AD NUMBER

AD854643

NEW LIMITATION CHANGE

TO

Approved for public release, distribution unlimited

FROM

Distribution authorized to U.S. Gov't. agencies and their contractors; Administrative/Operational Use; MAR 1969. Other requests shall be referred to Commanding General, US Army Electronics Command, Attn: AMSEL-BL-AP, Fort Monmouth, NJ.

AUTHORITY

Army Electronics Command ltr dtd 29 Nov 1971

AD

Research and Development Technical Report
ECOM-0319-F

APPLICATION OF RADAR TO MEASUREMENT OF SURFACE PRECIPITATION

FINAL REPORT

by

Pauline M. Austin

March 1969

ECOM

UNITED STATES ARMY ELECTRONICS COMMAND · FORT MONMOUTH, N.J.
CONTRACT DAAB 07-67-C-0319
MASSACHUSETTS INSTITUTE OF TECHNOLOGY
CAMBRIDGE, MASS.

Reports Control Symbol
OSD-1366
March 1969

Technical Report ECOM 0319-F

APPLICATION OF RADAR TO MEASUREMENT OF SURFACE PRECIPITATION

Final Report
1 September 1967 to 31 August 1968
Report No. 2

Contract No. DAAB 07-67-C-0319

Prepared by

Pauline M. Austin
Massachusetts Institute of Technology

for

U.S. Army Electronics Command, Fort Monmouth, N.J.

ABSTRACT

This report contains two major sections. In the first, consideration is given to the accuracy and practicality of measuring surface precipitation by radar. The second summarizes studies which have been made regarding mesoscale precipitation patterns and their relation to larger-scale circulations.

The radars which are in operation at the Weather Radar Laboratory at M.I.T. and auxiliary instrumentation for quantitative measurements are described, and the requirements for adequate radar calibration are discussed. Also included are estimates of the overall accuracy for the equipment and techniques which are employed. A data processor for printing digital maps or presenting data in other directly applicable form is described.

A number of raindrop-size measurements and the information they provide concerning Z-R relations appropriate for New England storms are summarized. Measurements of reflectivity in hailstorms and snowstorms are also discussed.

It is concluded that for convective storms a properly instrumented 10-cm radar can provide more accurate measurements of rainfall over an area than can a network of gauges. A wave length as short as 3 cm is shown to be unsatisfactory for measuring precipitation because of attenuation.

In widespread storms appreciable errors, occasionally a factor of two or three, may result from differences between the precipitation in the volume sampled by the radar and that reaching the surface. Observations of such effects are presented and discussed.

Advantages and liabilities both of the radar and of a network of gauges for measuring precipitation over an area are illustrated by experiments in which simultaneous measurements by the two methods are compared.

The second section of this report presents detailed descriptions of the structure and behavior of mesoscale precipitation areas and convective cells both in extratropical cyclones and in thunderstorm complexes. These descriptions will serve as a basis for physical and numerical studies of mesoscale phenomena.

Techniques have been developed for deducing the small-scale atmospheric motions from radar and rain-gauge data. Resulting contributions to the energetics and dynamics of larger-scale systems through release of latent heat and vertical transport of quantities such as sensible heat and momentum can be computed. In the analysis of a selected cyclonic storm it was found that the effects of small-scale convection were comparable in magnitude to those of the synoptic-scale circulations.

FOREWORD

The research described in this report represents work performed over a considerably longer period than that corresponding to contract no. DAAB07-67-C-0319. For a number of years, working under a series of contracts from the U.S. Army Electronics Command, the Weather Radar Research Project in the Department of Meteorology at the Massachusetts Institute of Technology has investigated the application of radar to measurement of surface precipitation. They have developed instrumentation, taken observations and studied the characteristics of the precipitation patterns. Many of these studies have been described in progress reports or in final reports of previous contracts, but in a rather fragmented manner. The aim of this report is a unified presentation of recent research.

The hardware and systems engineering for the WR-66 radar was obtained from the National Science Foundation under grant GP-2864. Also the laborious and expensive data processing described briefly in Section III, A, 1 and much of the analysis in III, A, 2 and 3 were accomplished under NSF grant G-19230. They are included here because of their relevance to work carried out under contracts from ECOM.

This report has been prepared by Dr. Pauline M. Austin, director of the Weather Radar Research Project. The research presented herein was accomplished by a number of individuals associated with the project. Specifically, all of the developments in instrumentation and the radar observations have been under the direction of Spiros G. Geotis, engineer for the Weather Radar Laboratory. His associate engineer, Donal Hoegl, has contributed significantly to the design and construction of the instrumentation. Design engineer for the digital equipment described in Sections II, B, 4 and 5 is Mario Schaffner. The extensive and detailed raingauge records were taken by machinist Edward M. Bean, who constructed and maintains the gauges at the field station.

Most of the research discussed in Section III was done by graduate students in the Department of Meteorology under the supervision of Dr. Austin:

Section III, A, 1 and 3: Charles K. Nason
A, 2: Michael J. Kraus
B: Robert A. Houze, Jr.
C: Elias A. Omotoso
Gary L. Melvin
E: M. Steven Tracton

TABLE OF CONTENTS

NOTICES

Disclaimers

The findings in this report are not to be construed as an official Department of the Army position, unless so designated by other authorized documents.

The citation of trade names and names of manufacturers in this report is not to be construed as official Government indorsement or approval of commercial products or services referenced herein.

Disposition

Destroy this report when it is no longer needed. Do not return it to the originator.

I. PURPOSE

The purpose of this contract is to investigate the application of radar to the measurement of surface precipitation. Aims of the research include: (1) assessment of the accuracy of radar measurements of precipitation rates and amounts; (2) development of instrumentation and techniques for improving the accuracy and reliability of such measurements; (3) quantitative observations of the distribution of precipitation in three dimensions; (4) meteorological analyses based on radar measurements of precipitation.

The operations of the project, in pursuance of the aims listed above, may be divided into four tasks: instrumentation, observations, data processing, and analysis and applications. In this report, rather than treat each task separately, the presentation is in two sections. In the first part consideration is given to the question of measuring surface precipitation with a radar. The problems which are encountered, the instrumentation which is required, and the accuracy which can be achieved are discussed. Contributions of the Weather Radar Research Project at the Massachusetts Institute of Technology, under sponsorship of the U.S. Army Electronics Command, are described. These contributions include design, construction and testing of instrumentation for accurate measurement of radar reflectivity over a large area with high resolution. There has also been considerable progress in developing instrumentation for automatic processing of the data in real time and presenting it in a form which is optimal for various applications. Many measurements have been made with both three and ten centimeter radars, and their respective advantages and limitations have been evaluated. Consideration has been given to the various sources of uncertainty which arise in interpreting radar measurements in terms of surface precipitation; experiments and observations are presented to illustrate their effects. Storm characteristics which are especially relevant to the problem, such as drop-size distributions, have been measured. Also, direct comparisons have been made of radar and rain-gauge measurements, and the results are discussed and evaluated. In this section emphasis is placed on recent developments, but description of earlier work which is pertinent to the subject is also included.

The second section of the report summarizes the studies which have been made regarding mesoscale precipitation patterns and their relation to the larger-scale atmospheric circulations. These studies include analyses of the cellular structure of storms and pilot studies to show the application of radar data to basic meteorological problems such as the effect of convective activity on the dynamics of extratropical cyclones.

II. RADAR MEASUREMENTS OF SURFACE PRECIPITATION

A. Introduction

It has long been recognized, even before the sharp spatial variations of precipitation intensity were dramatically portrayed by radar observations, that areal rainfall depths measured by precipitation gauges are accurate only if the network is exceedingly dense or if the data are integrated over very long periods of time. A radar can provide complete coverage over an area of 10^4 to 10^5 km^2 in about one minute and thus presents extremely attractive possibilities for measuring rainfall over an area. The difficulties and uncertainties involved, however, are so great that although attention has been given to this matter for over twenty years, nowhere are such measurements being made on a routine operational basis.

A question which has been frequently posed is, "How accurate are radar measurements of precipitation rate?" A concise and explicit answer to this question is not possible because of the many factors which affect it. It is better to examine the various factors involved and to ask more limited questions such as, "Under what conditions would radar measurements of precipitation be practical and desirable? What further developments are necessary to achieve satisfactory operational performance?" To these questions, more definite answers can be provided.

Radar measurement of surface precipitation rates or amounts involves the following aspects:

1. Measurement of the average signal intensity of fluctuating weather echoes;
2. Deduction of radar reflectivity in the storms;
3. Relation between precipitation rate and radar reflectivity;
4. Differences between the precipitation sampled by the radar and that which reaches the surface;
5. Automatic data processing and presentation of results in a form which is meaningful and immediately applicable.

Except for the relation between precipitation rate and radar reflectivity, all of these aspects are to a considerable extent concerned with the characteristics of the radar and the auxiliary instrumentation. In this part of the report a discussion of instrumental developments is first presented. Then the dependence of such measurements on storm characteristics is discussed. Finally, experiments which have been made to test the measurements and to evaluate their accuracy on precipitation rate are described.

B. Instrumentation

1. Description of the radars

Characteristics of the three radars in use at the Weather Radar Research Laboratory in the Department of Meteorology of the Massachusetts Institute of Technology are listed in Table 1.

Table 1. Characteristics of the radars for weather observations at M.I.T.

	SCR-615-B	AN/CPS-9	WR-66
Wave length (cm)	10.7	3.2	10.7
Beam width (degrees between half-power points)	3.0	1.0	1.3
Antenna gain (db)	33.2	41.6	43
Diameter of antenna (ft)	8	8	18
Pulse length (microseconds)	1.5	2.0 0.5	1.0
Pulse repetition frequency (cps)	400 600	400 931	350 700
Scopes	A/R PPI	A/R PPI, RHI	A/R PPI, RHI

All of the radars have remote scopes with camera attachments.

The SCR-615-B and a preproduction model of the AN/CPS-9 were provided by the U.S. Army Electronics Command and were in operation from 1946 and 1949, respectively, until 1964. Most of the data which have been analyzed have been taken with these radars, their limitations and advantages have been thoroughly explored, and early models of auxiliary equipment have been tested on them.

The major limitation of the AN/CPS-9 is the short wave length. When the radar was designed the wave length of 3.2 cm was selected because small particles such as hydrometeors have much greater reflectivities at short wave lengths, and because high antenna gain and good resolution can be obtained with a moderate sized dish. It was recognized that the radiation would be subject to attenuation by rain, but at that time statistics on rainfall intensities were not adequate to evaluate the seriousness of this limitation. Our analyses and observations discussed in section IIF, indicate that it is sufficiently serious to render this wave length inappropriate for measuring precipitation rates.

Limitations of the SCR-615-B are poor resolution and low sensitivity. Prior to 1964, when an improvement in sensitivity was achieved, rainfall of intensity below 5 mm hr^{-1} could not be detected except at very short range. In making observations, the AN/CPS-9 was used in snow and light rain and the SCR-615-B in moderate to heavy rain. The results are useful for evaluating the radars as instruments for measuring precipitation and for certain research studies, described in Chapter III of this report. But neither radar would be satisfactory for operational measurements of rainfall amounts because light and heavy precipitation frequently occur in the same storm.

In 1964, the laboratory was moved to the new Center for the Earth Sciences at M.I.T., a twenty-story building from which radars enjoy an unobstructed view in all directions. Through support from ECOM and a grant from the National Science Foundation, a newer AN/CPS-9 was installed and the WR-66 was constructed. Installation was completed in 1967. Because of its large dish and high power, this radar has a sensitivity and resolution comparable to those of the AN/CPS-9, but is free of rain attenuation. It can, therefore, make accurate measurements of the radar reflectivity in storms over a large area, usually out to 200 km in range. Because of the location of the new radars atop a high building, the

ground clutter is quite extensive, covering most of the area within 50 km. Therefore, observation of nearby precipitation must be made with the antenna slightly elevated.

In the fall of 1964 a new front end was put on the SCR-615-B radar, improving the sensitivity by about 12 db. Since then, it has been able to observe rain of 2 mm hr^{-1} out to a range of 80 miles. Because of the infrequency of storms during the extended drought in New England in the mid-nineteen-sixties and because of the preoccupation of the technical staff with installation of the new radars, observations taken since this improvement are relatively limited, but they are useful for evaluating the performance of a 10-cm radar with a moderate sized antenna for measuring precipitation.

2. Dynamic range

The radar was designed as a detector and is not easily adapted to the role of measuring device, especially if the target is precipitation. In this case the signal fluctuates at audio frequencies and a technique for averaging is required. The large dynamic range of weather echoes, which can be close to 80 db for a sensitive radar, also presents a problem, but this has been satisfactorily solved by the use of logarithmic receivers. A logarithmic receiver was constructed for the SCR-615-B at M.I.T. in 1955 (at that time they could not be purchased "off the shelf"). All of the weather radars at M.I.T. have logarithmic receivers, and they have now become standard equipment for all research and operational weather radars.

3. Measurement of average signal intensity

Signal fluctuations arise from changes in phase between waves scattered by individual hydrometeors as they move relative to each other. Analysis of the statistics (Marshall and Hitschfeld, 1953) has shown that for very many single observations of the same ensemble of scatterers in independent random configurations, the average power equals the sum of the power in the individual waves, and the standard deviation is equal to the average signal itself. When each observation is an average over k independent random configurations, the standard deviation is reduced to $1/\sqrt{k}$ times the average intensity. Accuracy of the measured power, therefore, depends primarily on the number of independent samples over which the average is made. If the receiver and amplifier are linear, the measured power is actually the square of the average amplitude and is 1 db less than the average power. With a logarithmic receiver the result is 2.5 db below the average power. These statistical relations have been checked experimentally by observing amplitude distribution functions from a series of single-pulse R-scope photographs and from the output of a boxcar generator (Austin, 1952) and by comparisons of the signal intensity from the same volume of precipitation-filled atmosphere as measured with the linear and logarithmic receivers (Austin and Geotis, 1960). Both of these experiments gave satisfactory verification to the assumed signal statistics.

The analysis of Marshall and Hitschfeld (1953) showed that the accuracy of an average over k statistically independent samples increases rather rapidly with the number of samples for small values of k up to about 20 or 30 but only slowly for large values. Therefore in practice, efforts are made to average about 20 to 30 samples. The length of time required for the relative motions of hydrometeors to produce a statistically independent random configuration varies considerably depending on the wind shear, the wave length, the beam width and other factors, but is on the order of milliseconds or a few hundredths of a second.

With typical signal decorrelation times of 5×10^{-3} sec for $\lambda = 3$ cm and 1.5×10^{-2} sec for $\lambda = 10$ cm, one would obtain 20 and 7 samples respectively for each 0.1 sec of averaging time. Independent samples in space occur at range intervals of one-half the pulse length and azimuth intervals of one beam width. For most weather radars the resolution in range is considerably better than in azimuth, and the combining of several range intervals may be advantageous since it increases the number of samples without degrading the resolution. In this type of averaging each sample contains a different ensemble of scatterers, and the statistical theory does not rigorously apply. Unless there is significant meteorological variation over the averaged range, however, it seems reasonable to assume that the several samples satisfactorily represent the same population.

Averaging signal intensity from a "point", defined as the volume of atmosphere between the half-power points in the beam and within a range interval of one-half the pulse length, is accomplished simply by holding the antenna stationary, gating off the signal from the desired range and averaging with a condenser. Over a period of a few tenths of a second an adequate number of independent samples is acquired while the ensemble of scatterers in the sampled volume does not alter significantly. This type of averaging is accomplished by the Pulse Integrator. The original model of the instrument was described by Williams (1949); modernized versions are part of the auxiliary equipment for all of the weather radars at M.I.T.

For averaging over an area, as the antenna scans, a storage device is required to accumulate and average the signals from each of the separate sections into which the observed area is divided. The sections or units of resolution should be kept sufficiently small to prevent combining echoes from precipitation which differs perceptibly either in composition or intensity. In practice this goal is rarely achieved since horizontal intensity gradients of 10 db or more in a few hundred meters are not unusual, and in the vertical the change from ice to water particles is accomplished in a few hundred meters. A practical criterion for resolution in signal averaging is that it should not degrade the resolution as determined by the beam width and pulse length of the radar.

Development of instrumentation for signal averaging, range normalization, and quantization into intensity levels has been one of the major accomplishments of the Weather Radar Research Project. Sweep integrators which use quartz delay lines for signal storage provide adequate time averaging without significant loss of range resolution. The time between pulses is synchronized to the delay time of the quartz line, and the signal returning from the atmosphere is added to the output from the delay line. In the first model, described by Kodaira (1959), the signal in the delay line is amplitude modulated, and stability requirements limit the additions to superposition of ten pulses. Limited frequency response of the circuit causes some space averaging, so that the average is taken over approximately twenty independent samples and reduces the standard deviation to 2 db. Range normalization is accomplished by adding a voltage proportional to $\log r^2$, and the signal is quantized into a series of intensity levels each covering an interval of approximately 5 db, which corresponds to a factor of two in equivalent rainfall rate. The intensity levels are displayed in sequence on the scopes (either PPI or RHI) by showing the regions where the signal exceeds the respective threshold values. An example is in Fig. 1.

The amplitude-modulated sweep integrator is used with the SCR-615-B radar. A second model which employs frequency modulation and thereby enjoys greater

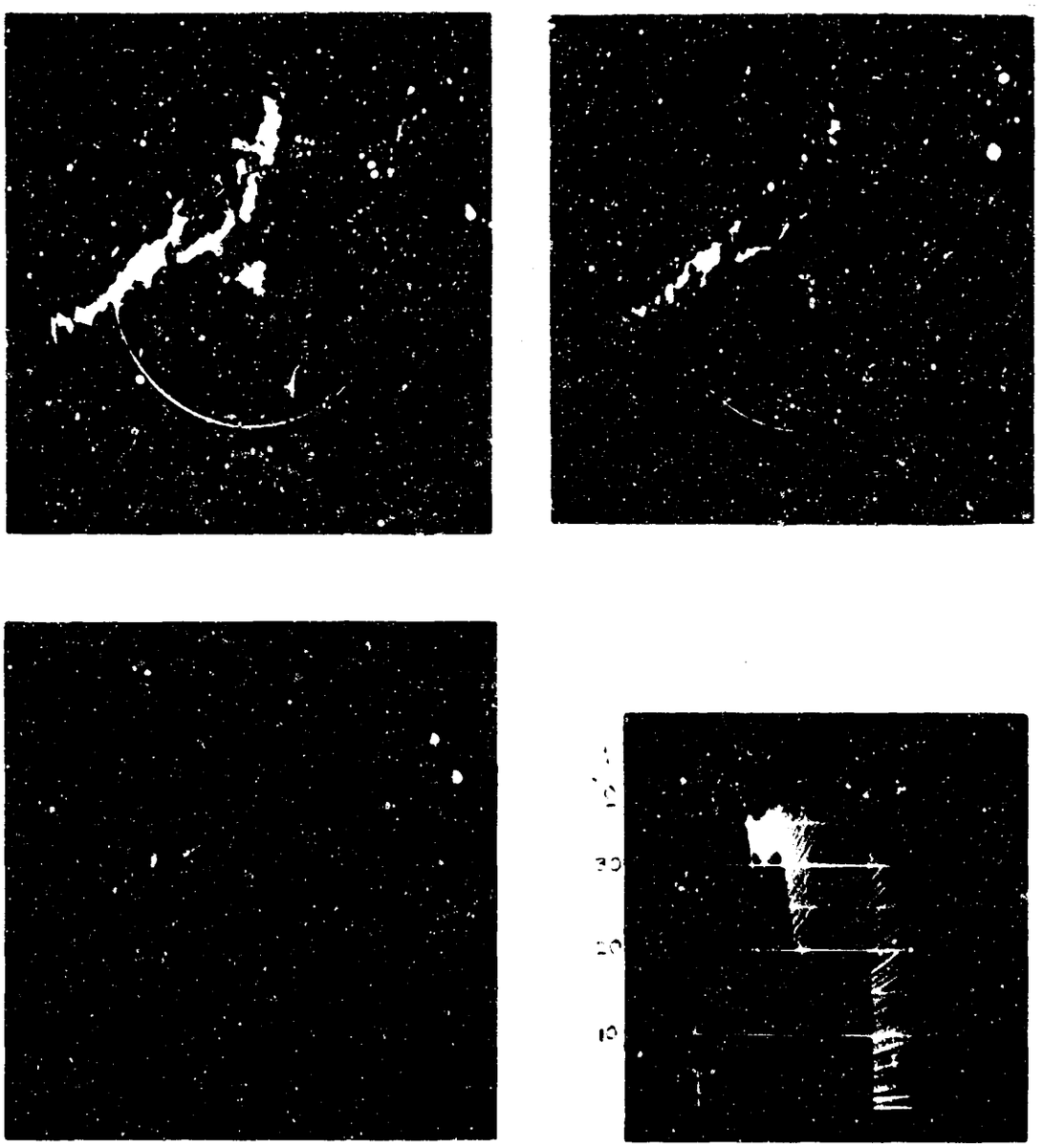

Fig. 1. Examples of averaged, range-normalized, signal intensity levels taken in squall line on 23 June 1965 with the SCR-615-B radar. PPI photographs are at 1900 EST and show areas with equivalent rainfall rates corresponding to 4, 16 and 64 mm hr^{-1}; range markers are at 20-mile intervals. On RHI range is 50 miles, azimuth 300 degrees, time 1940 EST. Shades of gray represent equivalent rainfall rates of 2 and 16 mm hr^{-1} with a very small intense core at 128 mm hr^{-1}.

stability has been described by Hoegl (1965) and is used with the AN/CPS-9 radar on short pulse. The sweep integrator for the WR-66 is entirely digital and is described in the following section.

Instrumentation for averaging and quantizing weather radar echoes has been developed or installed at only three or four laboratories, and the sweep integrators at M.I.T. provide the highest degree of resolution, coverage and accuracy available anywhere. Moreover, with the completion of the digital sweep integrator, we have provided a model which is suitable for operational and field use as well as research. The use of solid state components and integrated circuits makes it extremely compact, stable and flexible.

4. Digital sweep integrator

An ideal sweep integrator for weather radar measurements should have the following characteristics:

1. The capability to integrate any required number of samples from approximately 10 which is sufficient to produce an appreciable decrease in the standard deviation of the output, to several hundred, at which point further reduction in the standard deviation becomes negligible.

2. The capability to integrate signals over a range of amplitude as large as the maximum available in a weather radar, that is, about 80 db.

3. A resolution of the samples equal to the maximum resolution expected in a weather radar, on the order of 0.1 μ sec.

4. The ability to perform space integration by averaging a number of consecutive samples in range.

5. The ability to select samples at each desired range at different intervals of time, in order to vary the amount of independence between samples. The minimum interval is the radar pulse repetition period (PRP) and the maximum should be greater than the time required for total independence of the signals and might be as large as several seconds.

6. Accuracy of operations, regardless of the number of samples and the time required for the integration, within a precision limit of about 0.5 db.

7. Automatic normalization of the output, for all types of integration.

Sweep integrators previously used for weather radar observations are of the analog type and fail to satisfy the above specifications. The number of samples which can be integrated is limited by degradation of the signal during the integration process. Increase of resolution and dynamic range to the required levels is both costly and technically difficult. Exactness, freedom from drift, and stability are not typical characteristics of analog devices. The characteristics for the ideal integrator can be obtained with a digital computer. However, performance of the operations in real time for a radar of typical pulse width (0.5 μ sec) and with the desired dynamic range and precision, would require a computer of large capacity to be tied to the radar. The integration then becomes impractical from an economic point of view. A solution has been achieved with a simplified special purpose digital computer based on the circulating digital word system (Schaffner, 1966).

A block diagram of the system is in Fig. 2. The video signal of the radar is sampled and digitized by a quantizer. The digital values obtained are fed into the circulating word processor. This is composed of an operating unit and a circulation path for digital words. Each time a word enters the operating unit, new data are added and any necessary operations are performed; then the updated word returns again to circulation. The period of circulation is the same as the time between transmission of radar pulses; a special circulating signal triggers the transmitter. When an integration cycle is finished, the words present the output data; these data are decoded for the digital output and the analog output. The digital output has 16 levels; and the analog output has a resolution of 0.5% of the maximum signal.

The quantizer has sixteen levels. For a dynamic range of 80 db and signal fluctuations of the magnitude produced by meteorological targets, the quantization error is less than 1 db (Widrow, 1956). The integration consists of an accumulation of the values of successive samples at the same range interval, which is truncated when a preset number of samples is reached. The result is divided by the number of samples, subjected to range normalization, and presented as output. The number of accumulated samples can be set at 16, 32, 64, 128, and 256. The time interval between samples can be set at 1, 2, 4, 8, and 16 PRP. Consecutive samples in range (range integration) can be set at 1, 2, 4, 8, and 16. The corresponding lengths of the range integration are 325, 525, 1725, and 3323 meters, respectively.

The integrator can be set in two modes, automatic or manual integration. In automatic integration the following sequence of operations is repeated continuously:

1. Accumulation of the samples in each digital word. The number of samples, the space sequence, and the time interval are those previously set by the operator. This operation may need from 1 circulation (16 samples consecutive in space) to 4096 circulations (256 samples, no space integration and a time interval of 16 PRP between samples).

2. Addition of the range normalization factor in the words where a signal other than noise is obtained.

3. Scale normalization (division by the number of samples) and display. In order to have adequate brightness in the oscilloscopes, the display is repeated for eight circulations.

4. Reset of all words and circuits for new integration cycle.

In manual integration, the time interval between samples and the amount of range integration are set as in the automatic mode, but the number of samples is controlled manually. Accumulation progresses as long as a knob is depressed; when the knob is released, accumulation stops and the result is retained. Several accumulations, at different times, can be superimposed. No range correction is carried out in this mode, and the display is continuous. The manual mode is of particular use for measuring very small signals. The dynamic range can be set to a smaller value and at a low level comparable to that of the noise. With sufficiently long integration even signals well below the noise level can be detected and measured.

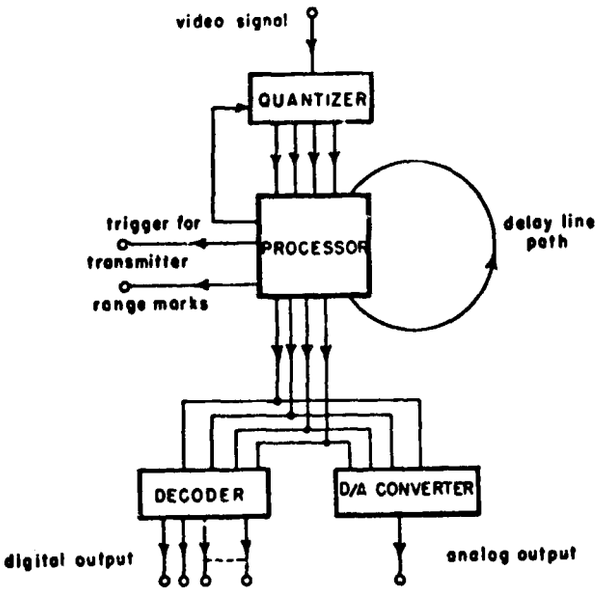

Fig. 2. Block diagram of digital sweep integrator

Fig. 3. Output of digital integrator on WR-66 radar. Range markers are at 20 km intervals.

The circulation path is composed of a cascade of glass delay lines working at a pulse rate of 6 Mc/s for a total delay of 1500 microseconds. All the circuits are solid state and some are of integrated type. All the operations are performed digitally, hence there is no calibration dependence at any time. Since the output is automatically normalized for all the different settings of the integration, it is possible to observe very clearly the effect on the output produced by changing the characteristics of the integration. These effects are illustrated in Figs. 4-6. Fig. 3 is a PPI representation showing three intensity levels in shades of gray.

Examples of integration on small signals are reported in Fig. 7. In the top two examples an artificial pulse signal radiation in front of the antenna was used; in the lower ones small meteorological echoes are present. The characteristics of the integrations are written on the figure.

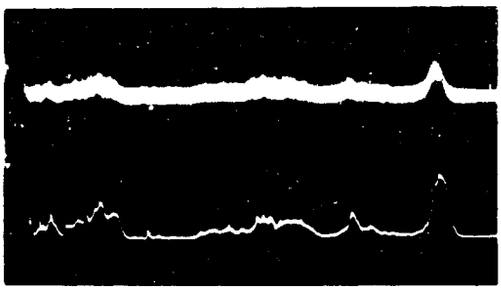

1 sample in range = 325 m resolution

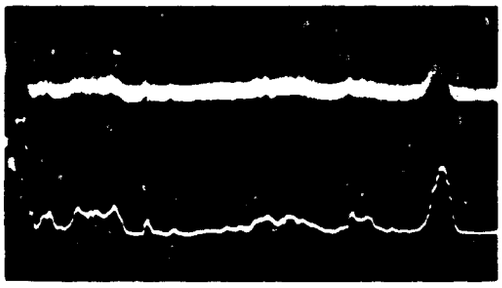

2 samples in range = 525 m resolution

8 samples in range = 1725 m resolution

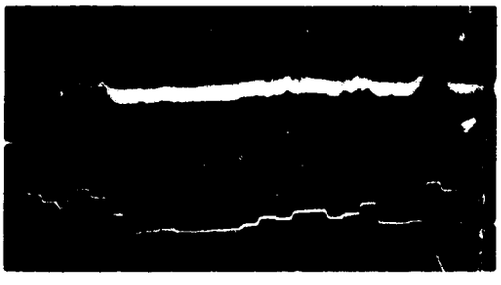

16 samples in range = 3325 m resolution

Fig. 4. Effect of varying range integration.
Upper trace: unintegrated video
Lower trace: integration of 256 samples with indicated range integration
Total range: 60 miles

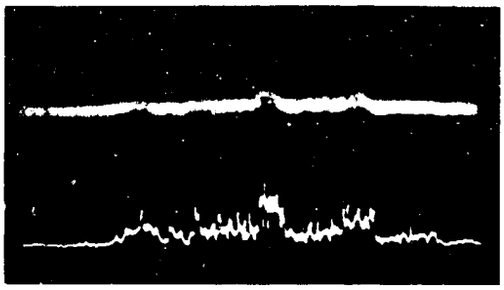

N = 16

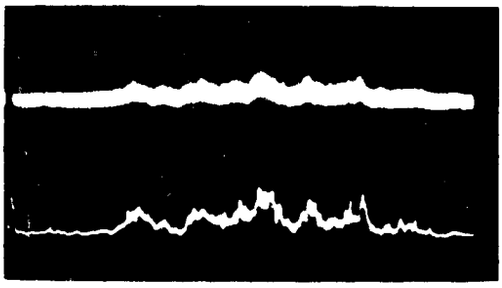

N = 32

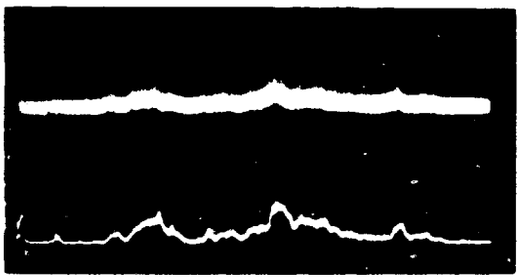

N = 128

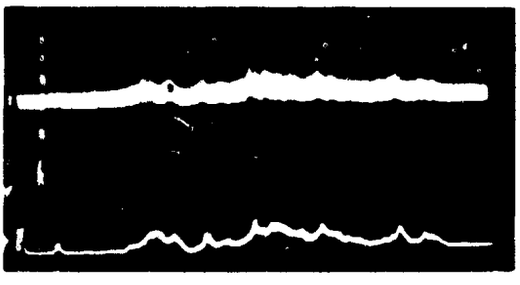

N = 256

Fig. 5. Effect of varying total number of samples
Upper trace: unintegrated video
Lower trace: integration of N samples in time, time interval of one PRP, no range integration.
Total range : 60 miles

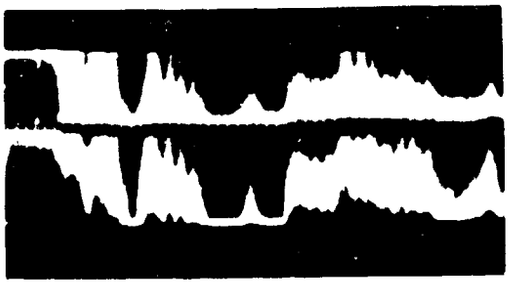

I = 1, S = 1, N = 16, T = 3

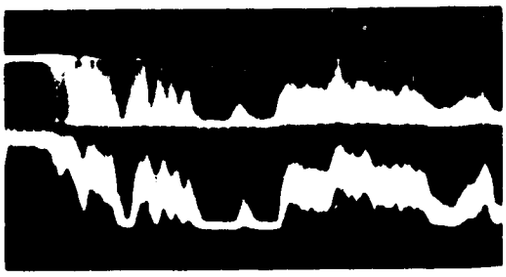

I = 8, S = 1, N = 16, T = 24

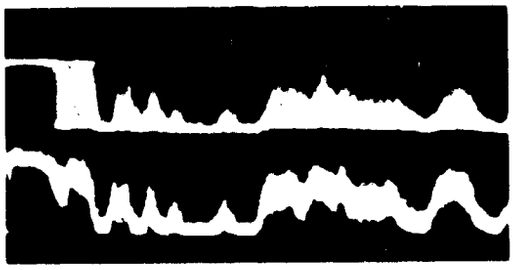

I = 8, S = 4, N = 16, T = 6

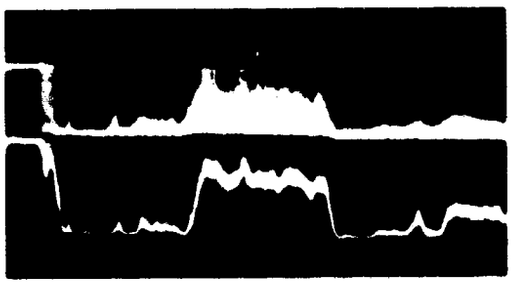

I = 8, S = 1, N = 64, T = 32

Fig. 6. Effect of varying interval between samples.
Upper trace: unintegrated video
Lower trace: superposition of 50 integrated outputs, each obtained with S consecutive samples in range, repeated at an interval I PRP for a total of N samples, covering a period T sec.

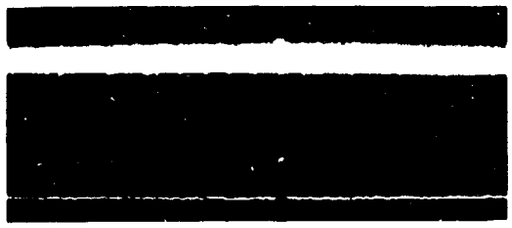

Pulse signal, -105 dbm
S = 2, I = 2, N = 256, with range correction

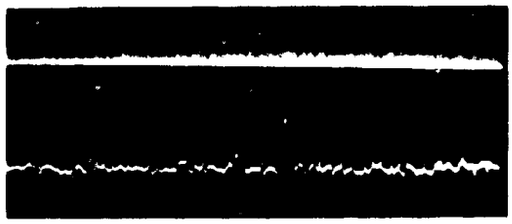

Pulse signal, -110 dbm
S = 2, I = 2, N = 13,300, manual integration

Weather echo
S = 2, I = 16, N = 333, manual integration

Weather echo
S = 1, I = 2, N = 2500, manual integration

Fig. 7. Examples of integration of small signals.
Upper trace: unintegrated video
Lower trace: integrated output for the indicated signal. Symbols are as in Fig. 6.
Total range: 60 miles

5. Digital data processor

A preliminary model of a processor for printing out, in XY coordinates, a quantized PPI representation and for computing statistics on integrated echo-intensities was constructed using a storage tube for integration and scan conversion (Schaffner, 1963). Limitations of the storage tube in retention of signals, dynamic range, and uniformity of characteristics, made this solution unsatisfactory.

A digital computer has the precision, reliability, and flexibility required for such processing. An incompatibility exists, however, between the large quantity of data produced at high speed by the radar and the characteristics of the conventional computer which is designed for executing one problem at a time. As a result, a high-speed, large-memory computer would be required, permanently attached to the radar--a solution which is neither economical nor practical for a common operational weather radar. A digital system which does not have this incompatibility, and was originally developed for processing signals of a meteor radar (Schaffner, 1966), is being constructed to process weather radar signals in real time.

The advantages of the system will become apparent upon comparison of its philosophy with that of the conventional computer. The basic structure of the conventional computer is represented in Fig. 8. A control unit calls for an instruction and one datum at a time from the memory; it controls the execution of the operation of an arithmetic unit on that datum and sends the result into the memory. For processing radar signals, a large memory is necessary to store the tremendous quantity of data continuously arriving from the radar, the intermediate results, and the final data waiting for the low speed output device. Moreover, many high speed arithmetic units are necessary in order to reduce all the input data to the desired output data in a reasonable amount of time.

The basic structure of the presented system is shown in Fig. 9. All the stored data circulates in a closed path suitable for digital signals. An operating unit is inserted in the path and therefore all the data can receive a cycle of processing at each circulation.

In this system the data related to a computation must arrive together at the operating unit. More precisely, these data are grouped and coded in a special form called a "page" -- so named because the data are organized as in a

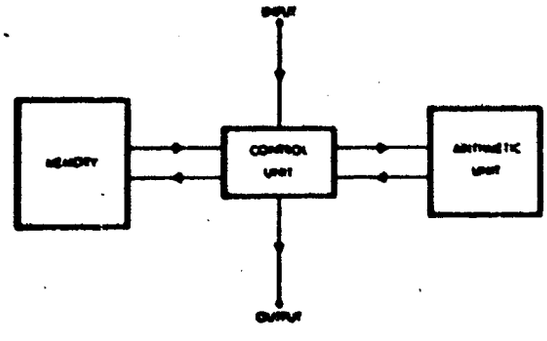

Fig. 8. Basic scheme of classical computer

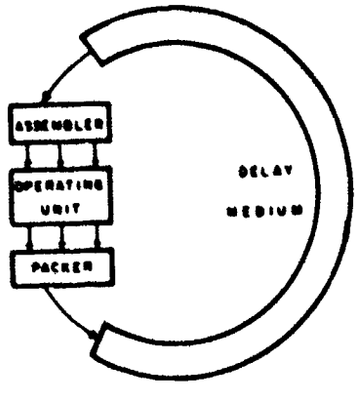

Fig. 9. Basic scheme of CPL system

written page. In a written page a sequence of symbols is made understandable by means of auxiliary symbols (space, punctuation) and by means of certain conventions (grammar, syntax). Here a circuit, called assembler, receives the continuous flow of digits and auxiliary signals from the delay medium, interprets them, and presents a page of organized data, related to a computation, to the operating unit.

The operating unit is composed of many operational elements loosely connected. The ensemble assumes an operational configuration when the program prescribes one. As a result the operating unit can be specialized for many different functions with high efficiency and speed. When the operating unit receives a page from the assembler, it executes a cycle of operations, as prescribed by the program of that page, and presents an output page to a circuit called "packer". The packer transforms the received page in a continuous sequence of digits and auxiliary signals for transmission into the delay medium.

Since the basic features of the system are the automatic circulation of the data, the organization of the data in pages, and the loose structure of the operating unit, it is called Circulating Page Loose (CPL) system.

When a CPL system is used for processing weather radar signals, the need for memory capacity is greatly reduced. All the data from the radar are acquired directly by the pages while they are passing through the operating unit. In the succeeding passages the pages, while they may continue to acquire data, perform the processing, which is executed in a short time because of the specialization of the loose operating unit. When the processing is completed, the same pages, reduced in size, perform functions of buffer and control for the output devices.

While the programming of a conventional computer consists of a sequence of elementary machine instructions, the programming of a CPL system consists of a list of states and transitions as used in the theory of the Finite State Machines (Gill, 1962). Consequently, the program for a CPL processor is very problem-oriented and extremely concise.

The CPL machine designed for processing weather radar signals is indicated in Fig. 10 with more details. The assembler, the operating unit, and the packer have register arrays, Ω_1, Ω_{2-3}, Ω_4 respectively, able to contain pages of maximum size of 5 words: one 8-bit key word and four 12-bit data words. The array Ω_1 of the assembler is duplicated four times for buffering purposes. Eight other registers are in the arrays Ω_1 and Ω_{2-3} for the program. The operating unit has four operating registers in order to execute operations on the four data words simultaneously. A loose logic circuit is available for implementing the several decisions requested by the program. The operating unit is provided with an auxiliary array Ω_5 for the transfer of data between pages. The circulation can be through the operating unit by the paths α_1 and α_2, or can bypass the operating unit through the path β. Data from the radar, video signal and antenna position, are fed into the operating unit. A high-speed printer of an electrographic type receives the output results from the operating unit.

The clock rate is 20 Mc; a page of maximum size, therefore, needs 3.4 μs to be transmitted. If the pages are kept as small as 20 bits, a page can be processed independently every microsecond, corresponding to independent values

of the video signal in a typical weather radar. The total capacity of the delay medium is 80,000 bits. Therefore up to 1170 independent pages of maximum size can circulate simultaneously in the system. If pages are smaller, a larger number can be processed at the same time. The program is not in circulation but is available for the assembler in an auxiliary storage. Up to eight programs can be started by push buttons; any other program can be inserted by plug-in cards. More than one program can be executed, in time sharing, on the same data.

As a first application of this processor, a program for polar to XY coordinate conversion and PPI printout with different resolutions is described. In this operation, the input data comes from the digital integrator and the printout is produced by the printer under a start command or in a programmed automatic sequence.

In this program, pages P_{i-j} are set in circulation, corresponding to the XY cells 1-1, 2-1, ...1-2, 2-2, ..., Fig. 11, in which the PPI representation is divided. At the beginning of the operation, these pages, hereafter called cell pages, are empty. The operation consists of five states. In state 0 the processor is awaiting the start order. During state 1, it is receiving the output from the integrator; the cell pages follow path β, Fig 10, leaving the operating unit free for pre-processing the data. This pre-processing puts onto a page called a carrier page the accumulated intensities for all of the sampled points within a single cell (word A), the number of integrated samples stored (word B) and a coded indication of the XY coordinates of the cell (word C).

When coordinates change the carrier page is put into circulation through path α_2 and data for the next cell are stored on another carrier page. Room in the circulation for inserting a carrier page can always be obtained at the desired time because an appropriate distance is maintained between pages, and the assembler has buffer capacity sufficient to hold up to four maximum-size pages. In this way a continuous sweep of integration outputs $a_1, a_2 \ldots a_k, b_1, b_2 \ldots b_\ell, c_1, c_2, \ldots c_m$, etc, Fig. 11, corresponding to the particular antenna direction crossing the XY cells 2-1, 2-2, 3-2 ..., is transformed into a set of carrier pages $C_{2-1}, C_{2-2}, C_{3-2}$ ..., carrying the accumulated data belonging to each cell.

During the several milliseconds between outputs while the integrator is occupied making a new integration, the processor is in state 2. In this state one carrier page at a time, C_{i-j}, sits in the array Ω_5 while the circulation is through paths α_1 and α_2. When the corresponding cell page P_{i-j} is resting for a cycle in Ω_{2-3}, the words A and B from the carrier page are added to it. When the transfer from all of the carrier pages to the corresponding cell pages is complete, the program returns to state 1 awaiting the next integrated sweep. On the cell pages, then, word A accumulates the sum of all integrated outputs for that cell during the entire antenna scan, and word B carries the number of these outputs.

When the antenna completes a full rotation, the program transfers to state 3. In state 3, at each passage of a page into the operating unit, the division of the content of A by the content of B is carried out and stored in word A. This means that each cell page will contain in A the average intensity obtained for that cell, and in B the number of samples which contributed to that average. When this division is accomplished for all the cell pages, the

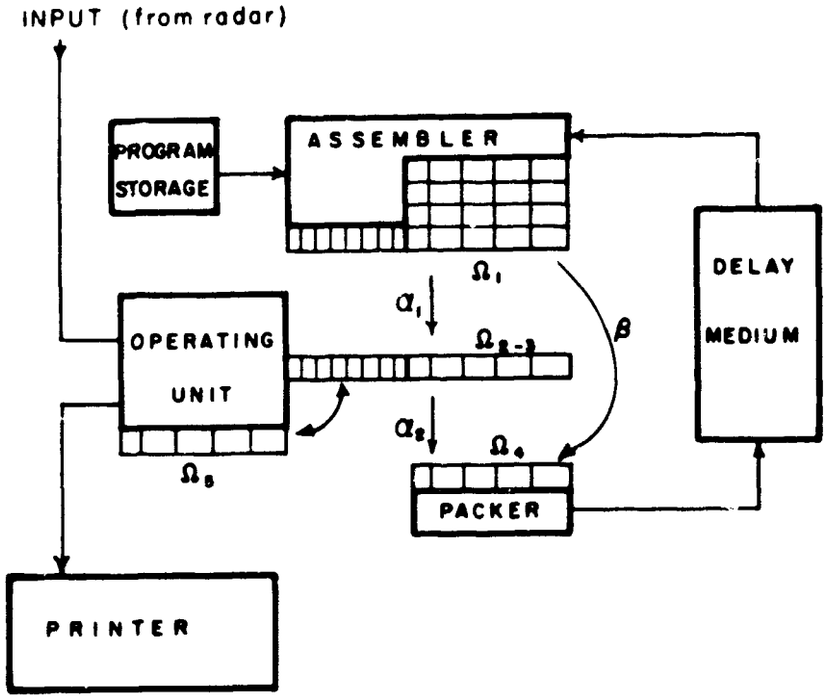

Fig. 10. Block diagram of the data processor

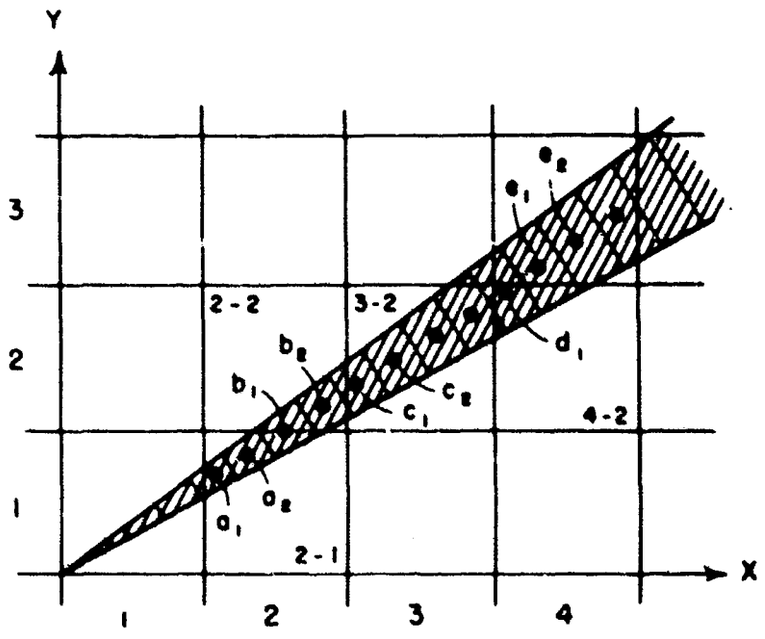

Fig. 11. Conversion from polar to XY coordinates

program transfers to state 4, in which the pages act as storage while the data is transferred to the output printer. The printer, Motorola model TP 4000, produces a PPI representation with a 54 x 54 grid, 2916 cells, in 15 seconds.

This processor is a general-purpose computer, oriented to the particular types of operations interesting for the weather radar signals. Therefore a large variety of programs can be attempted with the possibility of real time results. Those being planned are for computing: percent of total area covered by precipitation of each intensity, total rainfall, space and time correlations of integrated signal intensities, amplitude distribution and auto-correlation coefficient of unintegrated intensity, discrimination between weather and ground echoes.

The addition of a single memory unit to add precipitation amounts for one or several hours will provide detailed maps of total rainfall for the integration period, information of interest in hydrology and of importance in such problems as transport where knowledge of road and terrain conditions is needed.

6. Instrumentation for supplementary measurements

In addition to the radars, the laboratory maintains several tipping-bucket rain gauges, a modified Hudson-Jardi flowmeter gauge and a Fergusson weighing gauge at a field station seventeen miles away from the radar site. The tipping-bucket gauges each have two catch basins, one 38 inches in diameter and the other 19, the larger ones being used in the fall and spring and the smaller ones during the summer so that the high rainfall rates in thunderstorms will not cause saturation. The buckets tip every 10-12 cm^3, corresponding to rainfall depths of 0.006 and 0.0015 mm. The time scale permits resolution of only a few seconds, so that records are very detailed with respect to both intensity and variability. Three of the gauges are within about 30 meters of each other, and they generally agree to better than 10 per cent. Another tipping-bucket gauge is at a distance of 0.3 km; this one agrees with the others on the average, but not instantaneously since different showers or different parts of the same shower pass over it. A tipping-bucket gauge is also operated at the radar site. Except for midwinter months when the precipitation is primarily snow, records from these gauges cover almost all storms for nearly fifteen years. Not only are these data useful for direct comparison with radar observations as described in section II G, but in themselves they contain a vast amount of information regarding the showery structure and small-scale variability of surface precipitation. This information is proving extremely valuable in analyses of the type described in the third section of this report.

Several microbarographs were made available by ECOM in 1961, and since then records have been taken continuously at both M.I.T. and the field station. In addition, data have been taken during selected periods by voluntary observers at four other sites within the area covered by the radar.

A GMD-1A radiosonde set can provide information on atmospheric parameters and wind field in the immediate vicinity at times when the regular Weather Bureau observations are not sufficiently close to precipitation regions to supply the needed data.

7. Joss raindrop spectrometer

The close relationship between raindrop size and radar reflectivity is well

known, and many investigators have measured drop sizes in natural rain in order to obtain empirical relations between the radar reflectivity parameter, $Z = \Sigma D^6$ summed over a unit volume, and the precipitation rate, R. In addition to obtaining general Z-R relations, their dependence on geographical location and storm type have been studied statistically by Stout and Mueller (1968). Statistical analyses are not suitable, however, for investigations concerned with the development of hydrometeors in particular storms or storm types. Ideally, for such studies, one would make direct observations of the same hydrometeors at all stages of their growth, but there is no possible way to accomplish this. There is no doubt, however, that considerable insight could be gained by combining continuous sampling of the hydrometeors at the surface with detailed information of storm structure obtained with a high-resolution radar such as the WR-66. Joss has designed and built a raindrop spectrometer [Joss and Waldvogel (1967)] which records continuously and automatically, and is a very accurate and reliable device. Such an instrument would clearly be an extremely valuable supplement to the radar laboratory for studies in precipitation physics, and we have acquired one during the past year. Dr. Joss himself built the sensing unit for us; quantizing and counting circuits were constructed in our laboratory. The instrument has been completed, calibrated and tested. Already it has been successfully applied in making special measurements in Panama for the U.S. Army (contract no. DAAG25-69-C-0287).

The spectrometer is essentially an impaction device. The sensing surface is of very lightweight plastic, conical in shape, with the apex attached to the core of a coil, A in Fig. 12. At the impact of falling drops, the electric pulse induced in the coil is amplified and fed to another coil, B, which produces a counterforce and prevents any vertical motion of the sensing unit. This feedback system eliminates the "ringing" which has previously rendered impaction devices impractical for raindrop measurements. In this instrument the sensor is ready to accept another drop only six milliseconds after recording the previous one. The sensing surface is 50 cm^2 in area; counting rates vary from about 10 drops per second in light rain to 100 drops per second in heavy rain.

The magnitude of the damping pulse measures the impulse of the drop. Signals are quantized into twenty intervals; the drop sizes for the thresholds are in Table 2. Since there are many more small drops than large ones, the intervals

Table 2: Thresholds for channels in raindrop spectrometer

Channel	Drop diameter (mm)	Channel	Drop diameter (mm)
1		11	1.5
2	0.42	12	1.9
3	0.47	13	2.2
4	0.54	14	2.5
5	0.63	15	3.0
6	0.77	16	3.5
7	0.87	17	4.0
8	1.0	18	4.4
9	1.1	19	4.8
10	1.3	20	5.0

are made greater for the larger drops. An example of the output is in Fig. 13. It gives the actual time, the time interval over which the observation was made

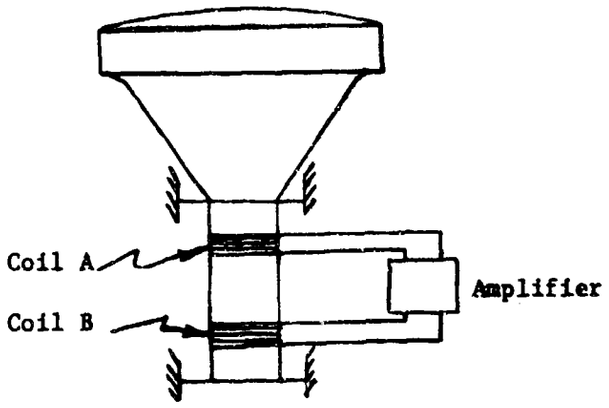

Fig. 12. Simplified sketch of Joss raindrop spectrograph

2	0		0	0	0
1	9		0	0	0
1	8		0	0	0
1	7		0	0	3
1	6		0	1	2
1	5		0	2	1
1	4		0	3	8
1	3		0	3	1
1	2		0	4	4
1	1		0	7	5
1	0		0	2	0
0	9		0	2	9
0	8		0	4	4
0	7		0	4	5
0	6		0	8	0
0	5		1	3	4
0	4		0	9	6
0	3		1	7	0
0	2		3	7	2
0	1		0	0	0
1	1	1 5		4	0
			0	2	5

Fig. 13. Example of printout. Data taken in Panama on 14 November 1968.

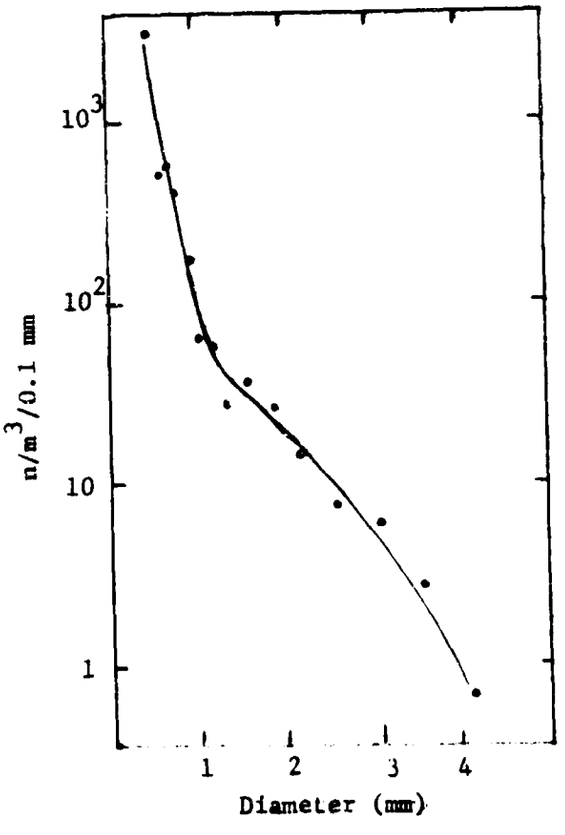

Fig. 14. Drop-size distribution from data in Fig. 13. Rainfall rate was 120 mm hr^{-1}.

and the number of drops in each size range. Printout can be obtained manually at any desired time by pushing a button or automatically either when the number of drops in any category reaches 999 or after a predetermined amount of rainfall. A tipping-bucket gauge connected to the spectrometer tips for every 0.1 mm of rain. Printout can be called for after every tip, every five tips or every ten tips. Fig. 14 shows the analyzed results of the output.

C. Radar Calibration

Radar reflectivity per unit volume, η, is deduced from measured average signal intensity, $\overline{P}_r$, by the radar equation

$$\overline{P}_r = \frac{P_t G^2 \lambda^2 h \theta \phi \kappa \eta}{512 \pi^2 r^2} \qquad (1)$$

Meanings of the symbols are described below. The accuracy of the deduced reflectivity depends on the accuracy of $\overline{P}_r$ and on the preciseness with which the parameters in equation (1) are known.

The transmitted power, P_t, is measured through a directional coupler which is in series with the transmission line. The accuracy of this method depends on how well the losses in the directional coupler and attendant cabling are known and on the accuracy of the power meter. Power meters of a high accuracy are easily obtained and the required measurements can be made to less than a db with little difficulty. It is important to recognize that this measure of P_t holds only for the power through the directional coupler and is not necessarily that which leaves the antenna. This might be important in radars which have rotary joints or other possible sources of loss after the directional coupler. These losses would, however, occur on the way out and back and therefore may be lumped in with the antenna gain.

The wave length, λ, is known very accurately through its relation to the carrier frequency, and the range, r, can also be measured very accurately because of the precise electronic timing mechanisms in the radar. The pulse length, h, can be measured to an accuracy of a small fraction of a db by looking at the RF output pulse with a spectrum analyzer.

In theory the gain of the antenna, G, is related to its size, and for a parabolic dish is given by $\frac{4\pi A}{\lambda^2}$ where A is the aperture. Actually, however, the gain is generally several db below the theoretical value and it should be measured on an antenna range.

In equation (1), θ and ϕ are the angles between half-power points in the beam and are assumed to define the illuminated volume of the atmosphere at any instant. However, for a parabolic dish the power pattern in the beam approximates a Gaussian function of the axial angle, and the effective solid angle is slightly less than that defined by the half-power points. The need for direct measurements of all radar parameters and especially of the antenna gain and beam power pattern was stressed by Austin and Williams (1951) and again by Austin and Geotis (1960).

Antenna gains for the SCR-615-B and the AN/CPS-9 have been measured both by tracking standard targets (metal spheres large compared with the wave length) and by direct measurements with a standard horn and power meter in the far field of the transmitting antenna. The direct measurements gave the values in Table 1. They are, as expected, several db below the theoretical values. Results from the standard targets were in fair agreement but were not so satisfactory because the echoes fluctuated considerably even though the spheres appeared to be quite smooth. Such fluctuations have also been observed by other investigators who have attempted to use standard targets for calibrating radars; the cause has not been determined. Because of these fluctuations, the uncertainty in values of antenna gain measured by observing standard targets is probably at least 2 db, and we have concluded that direct measurement on an antenna range is considerably more satisfactory and reliable.

Direct measurements of the entire beam pattern have shown that it does very closely approximate a Gaussian function and that the effective solid angle is ninety per cent of that subtended by the half-power points, so that the received power is 1 db less than indicated by equation (1). This correction for beam pattern is applied to all measurements.

The effect of attenuation, κ, is discussed in section II F.

It is recognized that some type of standard target or signal is desirable for frequent routine monitoring of radar performance, but a satisfactory one has not been found. Since we operate more than one radar at M.I.T., we have been able to monitor the performance by comparing apparent reflectivities from the same "point" (volume defined by the beam width and pulse length) in a storm. Fig. 15 shows minute-by-minute comparisons for about 360 points representing six hours of data on twelve days. Data were taken with the antennas stationary, elevation angle of 1° and range 17 miles. The graph shows a sharp peak at 1 db, which is probably the net error in measured radar parameters. There are relatively few points on the right-hand side of the peak, and they can probably be accounted for by differences in the volumes sampled by the two radars. The large number of points on the left-hand side, where the AN/CPS-9 reads relatively low, can be attributed to the effects of attenuation in moderate and heavy rain. In practice, if the relative signal intensities are within 2 db of the computed value, it is assumed that the radars are performing satisfactorily. If a larger discrepancy is found the cause is sought. One source of error which was uncovered by this method of monitoring is loss of power through deterioration of the magnetron spectrum. Although the total power output was normal, much of it was outside the frequency range of the receiver. Hence the spectrum as well as the total power output should be monitored.

Our experience has shown that with careful calibrations and techniques for signal averaging, measurements of radar reflectivity in storms can be made with an accuracy of 2 db or even slightly better. However, because of the complexity of the radar as a quantitative instrument, a reliable monitoring system is imperative.

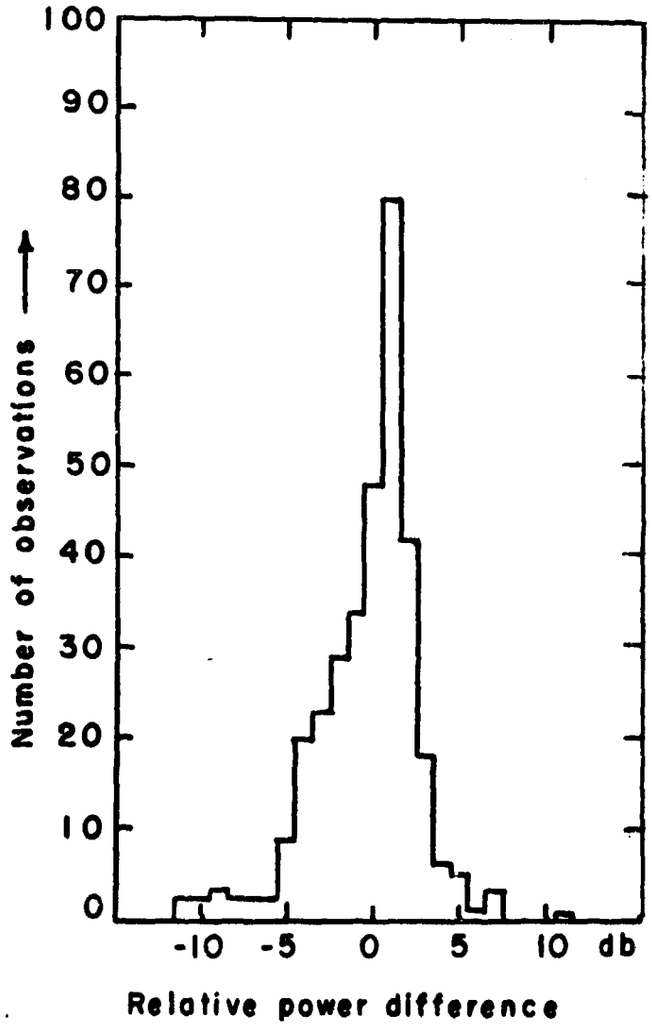

Fig. 15. Comparison of signals received on AN/CPS-9 and SCR-615-B radars from same precipitation target. Abscissa represents number of db by which measured power difference between the signals exceeds the value computed from radar equation and measured radar parameters. Positive values indicate that the AN/CPS-9 measures relatively high.

D. Relation Between Reflectivity and Precipitation Rate

1. Theory

For an assembly of spherical scatterers which are small compared with the wave length, the radar reflectivity is given by:

$$\eta = \frac{\pi^5 |K|^2 Z}{\lambda^4} \qquad (2)$$

where $Z \equiv \Sigma D^6$. Values of D are the diameters of individual spheres and the sum is taken over a unit volume. The quantity $|K|^2$ depends on the dielectric constant of the spheres and is equal to 0.93 for water and 0.197 for ice. Equation (2) is applicable to almost all rain for wave lengths greater than 3 cm, and also to snow provided the D's refer to the diameters of the melted flakes, and the appropriate value of $|K|^2$ is used.

The reflectivity factor, Z, and the precipitation rate, R, are not uniquely related, but both depend on the number and size of the hydrometeors, and they are related empirically to the extent that precipitation of any given intensity tends to have a particular particle-size distribution.

A direct measure of Z is obtained by sampling the hydrometeors and observing their diameters. If Z is deduced from radar measurements through application of equations (1) and (2) it is called equivalent Z and designated Z_e. Within the accuracy of the radar measurements Z_e has the same value as Z provided that the proper value of $|K|^2$ is used, the scatterers are sufficiently small compared with the wave length, and the scatterers are spherical in shape or the reflectivity is unaffected by the shape. Similarly a measure of precipitation rate deduced from a value of equivalent Z is called equivalent rainfall rate and designated R_e.

2. Z-R relations for rain

In the case of rain, measurements of drop-size distributions have been made by a number of observers, and the results generally fit quite well a curve of the form $Z = AR^b$.

A group of measurements surveyed by Marshall and Palmer (1948) fit the relation $Z = 200R^{1.6}$ with a standard deviation of about 3 db. Here Z is measured in $mm^6\ m^{-3}$ and R in mm hr^{-1}. Many observations have been made by Stout and Mueller (1968) in a variety of geographical locations. They found that if storms are grouped into thunderstorms, rain showers, and steady rain, slightly different regression lines are obtained. More significant differences occur between different geographical locations. Much of the empirical data are summarized in Figs. 16 and 17. The scatter of observed points about each of the regression lines is generally broader than the differences between the lines. The extent to which this scatter represents meteorological variations from storm to storm or from time to time within the same storm, and the extent to which it is caused by inadequate sampling of drops of all sizes has not yet been clearly established.

A number of drop samples have been collected at M.I.T., most of them during 1964 and 1965, in order to determine which of the empirical relations appear to be most suitable for New England storms. Measurements were made by exposing diazo treated filter papers about 9 inches in diameter for a few seconds. By this method a volume of air on the order of one cubic meter was sampled. Drop

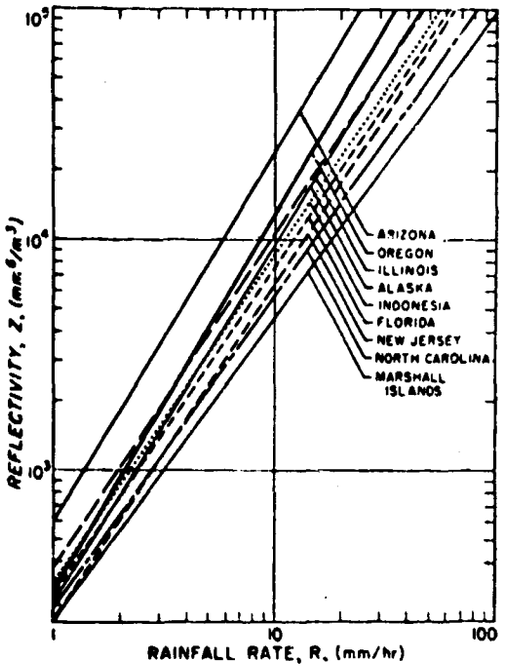

Fig. 16. Geographical variations of Z-R relation ships. (from Stout & Mueller, 1968)

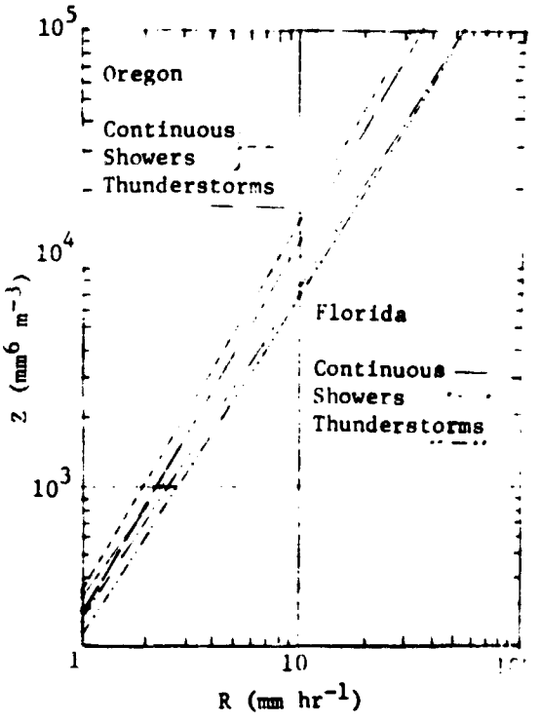

Fig. 17. Variation of Z-R relationships with rainfall type. (from Stout & Mueller, 1968)

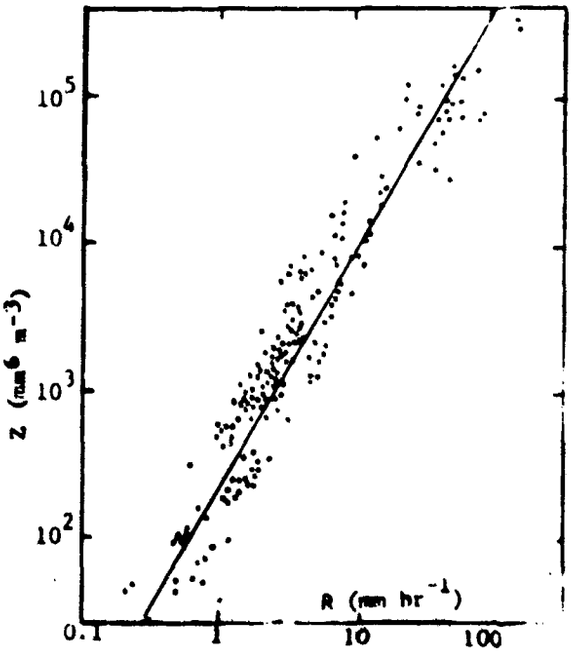

Fig. 18. Z-R relationships from individual drop-size samples taken at M.I.T. Line shows $Z=200R^{1.6}$

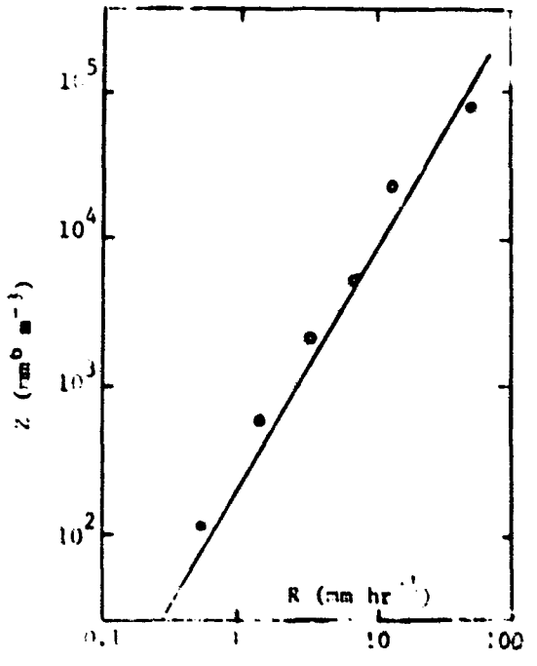

Fig. 19. Z-R relationships from M.I.T. data grouped according to rainfall intensity. Line is $Z=200R^{1.6}$.

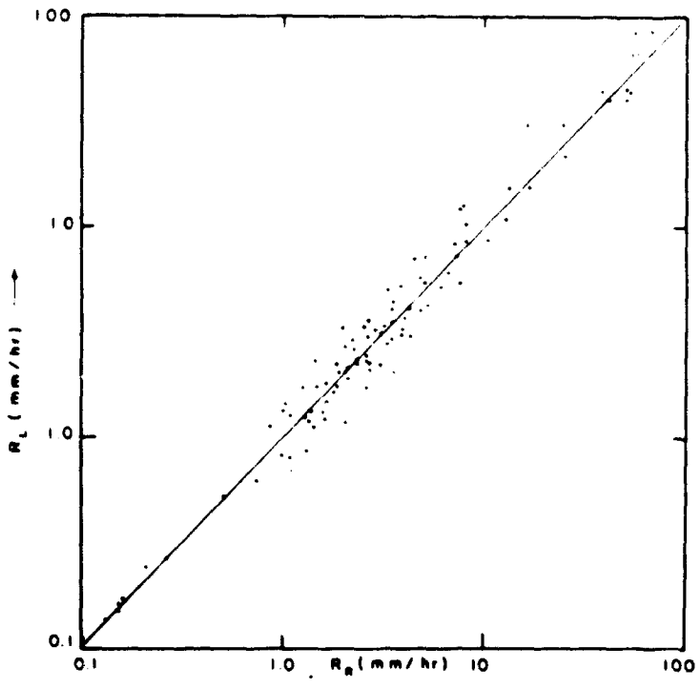

Fig. 20. Comparison of computed rainfall rates for simultaneously exposed right and left-hand drop-size samples.

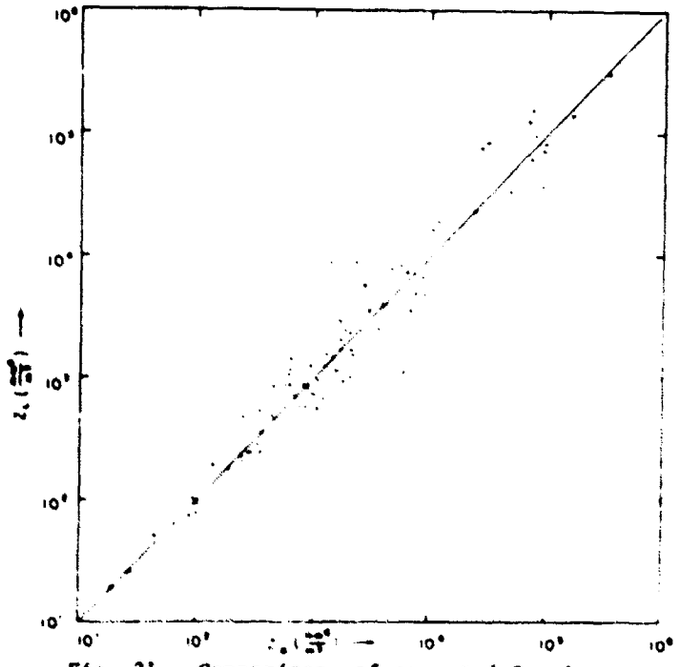

Fig. 21. Comparison of computed Z values for simultaneously exposed right and left-hand drop-size samples.

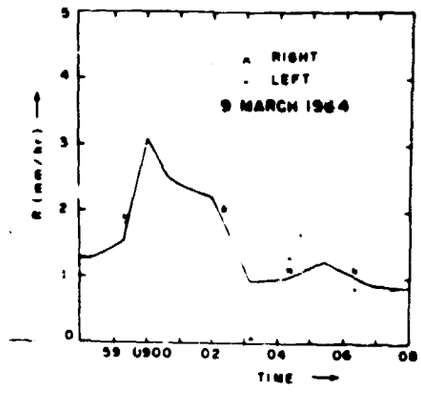

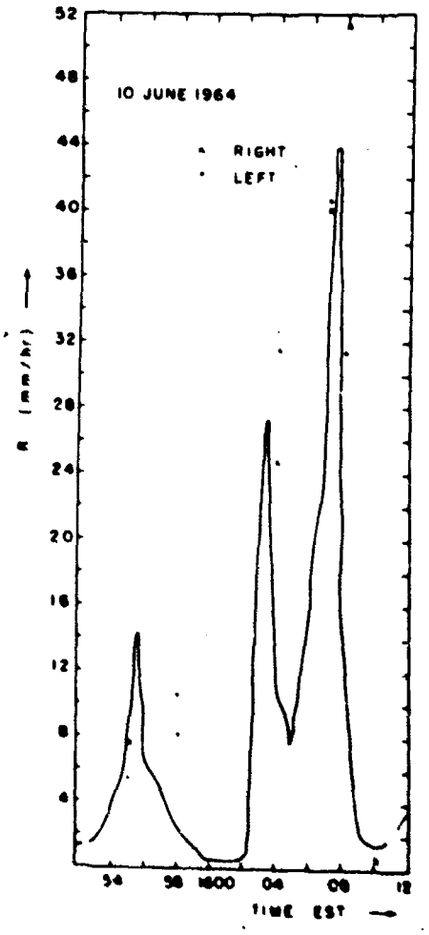

Fig. 22. Comparison of rainfall rate measured by gauge (solid line) with that computed from right and left-hand samples.

counting and sizing is done manually with a calibrated scale, the calibration having been made in the laboratory with drops of known volumes. Fig. 18 summarizes the results from 370 samples on 38 days. The line for $Z = 200\ R^{1.6}$ is drawn in and appears to be a good fit. This is in agreement with Boucher (1951) who sampled drops in a number of New England storms and obtained the relation $Z = 180\ R^{1.55}$. Fig. 19 shows the results when the data were grouped, that is, all the measurements within certain intervals of rainfall rate were averaged to give a single point.

On a number of occasions, two filter papers were exposed simultaneously side by side. The values of R and Z computed from the right and left-hand samples were then plotted against each other, Fig. 20 and 21. Examples in Fig. 22 compare rainfall rates computed from drop samples with those recorded by a rain gauge. The fact that the scatter of points in Fig. 21 is about as large as that in Fig. 18 supports the suspicion that much of the variation in observed Z-R relations results from sampling inadequacy.

From the various drop-size measurements and especially those made in New England, it appears that the empirical relation $Z = 200\ R^{1.6}$ is appropriate for rain in New England, and that on most occasions accuracy better than a factor of two can be expected from the use of this relationship.

3. Radar reflectivity of snow

Only a few measurements have been made of particle size distributions in snow. Those of Imai et al (1955) and Gunn and Marshall (1958) suggest that the relation $Z = 2000\ R^{2.0}$ is appropriate for snowflake aggregates. For non-aggregated snowflakes, Z would probably be lower by at least an order of magnitude. Moreover, for a given Z value, the radar reflectivity would be quite different for wet and dry snowflakes. It would seem, therefore, that until the processes of aggregation and melting are more fully understood, precipitation rates in snow cannot be measured even roughly by radar.

4. Reflectivity of hailstorms

Fairly comprehensive computations have been made of the backscattering properties of spheres composed of ice and water (Battan and Herman, 1961, 1962), and some observations of hail size distributions in Alberta, Canada, have been reported (Douglas, 1960, and Douglas and Hitschfeld, 1961). In general, however, sizes shapes and moisture contents of hailstones are so variable that a useful empirical relation between precipitation rate and radar reflectivity has not been formulated. Moreover, hail is often accompanied by heavy rain so that, in many storms, the rain contributes the bulk of the precipitation while the hail particles are responsible for the major portion of the reflectivity.

From measurements made with the SCR-615-B radar at M.I.T., Geotis (1963) has clearly demonstrated that the reflectivity of hailstorms in New England is closely related to the size of the largest hailstones they contain. Z_e values in excess of $10^{5.5}$ mm^6 m^{-3} were almost always associated with hail. Values of 10^6 were associated with hailstones as large as one-half inch in diameter, while those in the vicinity of $10^{6.5}$ or greater were produced by large hail, reported as "walnut" or "golf ball" size. Since the measurements were taken at a wave length of 10 cm, which is large compared with the dimensions of the hailstones, the values of Z_e were probably quite close to the actual values of Z in the storm; it was assumed in all cases that the hailstones were wet. A wave length of 3 cm would not greatly exceed the dimensions of the larger hailstones, and the relation

between Z_e and Z would be considerably less well defined. Moreover, attenuation of the 3-cm radiation would doubtless introduce serious errors.

It may be concluded, then, that measurements of reflectivity with a 10-cm radar can give a reliable indication of the presence of hail and of the maximum size of the hailstones. The reflectivity does not, however, give useful information regarding the precipitation rate in hailstorms.

E. Representativeness of Precipitation Sampled by the Radar

1. Location of volume sampled by the radar

With regard to measurement of surface precipitation by radar, it is necessary to consider any differences which might exist between the precipitation sampled by the radar and that which reaches the surface. Fig. 23 shows the height of the beam center as a function of range and elevation angle in a standard atmosphere. The volume of atmosphere sampled by a radar spreads above and below the central line by an amount roughly equal to half the beam width. It can readily be seen that at close ranges and with a narrow beam there is little opportunity for the hydrometeors observed by the radar to alter before they reach the surface. At large ranges, however, several kilometers of altitude may be involved.

2. Factors which affect representativeness

Discrepancies between radar and surface observations may be caused by:

(a) Evaporation, if air near the surface is relatively dry. The rate of evaporation of a raindrop of mass m and diameter D is

$$\frac{dm}{dt} = 2\pi D C_v k \Delta\rho \qquad (3)$$

where k is the diffusion coefficient of water vapor in air, C_v is the ventilation factor and $\Delta\rho$ is the difference in vapor density at the surface of the drop and in the environment. For raindrops up to 0.2 cm in diameter, the fall velocity V_t is roughly proportional to the diameter, so that if h is the distance fallen,

$$\frac{dh}{dt} = V_t = aD \quad \text{where } a = 4 \times 10^3 \text{ sec}^{-1} \qquad (4)$$

Then

$$\frac{dm}{dh} = \frac{2\pi C_v k \Delta\rho}{a} \qquad (5)$$

For $k \approx 0.3$ cm^2 sec^{-1}, $C_v > 1$ and $\Delta\rho = 2 \times 10^{-6}$ g cm^{-3}, which corresponds to a relative humidity of about 80 to 90 per cent at temperatures between 10C and 20C, each drop would lose at least 10^{-4} g while falling 1 km. A loss of this amount would reduce rain of 1 mm hr^{-1} by about 25 per cent and of 10 mm hr^{-1} by 10 per cent. These estimates are based on average drop-size distributions for eastern Massachusetts reported by Geotis (1968). Clearly the magnitude of this effect, when evaporation occurs, varies widely depending upon the circumstances. The above computations with representative values indicate that there doubtless are occasions when the effect is significant.

(b) Growth by condensation or sublimation. If there is convergence and lifting in the lowest layers of the atmosphere, any hydrometeors present will grow by condensation or sublimation. However, growth of raindrops by condensation is

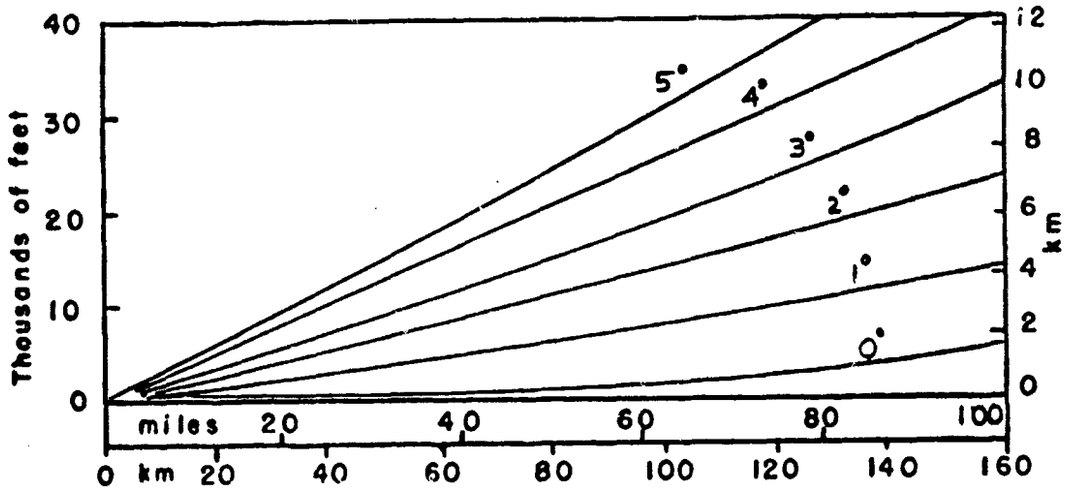

Fig. 23. Height of beam center above earth as a function of slant range and elevation angle.

slower, by roughly two orders of magnitude, than the evaporation rates considered above because supersaturations which can occur in the atmosphere are only a few per cent of the saturation deficits which may be encountered. If there is significant condensation near the surface, low cloud or fog is formed and growth of any raindrops is primarily by accretion.

In snowstorms the hydrometeors are numerous (perhaps 10^4 to 10^5 m^{-3} for unaggregated crystals) and fall slowly so that growth by sublimation may be significant. Austin and Wexler (1953) observed the variation of reflectivity with height in generally stratiform snow and compared the results with computations of growth rate by sublimation. They found increases of 3 to 5 db for each kilometer of altitude. In the layers where aggregation was occurring, the increase in reflectivity was much more rapid.

(c) Growth of hydrometeors by accretion in low stratus cloud or fog. Growth by accretion for a raindrop of diameter D is

$$\Delta D = \frac{EW\Delta h}{2\rho_L} \qquad (6)$$

where E is the collection efficiency, W the liquid water content of the cloud, ρ_L the density of water and Δh the distance fallen. In traversing a depth of 1 km a raindrop increases its diameter by approximately 0.4 mm for each g m^{-3} of liquid water in the cloud. An increase of 0.1 mm in the diameter of each drop would increase the rainfall rate by approximately 40 per cent at rates of 1 to 2 mm hr^{-1} and by about 20 per cent at 10 mm hr^{-1}. These computations are also based on the measurements by Geotis (1968).

(d) Presence of melting snow in the sampled volume. The reflectivity of melting snowflakes is usually 5 to 10 db stronger than that of the rain below it. There-

fore if the melting layer is in the upper portion of the radar beam, its higher reflectivity will cause the average value of η sampled by the radar to exceed that of the rain reaching the surface, perhaps by several decibels. If the melting layer is in the lower portion of the beam or below it altogether, then the volume sampled by the radar is filled mostly with snow which has a relatively low reflectivity. In this case, η in the radar sample may be several decibels less than in the rain.

3. Examples

All of the effects just described have been observed, on some occasions, with sufficient magnitude to affect radar measurements. Examples are in Fig. 24. Effects of evaporation are illustrated in Fig. 24a where equivalent rainfall rates measured by the AN/CPS-9 at 1630 EST on 28 May 1963 are shown. On this day the rain gauges in the area reported no measurable precipitation. The RHI shows that the echoes diminish considerably below 5000 ft. Surface stations were reporting relative humidities between 40 and 60 per cent. Skies were overcast; ceilings were generally about 10,000 ft but descended to near 5000 ft in the areas where radar echoes appeared.

On 12 February 1963, Fig. 24b, snow was falling at the ground and temperatures everywhere, except in the immediate vicinity of the coast were below 0C. Hourly precipitation data indicate that except for the band of heavier snow stretching across the area from southwest to northeast, there was fairly uniform moderate snow extending out to about 100 miles. The radar data suggest a continual decrease in intensity with range, an effect which is especially noticeable in the northwest quadrant. This apparent decrease in precipitation intensity with range is due to the fact that in the storm the reflectivity decreased steadily with height while the height of the sampled volume increased with range. The effects of accretion in low cloud or fog are similar to those in Fig. 24b in that as the range increases the rainfall rates indicated by the radar become progressively smaller as compared with those measured by gauges at the surface. It is not so clearly recognizable on the PPI, however, because the small-scale variability in rainfall intensity tends to mask the range effect, which can be detected only by painstaking comparison of radar and rain-gauge data.

On 21 December 1960, Fig. 24c, it was raining at the ground but the melting level was quite low, about 4000 ft. At a range of 17 or 18 miles the radiation in the top of the SCR-615-B radar began to encounter melting snow and the echo was consequently enhanced. Between 25 and 35 miles a sufficiently large portion of the beam was filled by melting snow so that an annular area of higher reflectivity appeared on the PPI. The reflectivity of the snow above the melting layer was lower by a factor of about five and it continued to decrease with height. Beyond 35 miles so much of the beam cross section was filled by snow that the signal ceased to be detectable. Such a clear-cut example of this effect is extremely rare because usually the variability masks the tendency to form a concentric pattern. A much more typical case is shown in Fig. 24d. The AN/CPS-9 radar showed light rain, approximately 1 mm hr^{-1}, covering the area continuously out to a range of about 35 miles with scattered areas of similar intensity between 40 and 60 miles, especially in the northeast quadrant. The rain-gauge network indicated that the precipitation was continuous, but beyond 35 miles detectability was marginal, and only patches were displayed on the PPI. A region of slightly heavier rain, $\sim$ 2 mm hr^{-1}, lay to the northeast between 10 and 30 miles, area A. On the SCR-615-B, rain of 1 mm hr^{-1} was presumably below the level of detection, with the lowest intensity level corresponding to a rainfall rate of 2 mm hr^{-1}. How-

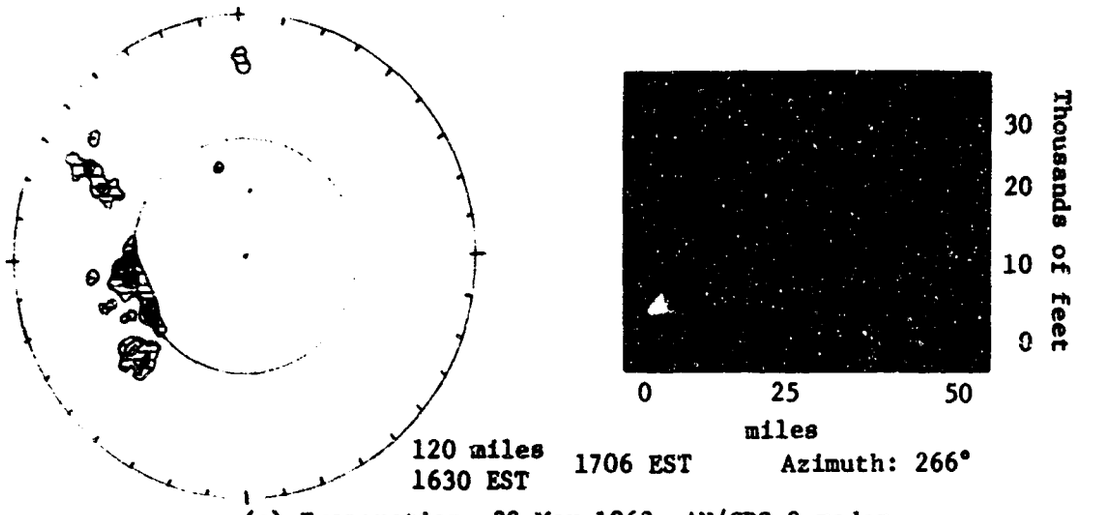

(a) Evaporation, 28 May 1963, AN/CPS-9 radar

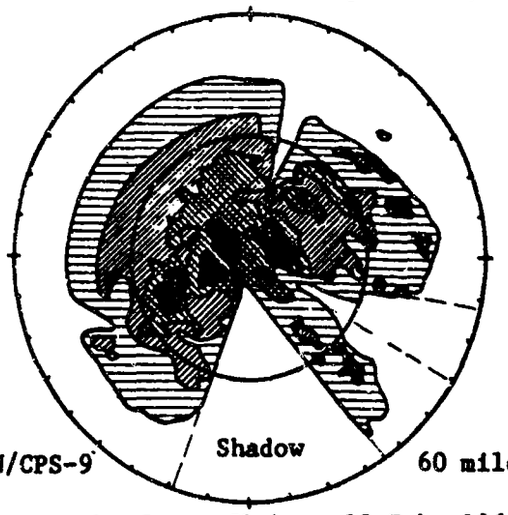

(b) Growth of snowflakes, 12 Feb. 1963

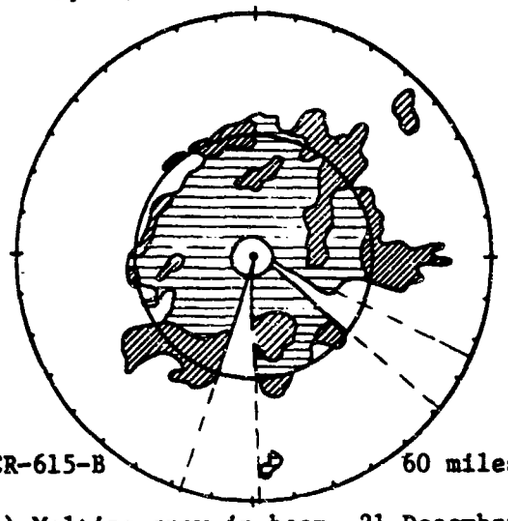

(c) Melting snow in beam, 21 December 1960

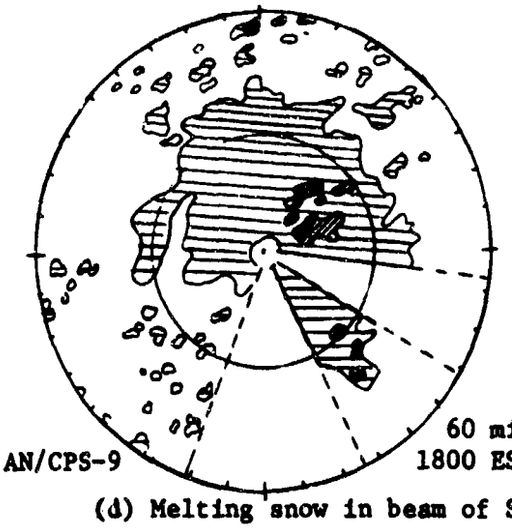

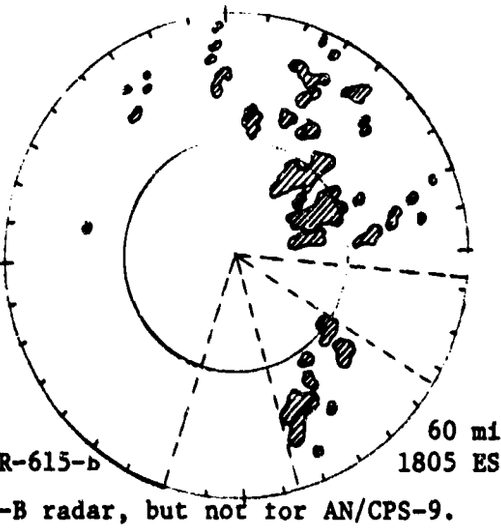

(d) Melting snow in beam of SCR-615-B radar, but not for AN/CPS-9.

Fig. 24. Examples illustrating effects of changes in hydrometeors in low levels of the atmosphere.

Key: R_e = 1 mm hr^{-1} 2 mm hr^{-1} 4 mm hr^{-1} 8 mm hr^{-1}

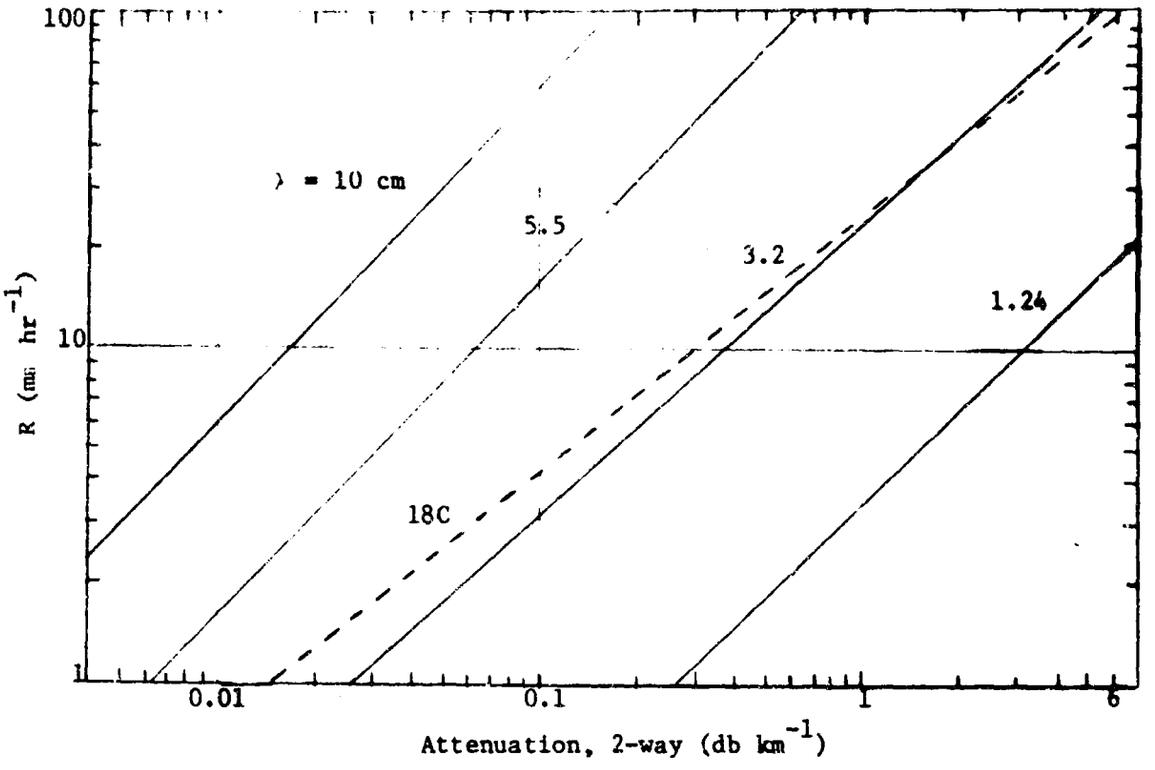

Fig. 25. Empirical values of two-way attenuation as a function of rainfall rate for radiation of various wave lengths. All except the dashed curve are for a temperature of 0C. (From summary in Atlas, 1964).

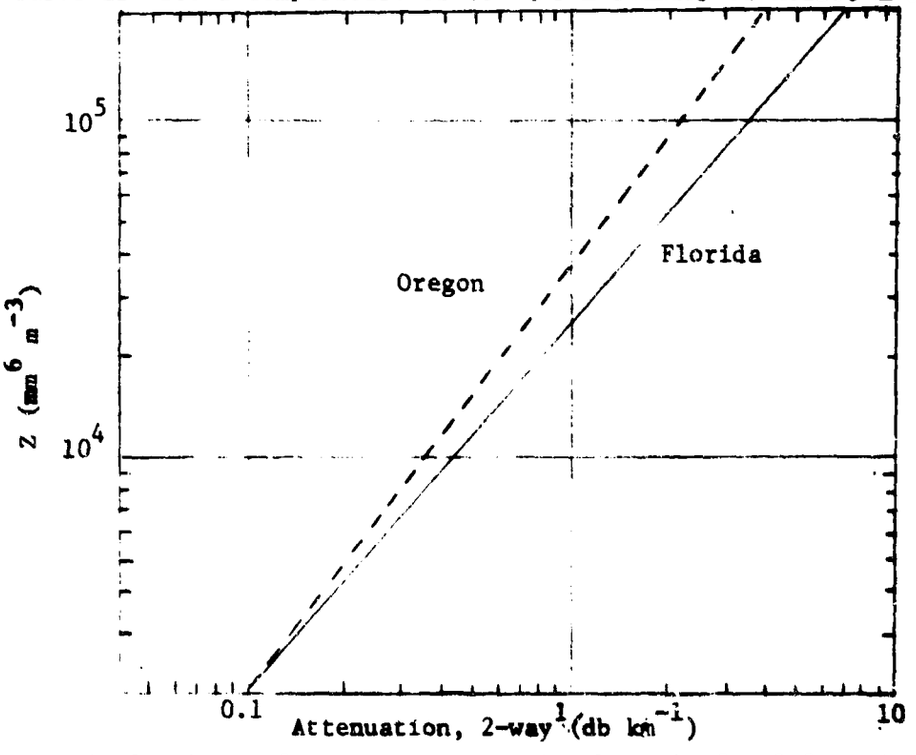

Fig. 26. Empirical values of two-way attenuation by rain for 3.2-cm radiation as a function of reflectivity factor. (From Mueller, 1966).

ever, the layer of melting snow lay just above 8000 ft, and at ranges beyond 30 miles it was within the 3° radar beam and enhanced the echo. On the display, therefore, area A with its rainfall of 2 mm hr^{-1} appears properly, but the lighter rain beyond 30 miles also appears at the same intensity level. The AN/CPS-9 with its narrower beam would not encounter the melting layer within a range of 50 miles.

4. Representativeness in stratiform and convective storms

The examples just presented illustrate how vertical variations in reflectivity may lead to errors in interpreting radar measurements in terms of surface precipitation. No attempt has been made to obtain statistics regarding the magnitude or frequency of occurrence of these effects because they vary widely from storm to storm so that a statistical correction would not be meaningful. In purely convective storms where the reflectivity is fairly constant with height up to 15,000 ft or more, there is unlikely to be any discrepancy between the precipitation viewed by the radar, at least out to ranges of 100 miles or so, and that which reaches the surface. In widespread precipitation, whether or not it contains convective cells, careful analysis of the vertical structure should be made in each storm by examining the RHI at a close range where the resolution is good. Then an estimate can be made of the representativeness of the precipitation sampled by the radar at various ranges. The observations can then be applied only over suitably limited ranges, or perhaps a correction could be devised.

It is obvious that when there are variations in reflectivity with height, the useful range is much more limited for a radar with a relatively broad beam. Also, in the cases shown, the necessity of scanning at an elevation angle of 1°, in order to get the beam above low hills surrounding the site, further shortened the useful range. The WR-66 radar with its narrow beam and elevated location can measure accurately over a much larger area than the SCR-615-B.

F. Effects of Attenuation by Rain

1. Computed values of attenuation

Computations of attenuation of microwaves by rain of various intensities, based on theoretical results by Mie (1908) and empirical drop size distributions of several investigators, have been summarized by Atlas (1964). Values for several wavelengths and temperatures are shown in Fig. 25. It should be remembered that these values are not exact because drop size distributions may vary from one storm to another, but they are sufficiently accurate to provide a good indication concerning the occasions when attenuation would present a serious problem in measuring radar reflectivities in storms. Fig. 26 shows the relation between the radar reflectivity factor Z and attenuation as computed by Mueller (1966).

Few comparisons have been made between computed and observed attenuation at centimeter wavelengths. A fairly long path through the rain is required to cause measurable attenuation, and it is very difficult to observe the exact distribution of rainfall along the entire path length. In early measurements, summarized by Battan (1959), the observed amounts of attenuation were generally somewhat greater than those computed from the rainfall rates. More recent measurements by Tokunago and Tanaha (1964) are in very good agreement with computed amounts; they used fairly short propagation paths and measured the rainfall rate at close spatial intervals.

From the values in Fig. 25, it can be seen that 10 cm radiation would suffer

only 2 db of attenuation when passing through 300 km of 10 mm hr^{-1} rain or through 30 km at 100 mm hr^{-1}. Since such extended areas of heavy rain do not occur, rain attenuation may be considered negligible at this wavelength. At 3 cm, however, 2 db of attenuation could result from 7 km of 10 mm hr^{-1} rain or only 0.3 km at 100 mm hr^{-1}. At this wavelength, therefore, attenuation can significantly affect measurements if moderate or heavy rain occurs along the path of propagation. At wavelengths shorter than 3 cm, rain attenuation would frequently affect quantitative measurements, while at 5.6 cm it would be significant only in very intense storms.

Because of the very low absorptive index of ice, dry snow does not cause appreciable attenuation at any wavelength. Wet snowflakes, on the other hand, attenuate as much as raindrops of equal mass, or perhaps even more if they can be simulated by water-coated ice spheres (Gunn and East, 1954). Also, for any particular precipitation rate, there are many more particles per unit volume of atmosphere in wet snow than in rain, because the raindrops fall more rapidly. Thus the attenuation in melting snow may be four or five times as great as in the rain below it.

2. Observations of attenuation

At M.I.T. attenuation of 3.2 cm radiation has been observed and measured by comparing echo intensities with those measured at 10.7 cm, the latter being unaffected by rain attenuation. The most severe attenuation is observed in thunderstorms, where rainfall rates of 50-100 mm hr^{-1} are not unusual. In rain of this intensity, equivalent Z values of $10^{5.0}$ to $10^{5.5}$ mm^6 m^{-3} are expected and are measured by the 10 cm radar. Figs. 27 and 28 illustrate typical thunderstorm patterns on the PPI and RHI. For these cases, where the storms were relatively simple in structure, computed and measured attenuation have been compared and are in quite good agreement. It may be noted, in Fig. 28b that at 20,000 ft, there is no attenuation, although Z_e values are in excess of $10^{5.0}$. It is apparent that the hydrometeors at that level were composed entirely of ice. At 30,000 ft, there was no attenuation, but the reflectivity measured by the 10 cm radar was consistently high relative to that measured at 3 cm. This effect is a result of the difference in beam widths of the two radars, as the more intense precipitation at lower levels penetrated the broader beam of the SCR-615-B radar.

In a single thunderstorm whose structure is not too complex, the effects of attenuation are to make the maximum reflectivity at levels below 20,000 ft appear much smaller than it actually is (by at least 15 or 20 db) and to indicate the location of intense cores very close to the front edge of the storm. An apparent reflectivity maximum aloft in the vicinity of 20,000 ft, as observed by Donaldson (1961) is also a result of attenuation in the lower portions; aloft where the hydrometeors are composed of ice more realistic reflectivities are indicated. For an entire squall line the pattern on the PPI is usually badly distorted. Since attenuation is greatest in the most intense storms, all the thunderstorm complexes in the squall line are reduced to approximately the same apparent intensity and the most severe ones cannot be identified. An example is the storm of 30 June 1960, Fig. 29. In the 10-cm depiction, four echoes have Z_e values in excess of $10^{5.5}$ mm^6 m^{-3}, and all four were confirmed as hailstorms by observers at the ground. The 3-cm radar indicates Z_e values less than $10^{4.5}$ for these storms; moreover, they do not even appear to be the most intense ones in the squall line.

Significant attenuation occurs in melting snow and in moderate widespread rain as well as in thunderstorms. For example, Fig. 30 shows the power received by both

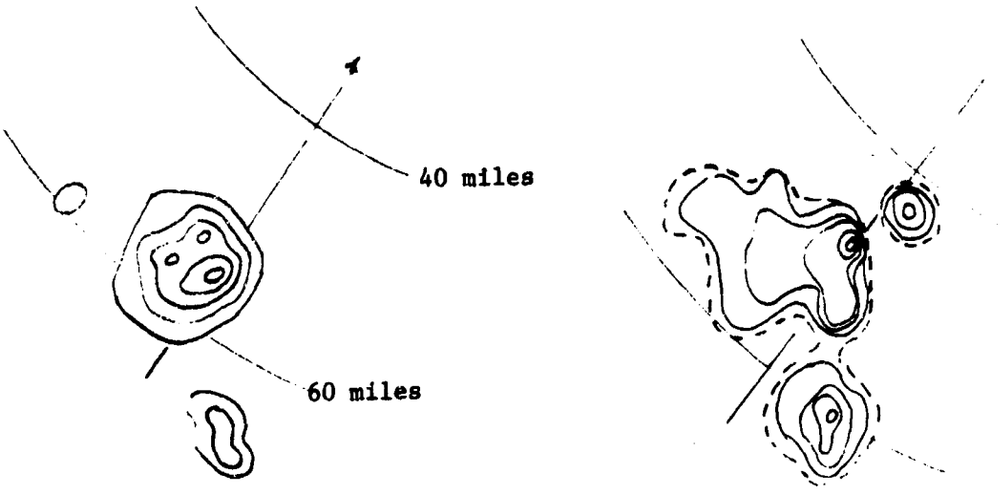

Contours on SCR-615-B
λ= 10.7 cm 1444 EST
Values of log Z_e:
4.0 4.8 5.6
4.4 5.2

Contours on AN/CPS-9
λ= 3.2 cm 1450 EST
Values of log Z_e:
2.0 3.2 4.2
2.7 3.7

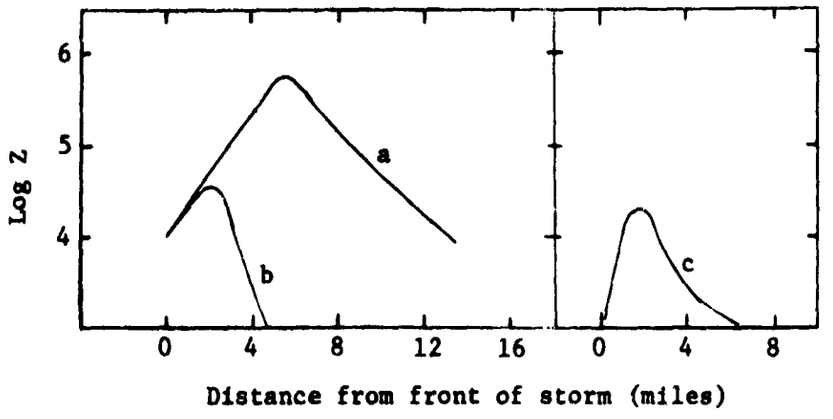

Fig. 27. Comparison of equivalent Z values measured at two wave lengths in thunderstorm on 14 July 1963. In the lower figure, curve a represents intensity profile along indicated radial direction measured at 10.7 cm; curve b is the same profile reduced by computed attenuation of 3.2 cm radiation; curve c is profile observed at 3.2 cm.

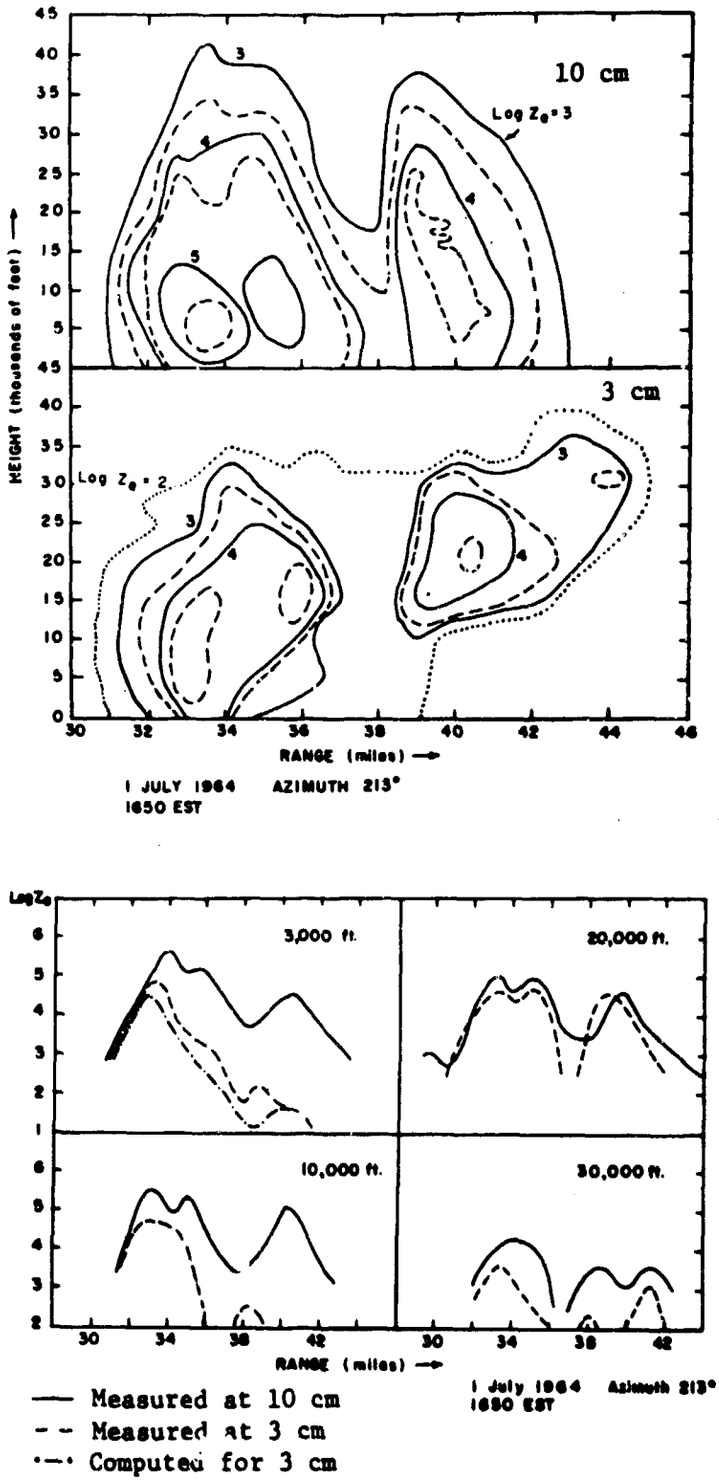

Fig. 28. Comparison of equivalent Z values in a thunderstorm as measured at two wave lengths on the RHI. Lower figure shows intensity profiles at several levels.

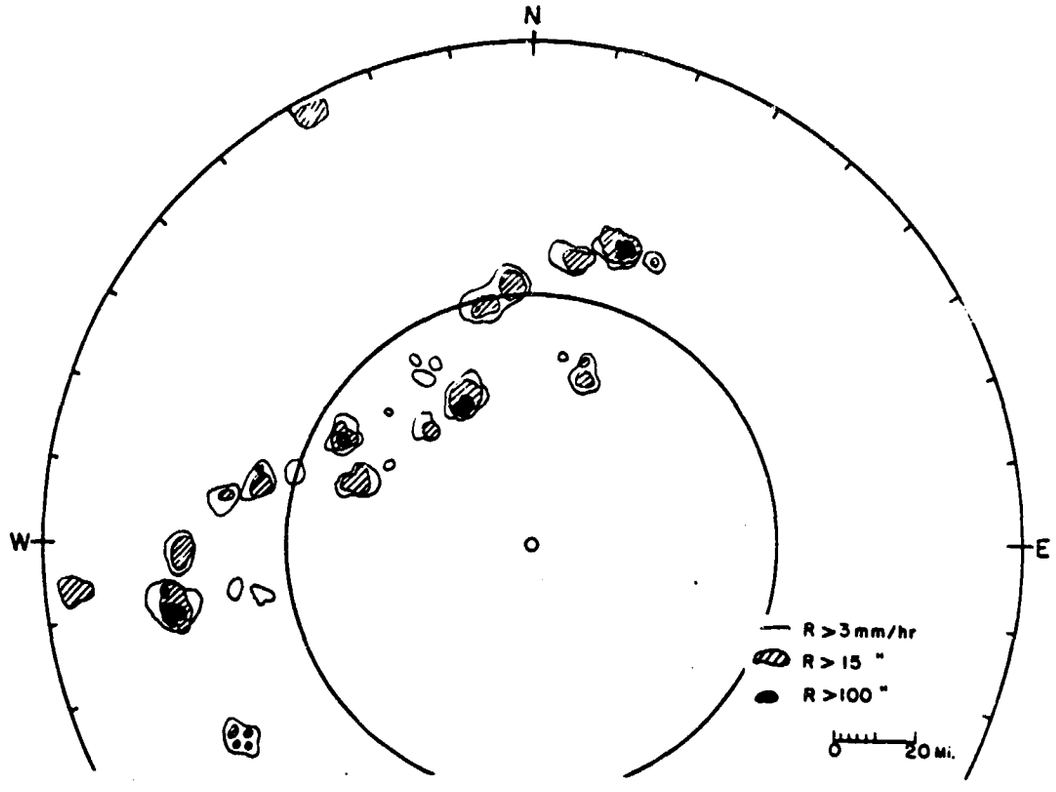

Intensity contours on 10-cm radar (SCR-615-B) 1221-1223 EST

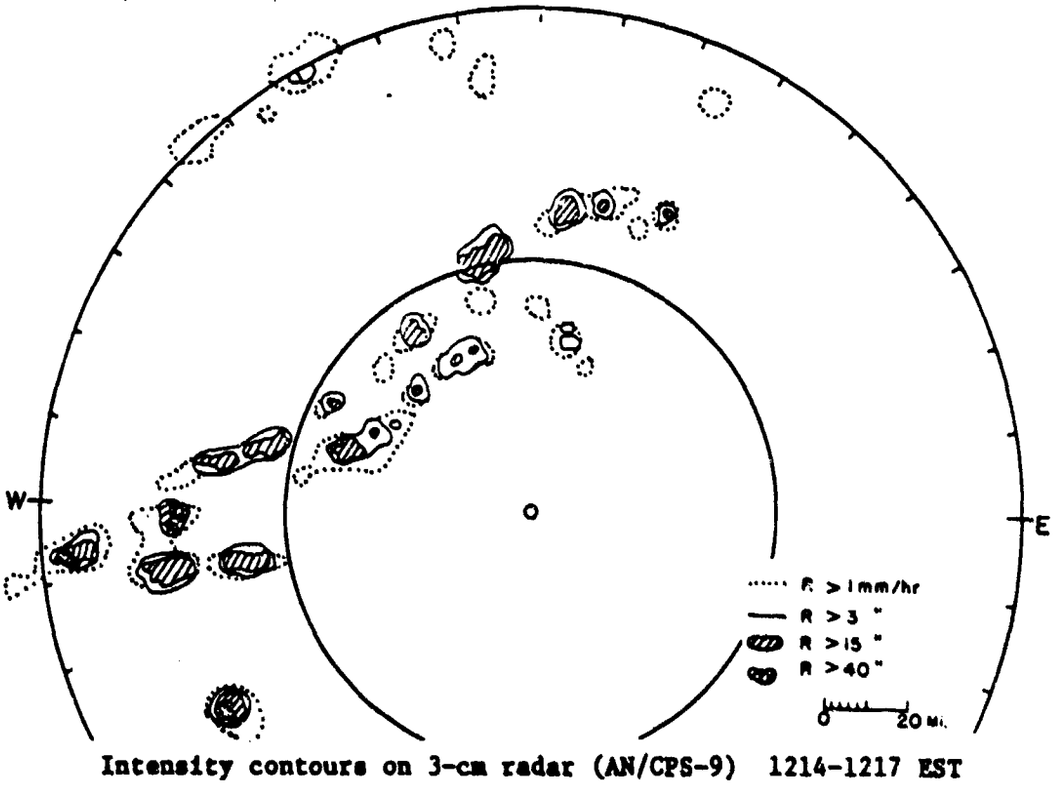

Intensity contours on 3-cm radar (AN/CPS-9) 1214-1217 EST

Fig. 29. Comparison of intensity contours on two radars. Squall line, 30 June 1960.

radars from the atmosphere just above the rain gauges at the field station during observations on 12 March 1962. Also shown is the power predicted from the observed rainfall rate with the assumption $Z = 200\ R^{1.6}$. Agreement between the gauges and the SCR-615-B radar is very good. On the AN/CPS-9, however, sharp drops of signal intensity at 1645 and 1655 EST indicate attenuation of 8 to 10 db as heavy showers passed between the radars and the field station which is at a distance of 17 miles. In this case comparison with computed attenuation is not possible because precipitation rates along the entire propagation path are not known; much of the heavy rain was in the ground clutter.

Attenuation by melting snow is illustrated by the data from 11 January 1963 in Fig. 31. During this storm the melting layer was observed on the RHI to be between 4000 and 5000 ft; at an elevation angle of one degree the center of the beam would be in the melting layer between 35 and 45 miles. At the beginning of the storm, precipitation which averaged 3 mm hr^{-1} was detected by the AN/CPS-9 radar at a range of 90 miles. Actually the beam was intercepting snow above the melting layer at this distance, but the reflectivity appears to be similar to that of rain of the intensity indicated by the gauges, and the storm is easily detected. At 1640, however, precipitation was not observed anywhere beyond the range where the beam passed through the wet snow, although the recording gauges indicate areas of rain fully as intense as that which was detected earlier. In Fig. 31a the signal from 80 miles was 8 db above minimum detectable. If precipitation of similar intensity was not detected at 1640 EST, there was apparently at least 8 db of attenuation. Only a very crude estimate of the expected attenuation can be made from the rain gauge data. For an average rainfall rate of 3 mm hr^{-1}, for example, two-way attenuation in the rain would be approximately 0.1 db $mile^{-1}$ while in the melting layer it would be about five times as great. If the beam travels through 35 miles of rain and 10 miles of melting snow, the total attenuation would be about 8.5 db, sufficient to make echoes from more distant precipitation of similar intensity undetectable.

3. Feasibility of correcting for rain attenuation

Some consideration has been given to the practicality of automatic correction for rain attenuation in observations made at 3 cm. In this procedure observed reflectivities would be continuously increased by a factor appropriate for the integrated attenuation along the path, the attenuation at each point being deduced from the corrected reflectivity values. Such a "bootstrap" operation appears plausible enough, but in practice is limited by the fact that any errors are compounded geometrically.

Computations for the model thunderstorm profile shown in Fig. 32 illustrate how extremely sensitive corrections for attenuation may be. Dashed lines 2 db above and below the assumed actual Z profile represent probable limits of error for good quantitative measurements at 10 cm. The lower full-line curve represents the Z profile depressed by the attenuation computed for a wavelength of 3 cm and integrated along the path of propagation. It, therefore, represents approximately what would be observed by a 3-cm radar; and if there were no error at all in either the measured reflectivity or the assumed relation between reflectivity and attenuation, the actual Z profile could be reconstructed from this curve. The dashed curves marked +1 and +2, however, show the reconstructed curves which would be obtained if the reflectivity were overestimated by 1 or 2 db respectively. In both cases the solution blows up to an infinite value of Z. On the other hand, an underestimate of 2 db (dashed curve marked -2 db) would produce a scarcely perceptible correction to the measured profile. Since there are uncertainties on the

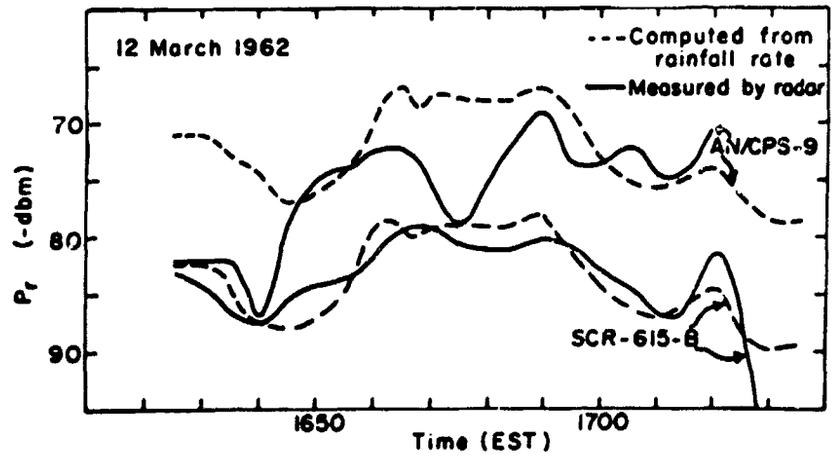

Fig. 30. Attenuation of 3-cm radiation by rain, illustrated by simultaneous radar and rain-gauge observations. Drops in signal on AN/CPS-9 at 1648 and 1655 are caused by heavy showers between radars and gauges.

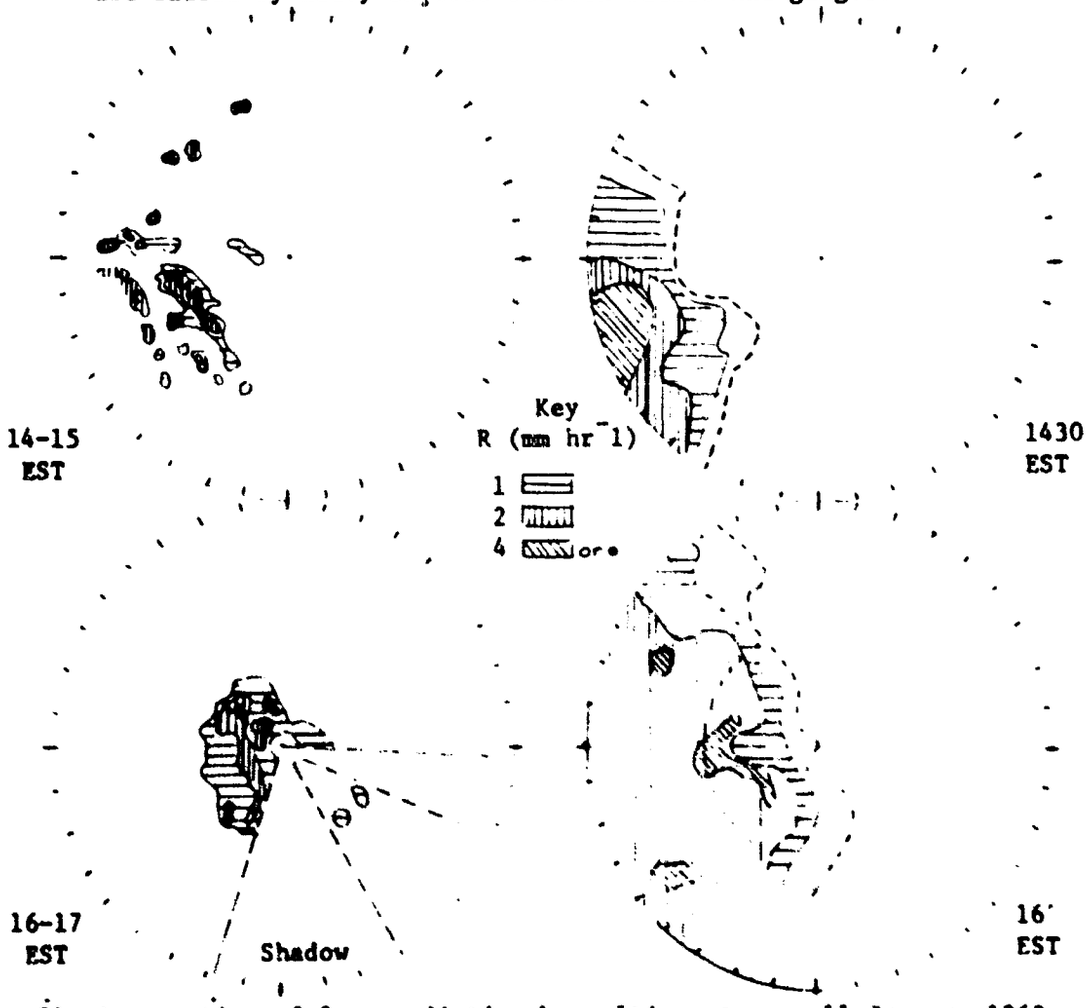

Fig. 31. Attenuation of 3-cm radiation by melting snow on 11 January 1963. Left hand figures show equivalent rainfall rate observed by AN/CPS-9 radar; right-hand figures show isohyets based on hourly amounts from rain-gauge network. Explanation in text. Outside circles: 120-mile range.

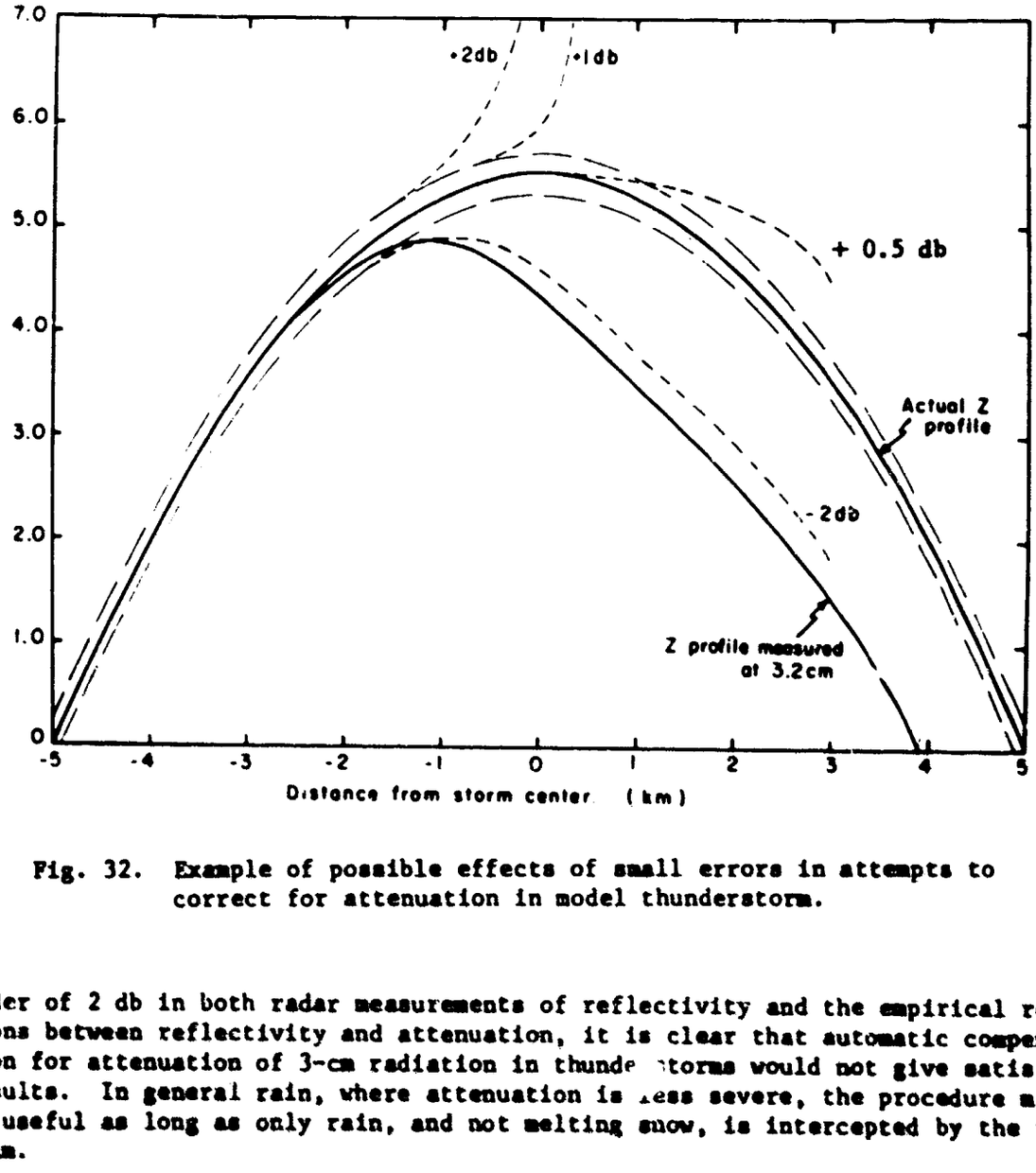

Fig. 32. Example of possible effects of small errors in attempts to correct for attenuation in model thunderstorm.

order of 2 db in both radar measurements of reflectivity and the empirical relations between reflectivity and attenuation, it is clear that automatic compensation for attenuation of 3-cm radiation in thunderstorms would not give satisfactory results. In general rain, where attenuation is less severe, the procedure might be useful as long as only rain, and not melting snow, is intercepted by the radar beam.

4. Frequency of significant attenuation at a wavelength of 3 cm

The observations show that in eastern Massachusetts attenuation on the order of 10 db or more for a wave length of 3 cm is generally encountered in thunderstorms, in winter rainstorms where the melting layer is low, and in moderate to intense cyclonic storms where heavy showers are embedded in widespread rain. For quantitative measurements even 5 db of attenuation would lead to significant error and 10 db would be quite serious. It is clear, therefore, that in this area satisfactory measurements of rainfall by radar cannot be obtained with a wavelength as short as 3 cm because they are seriously affected by attenuation in every type of storm which contains large amounts of rain.

In the tropics where much of the rain falls in very heavy showers a wavelength of 3 cm would be also useless for quantitative measurements.

G. Comparison of Radar and Rain Gauge Measurements

1. At a point

Since a rain gauge is an accurate and satisfactory device for measuring rainfall at any particular point, it is not suggested that a radar be used for this purpose. Nevertheless, comparisons of radar and gauge measurements at a point are useful in making an assessment of the reliability of the radar for measuring rainfall, especially if the point is at a close range so that discrepancies due to differences in the sampled volume are minimized.

Examples of data from a series of measurements made at M.I.T. are in Figs 33 and 34. The radars sample the atmosphere just above the rain gauges, which are at a distance of 17 miles. The received power, $\bar{P}_r$, is compared with the expected power computed from the rainfall rate, with the assumption $Z = 200\ R^{1.6}$, both quantities being plotted as a function of time. In the figures, traces for the rain gauge have been shifted forward in time by a few minutes to bring them into best agreement with the radar records. Since the upper portions of sloping showers are usually ahead of the lower parts, the radars record peak intensities sooner than the gauges.

Curves for equivalent Z computed from the radar signal intensities and from the measured rainfall rate generally parallel each other closely but not exactly, as in the example in Fig 33. Exact agreement should not be expected in view of the differences in respective sampled volumes. At a range of 17 miles and an elevation angle of 1°, and with the horizon at 0.5°, the volume defined by the half-power points and one-half the pulse length is approximately 10^8 m^3 for the SCR-615-B radar and extends vertically from 300 to 1500 meters. The AN/CPS-9 samples 10^7 m^3 between altitudes of 300 and 800 meters. Catch basins of the gauges vary from about one-half to four square meters.

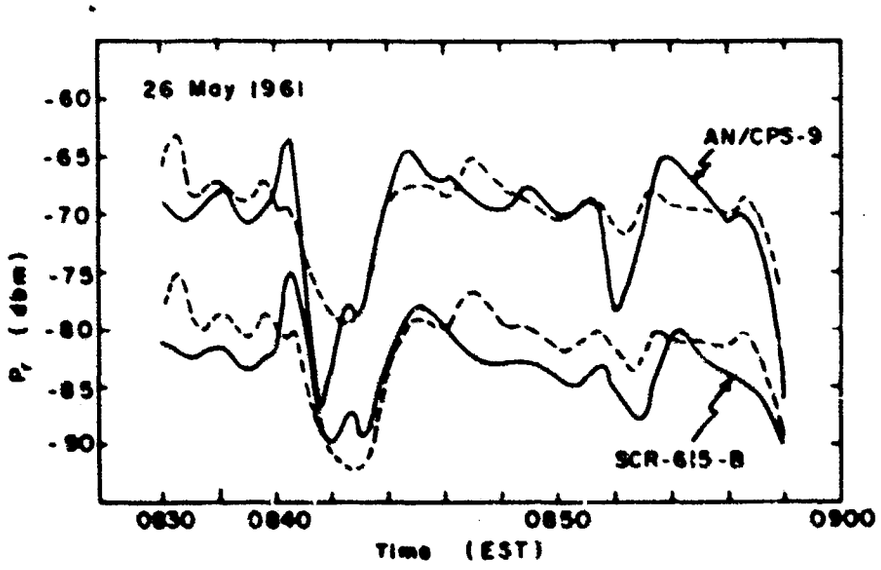

Fig. 33. Example of simultaneous radar and rain gauge observations. Solid lines show power received by the radars from a volume of atmosphere just above the rain gauge. Dashed lines show the power computed from the measured rainfall rate on the assumption that $Z = 200\ R^{1.6}$.

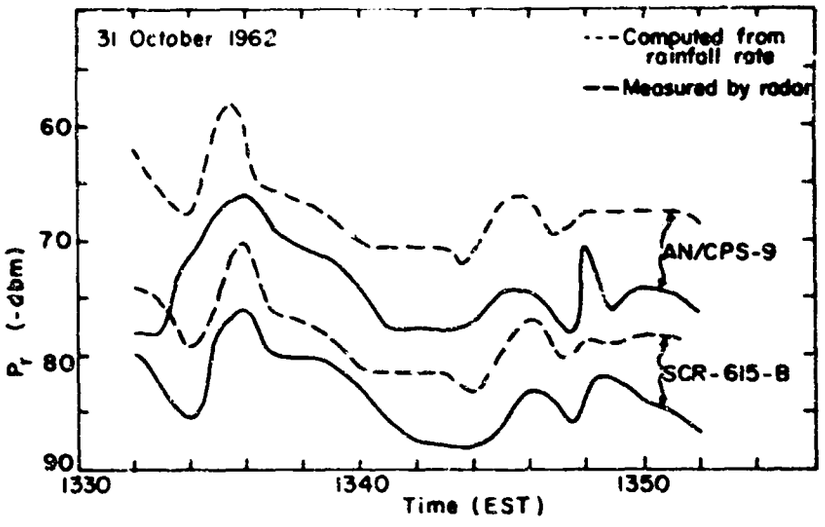

Fig. 34. Same as Fig. 35, in a storm where radar signals were relatively low.

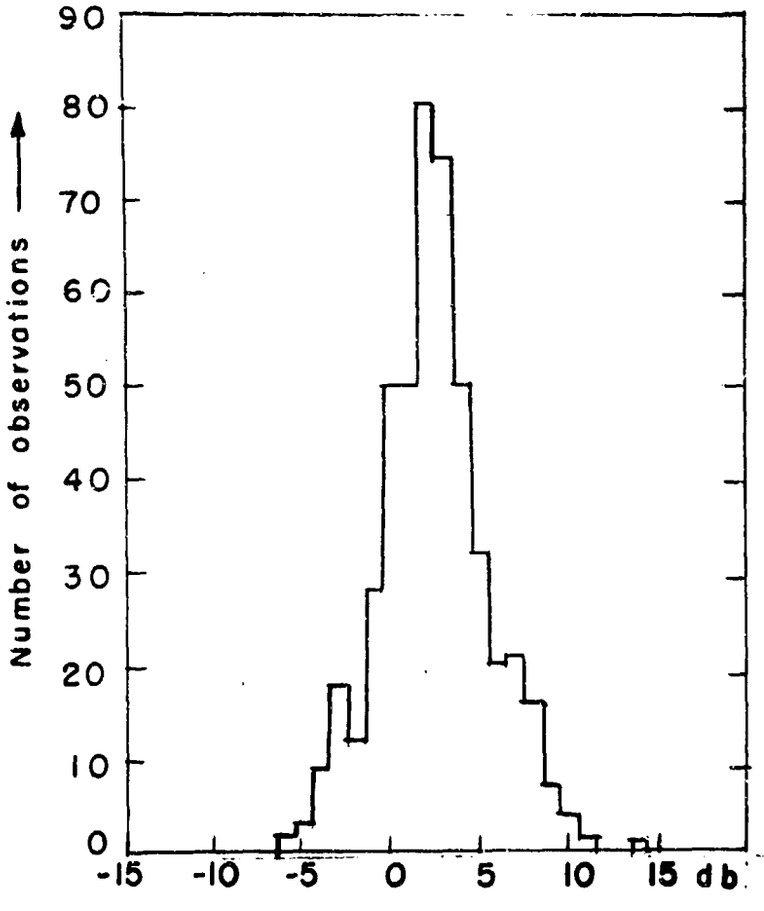

Fig. 35. Summary of differences between Z values computed from the rainfall rate (assuming $Z=200\ R^{1.6}$) and deduced from measured signal intensity on the SCR-615-B radar. Data represent comparisons at one-minute intervals in 6 hours of observations on 12 days. A positive difference indicates that the radar measures low as compared with the rain gauge.

After the time shift, measured and computed values are compared at one-minute intervals. Results of 380 points, representing six hours of data on twelve days during 1961-1963 are in Fig. 35. Data from the SCR-615-B are used for this comparison because, as pointed out in Section IIC, the AN/CPS-9 signal is sometimes depressed by attenuation. It was shown in that section, however, that in the absence of attenuation the two radars agree within 1 db.

The spread of values about the peak is due to differences in the sampled volumes and perhaps to variations in drop size distributions. The discrepancy in the position of the peak (at 2.5 db rather than zero) may be ascribed to errors in determining the radar parameters, to improper choice of empirical Z-R relation, or to occasions when there is significant drop growth in the lowest few hundred feet of the atmosphere. It is not possible to assess the precise contribution of each factor to the total discrepancy, but it has been shown that the calibration errors appear to be only about 1 db. The remaining 1 to 2 db are probably associated with storms of the type shown in Fig. 34. In these storms the radars are in agreement with each other, but indicate rainfall rates less than half as large as those measured by the gauges. About one third of the storms in the group were of this type, and in all of them the surface reports gave evidence of conditions suitable for low-level growth of raindrops by accretion. Since the discrepancy is so large (6 to 8 db), it is probably due to a combination of exceptionally small drops and a significant increase in precipitation rate below the region sampled by the radars.

In some earlier measurements made at M.I.T. (Austin and Williams, 1951) and some more recent ones in France (Dumoulin and Cogombles, 1966) the radar signals were very low (5 db and 11 db respectively) as compared with the expected values. It is probable that these large discrepancies were caused by an undetected power loss in the system, a result which emphasizes the importance of reliable calibration and monitoring of the radars.

For several reasons it does not seem desirable to use the results just described to derive a correction to be applied to all data from the particular radar at its given location, in this case a correction of +2.5 db for Z_e and 1.5 db for R_e, even if the sample were larger and the statistics thereby more reliable. In the first place, the storms appear to fall into two distinct groups; and for one of them, the majority of the storms in fact, there seems to be no consistent discrepancy beyond a probable error of only 1 db in the calibration. In the second place, it is not clear how much of the relatively large discrepancy for the storms in the smaller group is range dependent and therefore should not be applied equally over the entire area under observation. It is recommended, rather, that the storms where the discrepancies are found be studied more carefully, so that they can be identified and better understood. Then appropriate corrections can be applied selectively instead of statistically. Observations with the WR-66 and the Joss raindrop spectrometer are expected to clarify this question. Since most of the storms have very complex structure, as described in section IIIB, the rather ambiguous designations of "showers" and "continuous rain" which have been suggested for stratifying Z-R relations cannot definitively separate the two groups of storms found in this study.

2. Areal rainfall amounts

Because of the many factors which affect them, measurements of areal depths whether made by gauges or by radar, are accompanied by uncertainties which are usually large and also vary considerably from one situation to another. Hence

the results of experiments in which the two types of observations are compared are likely to be inconsistent or at least indeterminate. A summary of experiments reported by other observers will not be included here because the conditions under which they were performed vary considerably and they do not lend themselves to any meaningful generalizations. In some cases techniques for averaging and calibrating the radar signal were inadequate so that there were uncertainties of 5 to 10 db in the measured values of reflectivity; sometimes a short wave length (3.2 cm) was used in heavy rain so that the measurements were distorted by large and unknown amounts of attenuation. Some observers noted a deterioration in agreement between radar and gauges as the range increased, but did not specifically consider the problem of representativeness of the precipition sampled by the radar with respect to that reaching the surface. In some experiments the gauges were too widely separated to provide adequate sampling. It is not surprising, therefore, that in most of the comparisons agreement is poor, and the inference is often made that radar measurements of precipitation are not satisfactory. It should be noted, however, that in the one experiment where accurate radar data, a dense network of gauges, and convective precipitation were all combined (McCallister, Teague, and Vicroy, 1966) the agreement was excellent as shown by the depth-area comparison in Table 3.

Table 3: Comparison of depth-area measurements by radar and rain-gauge network, for storm of 8-9 February 1966, in Texas and Oklahoma (from McCallister et al, 1966)

	Observed Rainfall	Radar Rainfall
1 inch	12,100 sq. miles	13,500 sq. miles
2 inches	6,000 sq. miles	8,300 sq. miles
3 inches	3,800 sq. miles	4,300 sq. miles
4 inches	1,950 sq. miles	1,500 sq. miles
5 inches	400 sq. miles	350 sq. miles
6 inches	22 sq. miles	20 sq. miles

At M.I.T. we have not made observations or performed experiments specifically designed to compare areal depths of precipitation as measured by radar and rain gauges. It seemed that more would be learned by examining the various aspects of the problem individually than by accumulating statistics wherein uncertainties due to different effects are mixed in varying amounts. Some comparisons have been made, however, and they are illuminating in pointing up the different problems associated with various storm types. The radar reflectivity is measured with an accuracy of about 2 db, but the network of gauges in the area is not particularly dense. Recording gauges, from which hourly precipitation amounts are published by the U.S. Weather Bureau average about one gauge per 1000 km^2; the network from which daily amounts are reported in the Climatological Summaries is about six times as dense.

Fig. 36 shows a comparison in which radar digital maps were integrated over the entire day so that the relatively dense network of gauges reporting daily precipitation amounts could be used. The radar data were sampled every ten minutes at grid points separated by five miles. The equivalent rainfall rate assigned to each intensity level was halfway between the threshold values for the levels. Maps showing selected radar data contain measurements only from points which have rain gauges within the 5 x 5 mile squares which they represent. For 16 May 1961, when a mesoscale rain area (about 30 miles in dimension) moved from southwest to northeast across the grid, agreement is good. On 10 July 1961, when small intense

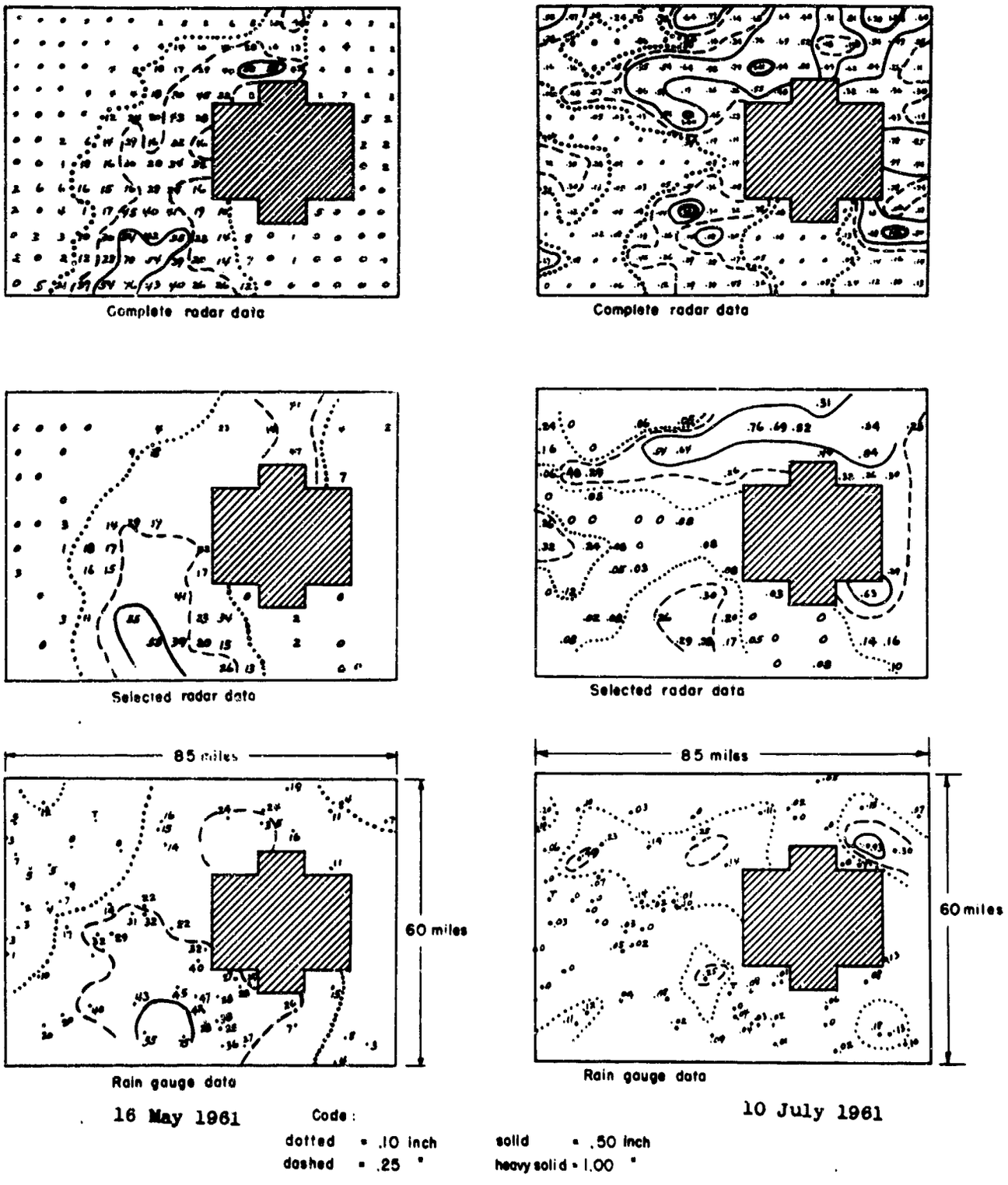

Fig. 36. Comparison of daily rainfall amounts measured by radar and by rain gauge network. Shaded areas cover radar ground clutter.

air mass showers occurred, agreement is good at points where rain gauges are located, but several small areas of intense rain which were observed by the radar missed the gauges entirely. For both storms, the isohyetal maps from the selected radar data are in better agreement with those from the rain-gauge network, but it is obvious that the complete radar data provide more realistic information. On both days the precipitation was primarily convective and the SCR-615-B radar was used.

For the analysis of mesoscale precipitation patterns and their relation to the larger-scale circulations, which is presented in section IIIA of this report, all radar data from storms during 1962 and 1963 were reduced to digital maps with a grid of 5 x 5 mile squares. Equivalent rainfall rates were assigned to each intensity level based on the relations $Z = 200\ R^{1.6}$ for rain and $Z = 1000\ R^{1.6}$ for snow. The latter relation was used for snow because it differs by only a few decibels from the suggested empirical one, $Z = 2000\ R^{2.0}$, and has the advantage of greatly simplifying the data processing. From these digital maps areal rates could be readily obtained by averaging the rates for individual squares over any desired area.

For the same mesoscale study areal amounts were computed from the hourly precipitation data for an area of 1.5×10^4 mi^2 within an 80-mile range of the radar site. Within this area there are 37 recording gauges but they are not uniformly spaced. A computer program weighted the amount reported by each gauge according to the area it represented and computed the number of cubic meters of water which fell on the entire area during each hour. Typical comparisons of areal amounts over 1.5×10^4 mi^2 for various types of storms are in Fig. 37.

(a) Intense thunderstorms. On 31 May 1962 a squall line moved through the region. Equivalent rainfall rates up to 100 mm hr^{-1} were observed and also some hail. The radar and gauges are in good agreement regarding the total precipitation for the whole storm but show considerable variance in the hourly amounts. In this type of storm the radar probably gives the more accurate information. If an intense thunderstorm complex moves between gauges the rain-gauge network underestimates the total rainfall; if a strong core moves directly over a gauge, it is weighted by too large an area and the amount of rain is overestimated.

(b) Strong convective showers surrounded by general rain. On 12 September 1963 showers with peak rainfall rates up to about 60 mm hr^{-1} surrounded by widespread light rain accompanied the passage of a cold front. In this type of storm the radars tend to underestimate the total precipitation. The SCR-615-B fails to detect the light rain and records only the showers. The 3-cm radiation of the AN/CPS-9 is attenuated in the heavy showers and therefore records less rainfall. In this type of storm, the WR-66 with its long wave length and high sensitivity should provide very satisfactory measurements.

(c) Intense cyclonic storms. Intense coastal cyclones or those which move up overland but bring large amounts of moist tropical air are often accompanied by a great deal of rain. Groups of fairly intense showers are embedded in widespread rain, and the precipitation may continue for several days. These storms generally contain relatively small drops and there is appreciable low-level accretion, so that even at a range as short as 17 miles the radars seriously underestimate the rainfall rate, as illustrated in Fig. 34. Over a large area the underestimate is severe, as shown by the comparison for 5 October 1962 in Fig. 37. The general light rain is missed altogether by both radars, except at extremely

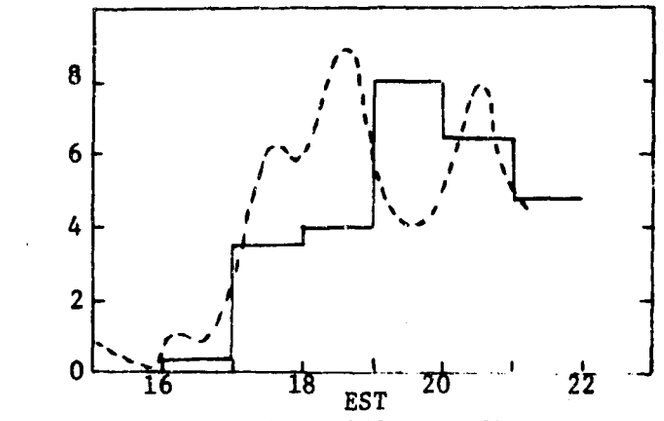

a. 31 May 1962 SCR-615-B

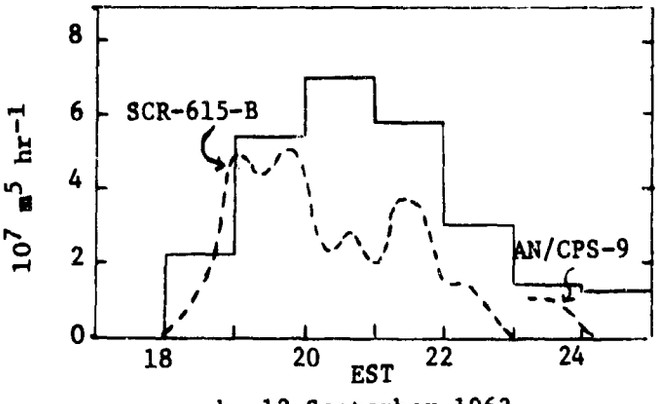

b. 12 September 1963

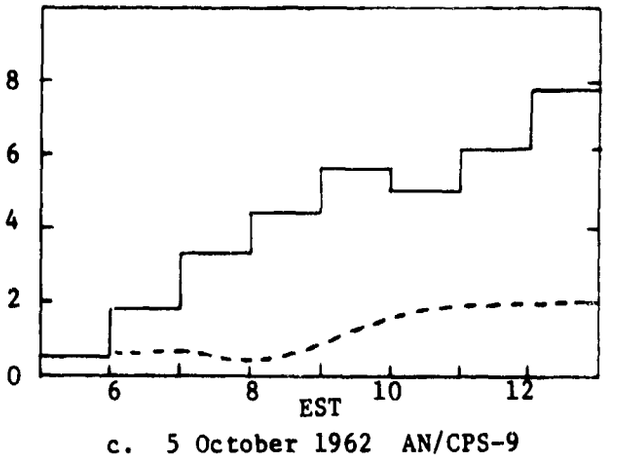

c. 5 October 1962 AN/CPS-9

Fig. 37. Areal rainfall rates indicated by radar (dashed line) and gauge network (solid line) for various storm types. Units are 10^7 m^3 hr^{-1} for an area of 4 x 10^4 km^2 surrounding Cambridge.

short ranges on the AN/CPS-9, and the showers which they do detect appear to be only one-third or one-half as intense as they actually are. The AN/CPS-9 signals are further reduced by attenuation. The radars are very useful for providing information regarding the structure of these important storms, but clearly are not adequate for measuring rainfall amounts in them, unless special techniques can be devised to identify such storms and to process the data in a manner which is appropriate for them.

(d) Snowstorms. Snow is rarely detected as far as 80 miles, so that in a comparison over such a large area the radars would tend to underestimate the total amount. Even over smaller areas, the results are inconsistent, since there is no well-established Z-R relation for snow and there may be considerable differences between the snow sampled by the radar and that which reaches the surface.

H. Summary and Conclusions

There are two assumptions frequently made by people concerned with the problem of measuring precipitation by radar which have confused the question rather than clarifying it. The first assumption is that if there are discrepancies between radar and rain-gauge observations, then the radar measurements are in error. Admittedly, there is very little uncertainty regarding the amount of water which falls into the catch basin of a gauge; but discrepancies between the two types of measurements may well arise from small-scale variability in the storm and differences in the volumes which are sampled rather than from errors associated with either instrument. Moreover, when observations are applied over an area, there may be large errors in the gauge measurements because of sampling inadequacy.

The second misleading assumption is that the empirical relation between radar reflectivity and precipitation rate is the overwhelmingly predominant source of uncertainty in radar measurements of precipitation. This attitude has arisen because this particular uncertainty is inherent in the storms and therefore may represent the ultimate limitation in accuracy. However, because of the tendency to identify problems of radar measurements of rainfall with evaluation of the Z-R relation, other important aspects have failed to receive proper attention.

In this report we have considered four sources of uncertainty, none of which is either definitely predominant or clearly negligible: (1) methods of signal averaging; (2) radar calibration; (3) Z-R relation; and (4) differences in the precipitation sampled by the radar and that reaching the surface. The first two are mainly instrumental and can be controlled and evaluated more readily than the others. But they have not always been properly recognized in experiments presented in the literature. On more than one occasion, in fact, experimental results have been interpreted in terms of Z-R relationships when the radar instrumentation and techniques employed were such that there could easily have been errors as large as 10 db in the measured values of average signal intensity and radar reflectivity.

In theory, average signal intensity can be obtained to any desired degree of accuracy simply by averaging the signal from the same volume of precipitation over a sufficiently long period of time. For observations over an area, however, a practical limit is set by the need to scan with the antenna and by the time variability in the storm structure as small precipitation areas build, move and dissipate. In practice, an average of about thirty independent samples can be achieved. The standard deviation for such averages is 1 db, so that they are accurate within

2 db ninety-five per cent of the time. Instrumentation for signal averaging has been developed at M.I.T. and is described in section II, B, 4. It operates digitally, is built of solid state components and is suitable for adaptation to routine field and operational use.

Calibration of the radar consists of measuring the various quantities which enter into the equation relating average signal power to radar reflectivity. Most of these parameters can be measured easily with an accuracy of a few tenths of a decibel or better. The antenna gain and the effective solid angle in the beam, however, are not so easy to measure accurately and they may differ appreciably from their theoretical values. Direct measurements of these quantities have been made for the radars at M.I.T. and the overall accuracy is estimated to be better than 2 db; comparison of simultaneous measurements on two radars support this estimate since they differ by only 1 db. It should be pointed out that the calibration error cannot be reduced indefinitely by making more careful measurements of the parameters. Since the power tapers off at the edges of the beam and into the side lobes, a somewhat arbitrary decision must be made as to what axial angle is considered to be the edge of the beam; moreover, the error involved depends on the storm structure as well as the power pattern in the beam.

The Z-R relation has received considerable attention and it has been shown that the most suitable empirical relations differ for different geographical locations (Stout and Mueller, 1968). Differences are usually less than a factor of two, but in extreme cases may be as much as a factor of five in the rainfall rate associated with a given value of reflectivity. For given geographical locations the standard error due to variations in drop size was computed by Mueller and Sims (1966) to be between 1.4 and 1.9 db in rainfall rate, so that the 90 per cent confidence limits are approximately a factor of two. Observations at M.I.T. suggest that in New England the variations are not entirely random but that certain storms have exceptionally small drops. Identification of such storms and grouping them separately should improve the accuracy of the empirical Z-R relation.

Errors due to differences in the precipitation sampled by the radar and that reaching the surface can be caused by evaporation, accretion, or melting snow in the lowest layers of the atmosphere. These errors are slight for thunderstorms or intense convective showers; but for widespread rain, especially in winter, or snowstorms they can be appreciable, as large as 5 db in reflectivity in the vicinity of 30 miles and increasing progressively with range. The effect of such errors is to severely limit the range to which accurate measurements can be made, and they are especially pronounced if the radar has a broad beam.

Both computations and observations have clearly demonstrated that satisfactory measurements of surface precipitation cannot be made with a wave length as short as 3 cm because of attenuation in heavy rain and melting snow. It is recognized that advantages of high resolution and sensitivity are more easily obtained with a short wave length, but they can hardly be considered advantages if frequently large and always unknown amounts of attenuation render the resulting data practically meaningless.

In brief, for storms which are primarily convective, a properly instrumented and calibrated 10-cm radar can measure surface precipitation rate with an accuracy of 2 to 3 db (50-100%) out to ranges on the order of 100 miles. For areal amounts, the information from the radar is considerably better than can be obtained from a network of gauges, except for a very small area with an extremely dense network.

In fact, because of the difficulty of sampling representatively, it is unlikely that gauges would even provide useful supplementary information unless there is a very dense mesonetwork of gauges in the region under observation. For widespread storms, on the other hand, radar measurements must be interpreted with a great deal of caution. The vertical structure of every storm should be scrutinized and the radar data supplemented by whatever gauge information is available. It is strongly recommended that in the tropics and other regions where the rainfall is primarily convective, 10-cm radars be installed and instrumented for rainfall measurements. It seems very doubtful that satisfactory measurements of the precipitation can be obtained by any other means.

At the present time radar weather information is presented in the form of maps showing the instantaneous distribution of equivalent rainfall rate. To further reduce it to a form suitable for hydrological uses or other immediate applications requires a rapid and expensive recording device and immediate access to a large digital computer. A data processor specifically designed to handle weather radar data has been designed and is being built at M.I.T. The description is in section II, B, 5. This device is sufficiently modest to be part of the instrumentation for an operational weather radar, yet it is capable of handling the large amounts of data without degradation in quality or resolution.

III. ANALYSES OF SMALL-SCALE PRECIPITATION PATTERNS

A. Mesoscale Precipitation Patterns in New England and Their Relation to Larger-Scale Parameters

1. Description of data and methods of analysis

Radar observations have shown that most storms have a great deal of small-scale structure, but attempts to classify or even describe the patterns have not been very successful. In the early days part of the difficulty lay in the fact that data were qualitative and the appearance of the echoes depended greatly on the characteristics of the radar as well as those of the storm. During the last decade we have been obtaining quantitative radar records, so that it should be possible to deduce statistics regarding frequency of occurrence, dimensions and duration of precipitation areas of various intensities. Such statistics would not be meaningful, however, unless the survey included a large and representative sample of all types of storms which occur in this region. Nor would they be meaningful unless the storms were stratified and weighted appropriately because some storms deposit very large amounts of precipitation while others are relatively insignificant. Also, it does not seem desirable to lump together such diverse types as, say, air mass thunderstorms and the widespread snow from a winter "northeaster". It was decided to use a two-year sample, and the years 1962 and 1963 were selected because good radar coverage was available in most storms, and they were prior to the unusual drought in New England during the middle 1960's. All precipitation within an area of 15,000 square miles would be included in the study. For the radar data, the area is a circle with radius of 80 miles, since beyond this range quantitative measurements are somewhat uncertain even for convective storms. The region within 15 miles is excluded because of ground clutter and the southeast quadrant is also excluded because of numerous shadows cast by nearby buildings.

Identification of storms and computations of the amount of rainfall associated with each were based on Hourly Precipitation Amounts for New England published by the U.S. Weather Bureau. There are 69 recording gauges within a range of 120 miles (the range of the radar PPI) and 37 within the 80-mile circle. For the gauge data the eastern quadrant, over the ocean, is omitted. Maps were plotted showing the distribution of rainfall for each hour and for each day when rain occurred within 120 miles. Also, the number of cubic meters of water which fell within a range of 80 miles was computed for each hour and each entire storm. Since the gauges are not uniformly spaced, the amount recorded by each was weighted by the area it represents. A situation was deemed a storm if any one of three conditions was fulfilled: (1) 10 or more of the 69 gauges reported some precipitation and at least one had a 24-hour total of 0.2 inch or more; (2) 20 or more gauges reported some precipitation and at least one had a 24-hour total of 0.1 inch; (3) 30 or more gauges reported with at least one 24-hour total of 0.05 inch. If as much as two hours elapsed with none of the gauges recording precipitation, any subsequent precipitation was considered to be a new storm. To the storms selected on the basis of the rain-gauge reports a few were added where the SCR-615-B radar observed thunderstorms which passed between the surface gauges and one where light rain observed by the AN/CPS-9 radar apparently evaporated before it reached the surface. The total number of storms for the two years was 188.

Macroscale classification of the storms was based on surface synoptic maps and is discussed in the following section. In addition, divergence of air and moisture for layers one kilometer in depth and the associated large-scale vertical velocities and condensation rates were computed from radiosonde data from the

three nearest stations. The triangle defined by these stations is also 15,000 square miles in area.

Mesoscale storm patterns were deduced from the radar data which was available for 115 storms during the two years. PPI displays at 10 minute intervals were reduced to digital maps with a grid of 5 x 5 mile squares. Equivalent rainfall rates were assigned to each intensity level based on the relations $Z = 200\ R^{1.6}$ for rain and $Z = 1000\ R^{1.6}$ for dry snow. Since the interval of 5 db for each intensity level corresponds to a factor of two in equivalent rainfall rate, assigned values of R_e were 0.5, 1, 2, 4 ... mm hr^{-1}. The digital maps show at a glance the mesoscale patterns in the horizontal, but not the cellular structure because the grid squares are too coarse to resolve individual convective elements. Areal precipitation rates as indicated by the radar were obtained by averaging the rates in the individual squares.

Cellular structure and vertical variations in reflectivity are considered to be microscale features. These were investigated from the RHI displays.

The plan of the survey was to make separate groupings of all storms according to macroscale type, mesoscale pattern and cellular structure and then to determine the extent to which the same storms tended to be grouped together in all cases. This would provide an indication as to whether certain mesoscale or microscale characteristics tend to be associated with specific types of synoptic-scale events.

2. Macroscale analysis

The storms were divided into seven types on the basis of large scale features, the grouping being determined by the position and history of the low pressure center or front with which the precipitation was associated. Brief descriptions and designations for the groups are as follows:

1. Low pressure center moves up the Atlantic Coast, generally in a north-easterly direction (coastal low, CL).

2. Low pressure center moves in an easterly or northeasterly direction from the Great Lakes area (designated GL). These cyclones may have developed further to the west or southwest, but they come from the Great Lakes as they approach New England.

3. As a cyclonic center approaches from the Great Lakes, a secondary forms off the coast and becomes an equally dominant feature of the map (overland low with coastal, OL + CL).

4. Low pressure center approaches New England overland from a southwesterly direction (SW).

5. Passage of a cold front (CF).

6. A stationary front is in the area, and a wave forms on it producing precipitation (SFW).

7. Air mass precipitation (AM). There are no cyclones nor fronts in the region.

A storm was classified as frontal only when the primary low with which the front was associated was many hundreds of miles away. If, for example, a Great

Lakes low passes to the north of New England, the observed precipitation may well be associated with a cold or occluded front. Such a storm would, however, be classified as GL. In order that such effects might also be taken into account, the position of each low pressure center at the time of heaviest precipitation has been recorded. It is believed that the emphasis on positions and paths of low pressure centers rather than on fronts, especially warm fronts and occluded fronts, has reduced the subjectivity of the grouping to a minimum. It is recognized that the upper-air features of the large-scale circulations very probably influence the precipitation patterns. The macroscale grouping was based on surface features only for the sake of simplicity. Certainly as a better understanding is gained of the interdependence of circulations on the various scales, the upper-air characteristics should be included in the analysis.

The following quantities were computed and tabulated for the individual storms in each macroscale group and also for each group as a whole:

1. Total amount of water deposited in the area within 80 miles of Cambridge.
2. Spatial distribution within this region on the basis of four equal-area subsections.
3. Duration of entire storm.
4. Period of heaviest precipitation.
5. Maximum hourly amount for the entire area.

Results concerning the amount of precipitation associated with the various storm types are in Tables 4 and 5 and in Fig. 38. It can be seen that if the two selected years are reasonably representative, the storm types which occur most frequently are waves on stationary fronts and cyclones from the Great Lakes area. Neither of these types, however, tend to have large areal precipitation rates, and the coastal lows are the storms which actually deposit the largest amounts of water. Individual storms with unusually large hourly rates and total amounts are often in the SW group, but these storms are not nearly as frequent as the coastal lows. It is interesting to note from Fig. 38 that while most of the storms deposit less than 5×10^8 m^3 of water in the area under consideration, there were eight storms during the two years which deposited more than 1.5×10^9 m^3, and these eight storms accounted for 26 per cent of the total precipitation. Six of these intense storms were in the CL and SW groups. The importance of relatively few deep extratropical cyclones to the entire precipitation regime suggests that they should be studied in considerable detail.

Time variations of hourly areal amounts were plotted for all of the storms, as in Fig. 39. In 153 of the storms the variation was similar to that for 23-24 November 1963 where areal amounts increase more or less steadily to a peak and then drop off. There might be one or more very minor secondary peaks preceding or following the time of maximum areal intensity by periods of roughly 4 to 6 hours. In 25 storms there were two distinct peaks as on 19-20 January 1963; times between the peaks varied from 3 to 20 hours, but 4 to 5 hours was by far the most common. Ten storms had three or more peaks. A summary according to groups is in Table 6; the air mass and OL + CL storms appear to be the most prone to multiple peaks. The times of day when peaks occurred were tabulated in order to investigate possible diurnal effects. No significant ones were found except for a late afternoon peak in cold front and air mass storms, reflecting the period of maximum thunderstorm activity.

Spatial variations in precipitation amounts were explored by dividing the area

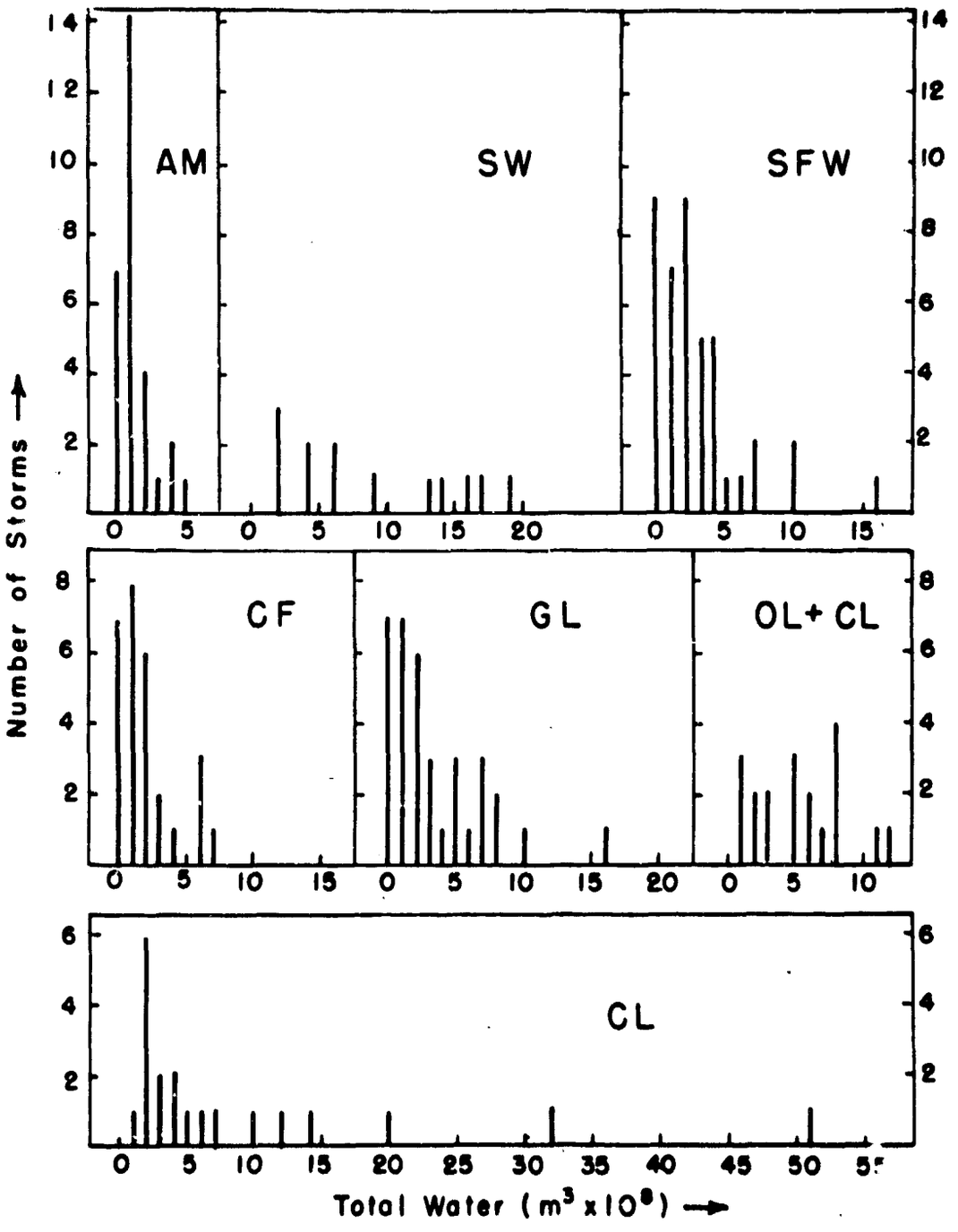

Fig. 38. Distributions of total water in the various macroscale storm groups.

Table 4. Distribution of precipitation in various groups.

Storm Type		CL	GL	OL+CL	SW	SFW	CF	AM	Total
Number of storms	1962	13	17	9	6	16	12	17	90
	1963	8	18	10	7	26	17	12	98
	Total	21	35	19	13	42	29	29	188
	Per Cent	11	19	10	7	22	15	15	
Total water deposited in area ($m^3 \times 10^8$)*	1962	115	44	53	67	62	23	21	386
	1963	68	64	48	46	57	33	11	327
	Total	183	108	101	113	119	56	32	713
	Per Cent	26	15	14	16	17	8	4	
Duration (hours)	1962	369	269	207	190	379	117	252	1783
	1963	285	364	224	159	481	194	154	1861
	Total	654	633	431	349	860	311	406	3644
	Per Cent	18	17	12	10	24	9	11	

Table 5. Distribution of mesoscale quantities within each macroscale group.

	Group	CL	GL	OL+CL	SW	SFW	CF	AM
Number of storms		21	35	19	13	42	29	29
Total water: ($m^3 \times 10^8$)*	Mean	8.7	3.1	5.4	8.7	2.8	1.9	1.7
	Median	4.2	1.9	5.4	6.1	2.1	1.2	0.7
	Mode	1.5	0.2	-	-	0.4	0.4	0.6
	Range	1-51	0.2-16	0.5-12	2-19	0.1-16	0.1-7	0.1-5
Duration: (hours)	Mean	31	28	23	27	20	11	14
	Median	23	14	22	29	18	10	11
	Mode	22	14	16	-	19	9	11
	Range	8-93	5-47	11-38	14-42	6-65	5-18	5-45
Maximum hourly amt. ($m^3 \times 10^7$)	Mean	6.6	4.3	6.5	10.9	3.8	5.0	2.4
	Median	5	4	5	8	3	3	2
	Mode	3	2-5	3	5	1-3	1	1
	Range	1-17	1-13	1-16	4-24	1-20	1-17	1-8

*10^8 m^3 of water on the total area (4×10^{10} m^2) corresponds to an average depth of 2.5 mm or 0.1 inch.

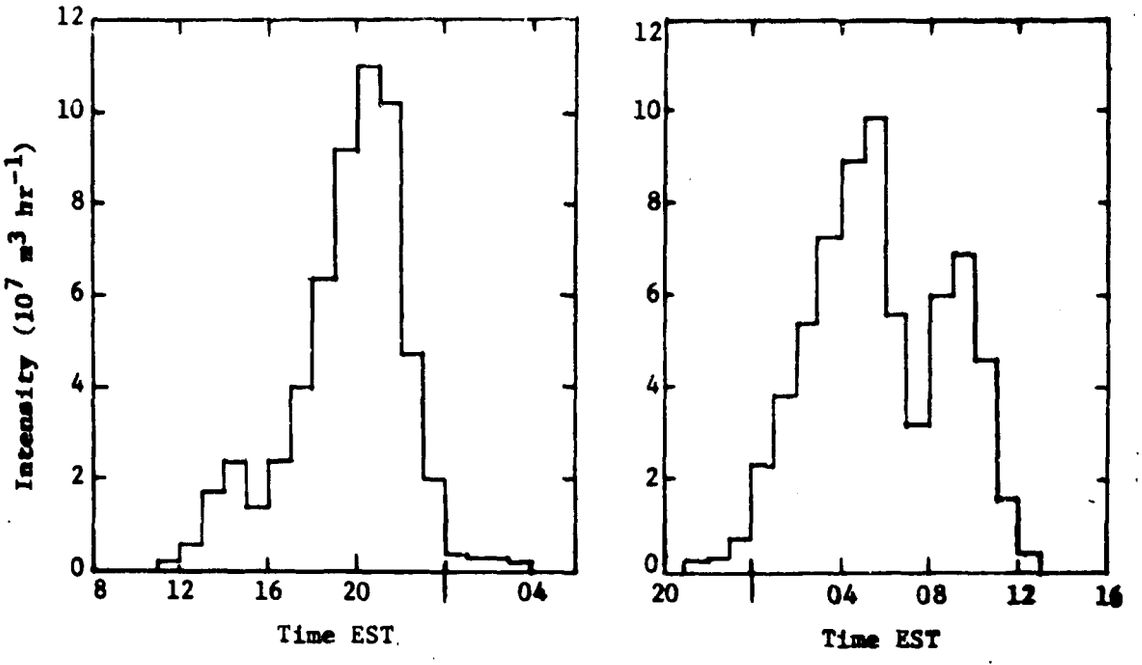

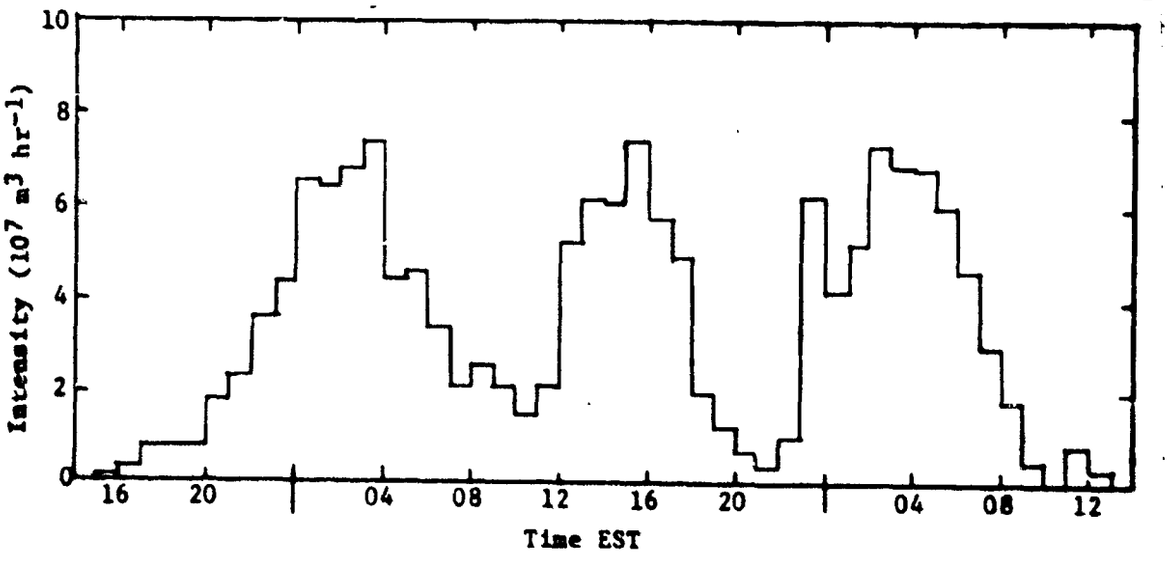

Fig. 39. Examples of time variations in hourly areal intensity over 4 x 10^4 km^2.

Table 6. Number of storms in each group having N peaks in areal hourly precipitation amounts.

	CL	GL	OL+CL	SW	SFW	CF	AM	Total
1	18	29	14	12	36	24	20	153
2	2	4	4	1	3	4	7	25
3 or more	1	2	1	0	3	1	2	10

into four equal subsections: central, northern, western, and southern. There are no gauges to the east over the ocean. Results are summarized in Table 7. The spatial differences are not striking, but for cyclonic storms there is a tendency for the greatest depth to be received by the section nearest to the path of the cyclone center and the least by the most remote section. Coastal cyclones have their centers toward the east or southeast, and the western portion of the area receives least precipitation. Overland lows from the Great Lakes area either go di-

Table 7. Average depth of water per year, in cm, deposited on each subsection by storms in the various groups. Amounts definitely above the average are underlined by solid lines, those below by broken lines.

	Center	North	West	South	Average
CL	30	25	20	27	26
SW	17	16	14	15	15
GL	13	16	14	13	14
OL+CL	15	14	12	13	14
SFW	17	15	17	19	17
CF	8	5	8	8	7
AM	6	5	3	3	5
Total	105	96	90	98	97

rectly over the region or to the north, and the northern subsection receives the greatest amount for this group. The stationary fronts usually lie to the south as the waves move along them. Air mass showers tend to be heavier in the hilly regions to the north and west. We do not know the reason for the relatively low amount of cold front precipitation in the northern section.

The seasonal variation in precipitation amounts is slight when all the storms are considered together, but some of the groups show very pronounced seasonal tendencies which are summarized in Table 8. Coastal storms predominate in the fall; overland lows from the southwest provide the bulk of mid-winter precipitation, while the overland lows with secondary coastal cyclones peak up sharply in February and March. Cold fronts are primarily summer storms.

In order to check the representativeness of the sample, monthly amounts in Table 8 were compared with climatological values and variations based on data from 1931 to 1960 for a number of rain gauge stations in New England. The total amounts for 1962 and 1963 were slightly below normal, especially 1963, but the monthly variability is close to the climatological standard deviation and the two years

are considered to be reasonably representative.

Table 8. Amount of water ($m^3 \times 10^8$) deposited in observed area (15,000 sq. miles) by each type of storm during indicated months in 1962 and 1963. Maximum contributions during each month are underlined.

Storm Type	CL	GL	OL+CL	SW	SFW	CF	AM	Total
Month								
January	1.7	6.3	14.5	24.7	9.6	0	0	56.8
February	9.8	7.3	28.2	0	14.5	0	0.7	60.5
March	1.5	0.9	30.2	8.2	3.7	0.4	1.4	46.4
April	4.9	7.3	5.9	4.1	24.4	1.6	0.5	48.8
May	0	21.0	7.6	0	11.3	4.8	4.2	48.8
June	3.6	4.9	0	0	22.0	8.7	7.3	46.4
July	0	10.6	10.4	0	6.1	15.3	5.3	47.8
August	12.2	12.6	0	1.9	13.5	11.2	3.2	54.6
September	27.4	2.1	0	13.8	9.9	6.1	2.0	61.2
October	68.1	18.0	0	0	0	1.2	1.5	88.9
November	36.3	7.7	0	37.4	3.9	5.6	5.7	96.6
December	17.9	9.4	3.9	23.3	0.4	0	0.1	55.0

3. Mesoscale patterns

Commonly observed patterns on the radar are bands of precipitation, large areas of more or less continuous precipitation, and assortments of small and often irregular areas. In an attempt to formulate objective criteria for describing such patterns a preliminary study was made in which a number of storms with well defined structure were selected and analyzed. Selection was subjective and based on the appearance of the digital maps. Sixty-four storms were chosen from the years 1960-1963. In 28 storms relatively large areas (on the order of 100 miles in dimension) of continuous precipitation were observed; 24 storms contained lines or bands of precipitation; and 12 storms which were comprised of either broken areas or several small areas with no well-defined bands were classed as miscellaneous. Dimensions, intensities, and internal structure of the areas and bands were considered.

In the case of the areas, it soon became apparent that dimensions could not be determined from the radar data alone because much of the time the edges of the echoes depended upon the limit of detectability rather than on the edge of a precipitation area. The rain gauges would show precipitation continuing beyond the regions depicted by the radar. The rain-gauge maps covered an area of approximately 4×10^4 square miles, and in many of the storms all of the gauges were recording a millimeter or more of rain during several hours. From the rain-gauge data, it was concluded that 21 of the storms contained areas of continuous precipitation which were at least as large as 10^4 mi^2, while in the other seven the observed areas were 2×10^3 mi^2 or greater. In only one storm did the precipitation appear to be fairly uniform in intensity throughout the area. In all of the others there were one or several regions of more intense rain (ranging from 4 to 32 mm hr^{-1}) imbedded within the lighter rain. These more intense areas had dimensions of about

30 miles and contained roughly 10^3 mi^2.

The bands ranged in length from 80 to 200 miles with over half between 120 and 160 miles. Widths varied considerably along the lines but were generally about 20-30 miles. There appeared to be no relation between the dimensions of the bands and the intensities or amounts of precipitation. None of the bands were uniform in intensity, all had small regions (10-30 miles in dimension) of relatively heavy precipitation scattered along the lines.

On the basis of the observed characteristics of the selected areas and bands, the following criteria appear suitable for describing mesoscale patterns:

(a) An "area" displays continuous echo over a region whose dimensions are at least 50 miles in every direction.

(b) A "small area" is not as great as 50 miles across in all directions, but exceeds 20 miles in at least one dimension.

(c) A "spot" is 20 miles or less in every direction.

(d) A "band" or "line" is at least four times as long as it is wide and extends 80 miles or more in length. A band may be solid, broken or spotty.

(e) In a "small band" the length is less than 80 miles but is at least four times as great as the width.

Attempts to sort all of the 115 storms in 1962 and 1963 for which we have radar data into groups typified by the patterns listed above met with only very limited success. Several pattern types would often occur during the course of a single storm. Moreover, most of the definite areas and bands had already been selected for the preliminary study, and the remaining storms presented an assortment of small areas, small bands and spots. In Table 9 the storms in the preliminary study are grouped by synoptic type.

Table 9. Summary of mesoscale patterns. Number of storms in each category during 1962-1963 is given.

Storm type	With radar data	Selected as:		
		Area	Band	Misc.
CL	14	2	0	2
OL+CL	12	6	0	0
SW	9	3	0	3
GL	20	2	5	2
SFW	28	5	3	4
CF	18	0	6	1
AM	14	0	4	0
Total	115	18	18	12

From the table it would seem that definite areas appear in only about 15 per

cent of the storms. However, there may be some instrumental bias in this result. Half of the OL+CL storms appear in this pattern type and many of them were late winter snowstorms. Some of the very intense coastal cyclones and lows from the southwest either appeared in the miscellaneous group or were not selected at all, although the rain gauges usually indicate extensive areas of light rain in these storms with small areas of heavier rain and intense showers imbedded in them. However, the SCR-615-B is not sufficiently sensitive to detect the light rain and the AN/CPS-9 suffers from attenuation in the heavy showers, so that neither radar shows the areas. We may conclude then that in intense cyclonic storms precipitation areas exist but are not well depicted by the radars; in moderate cyclonic storms precipitation areas exist and are usually well depicted by the AN/CPS-9, especially in snowstorms where attenuation is not a factor; in weak cyclonic storms there is probably widespread cloudiness but precipitation occurs only in small areas.

Persistent bands appear most frequently in frontal and air mass storms; it may be noted that in many of the GL storms most of the precipitation in this area is associated with a cold or occluded front. But there are also a great many, probably the majority, of frontal storms where small areas and spots are the predominant pattern type.

One of the most important results from this analysis is the observation that almost all of the storms contain small precipitation areas, either alone, spaced along a band or embedded in larger areas of light precipitation. Meteorologists have an understanding of the basic physical processes involved in synoptic-scale areas of lifting and condensation associated with cyclones and also for the buoyant lifting in convective cells. Very little is known, however, concerning atmospheric circulations in the mesoscale and their relation to precipitation processes. The ubiquitousness of mesoscale precipitation areas points up the need to study them more carefully.

4. Cellular structure

Five types have been defined to describe the extent and nature of cellular structure as shown on the RHI:

(a) Medium to large convective cells. These cells are 3 miles or greater in horizontal dimension; usually no "bright band" is seen, but it may appear during the dissipating stages of the convective storms.

(b) Small convective cells, no bright band. A small convective cell is two miles or less in horizontal dimension.

(c) Well-defined small convective cells and bright band. In this configuration the bright band may not appear as an enhanced horizontal echo, but the strongest echo within the cells is consistently observed at a level just below the 0C isotherm.

(d) Bright band visible, but no well-defined cellular structure.

(e) Neither bright band nor cellular structure well-defined.

It is considered that storms of types (a) and (b) are primarily convective in nature; those of types (d) and (e) are primarily stratiform, while type (c) results from a combination of stratiform and convective lifting.

Table 10 shows the distribution of cellular structure for the various synoptic groups. It should be mentioned that seasonal effects are very strong. Large convective cells (type a) are found in all groups except the SW cyclones but all of these cases were summer storms which occurred between late May and early September. Moreover, there were only two summer storms which were not type (a); both were coastal cyclones with small cells and general rain (type c).

Table 10. Summary of cellular structure for various synoptic groups. Number of storms in each category during 1962-1963 is given.

Synoptic group	Cellular type a	b	c	d	e	Total
CL	2	3	7	1	1	14
OL+CL	3	4	4	0	1	12
SW	0	1	7	0	1	9
GL	8	2	7	1	1	19
SFW	12	3	5	2	2	24
CF	14	0	3	0	0	17
AM	6	0	5	0	0	11
Total	45	13	38	4	6	106

When the total amount of precipitation is considered rather than the number of storms, it is found that less than 15 per cent is deposited by storms that are primarily stratiform, less than 25 per cent by storms that are almost entirely convective, and roughly 65 per cent is associated with storms of type (c).

Because so many storms, including most of the intense extratropical cyclones, contain both stratiform and convective precipitation, a pilot study was performed to demonstrate how the relative contributions of the two types of lifting can be determined from radar and rain-gauge data. The coastal cyclone of 7-9 November 1963 was selected for the pilot study; examples of the basic data are in Figs. 40-42. On the SCR-615-B the lowest intensity level depicts showers with equivalent rainfall rate in excess of 8 mm hr^{-1}. The second intensity level corresponds to 20 mm hr^{-1} or greater; in the heavier rain areas some showers of this intensity were observed. None were recorded at the third level, which would correspond to rainfall rates in excess of 40 mm hr^{-1}. These radar-indicated rainfall rates are in good agreement with those recorded by the sensitive tipping-bucket gauges at the field station 17 miles north-northwest of the radar site.

Estimates of the relative contribution of stratiform and convective lifting to the total precipitation are based primarily on detailed records of the rainfall rates, as in Fig. 41. The fairly steady rates or plateaus, out of which the sharp shower peaks rise, are measured for each hour. The difference between this amount and the total for the hour, as indicated by both tipping-bucket and weighing gauges, is attributed to convective activity. For the entire day on 7 November 1963, 55 per cent of the precipitation was stratiform and 45 per cent convective. Further corroboration of the relative amounts is supplied by the computations of large-scale lifting and condensation rates. In the intense cyclonic storms, the computed large-scale condensation rate was usually one-half to two-thirds of the areal rain-

fall rate measured by the network of gauges for the same hour. This was the case for 7 November 1963.

In order to appreciate the very large number of cells which appear in storms of this type, a composite tracing was made to show all of the rain within a 200 x 200 km square (15,000 mi^2) at 1330 EST (Fig. 43). For this figure, precipitation areas were added in the following manner to what was actually observed on the scope at that time (Fig. 40). Echoes observed one-half hour and one hour previously were advected towards the west northwest according to their observed motion. Similarly echoes observed later were advected backwards. The individual cell echoes had a life-time of only 5 to 10 minutes, so that the same cells would not be in existence an hour after they were observed. It is assumed, however, that the group would still be in existence, and that the number and intensity of the cells within the group remained approximately the same. In the directions normal to the echo velocity, the pattern was extrapolated maintaining a similar density of cells and groups of cells. A check was then made to see whether the pattern so constructed would, if it moved in the observed manner, actually deposit over each rain gauge the amount recorded for the hour.

In this storm the groups of showers were arranged in elongated areas or loose bands as shown schematically in Fig. 43. These bands can also be identified in Fig. 41; band A went over the rain gauge at 1230 EST, B at 1300, C at 1330 and D at 1350-1420. In the composite there are 1200 cells at the lowest intensity level, including those assumed to be in the regions where the patterns were extrapolated. There are 75 cells at the second intensity level, almost all of which were actually observed by the radar. The gauges over which these more intense cells passed invariably received proportionately greater amounts of precipitation than the surrounding ones.

On the average, the showers were observed to have areas of 1.7 km^2 and durations of 8 minutes, with rainfall rates of 15 mm hr^{-1} in the level-one cells and 40 mm hr^{-1} in the level-two cells. During the hour, nearly 10,000 cells would build and dissipate in the area under consideration and would deposit approximately 3×10^7 m^3 of water. The rain-gauge data showed that the average rainfall rate in the synoptic-scale area outside of the bands is 2.5 mm hr^{-1} while the steady rain in the bands but between the cells was 5-6 mm hr^{-1}. The synoptic-scale lifting then contributed 10^8 m^3 of water and the enhancement in the mesoscale areas contributed 4×10^7 m^3 giving a total of 1.7×10^8 m^3 of which slightly less than 20 per cent was attributed to the cells. This detailed example has been included to illustrate the extreme complexity of pattern which may be encountered and the extensive convective activity which often occurs in cyclonic storms.

In general it may be concluded that the cellular structure is more dependent on the season than on the macroscale storm type and that precipitation which is almost entirely stratiform is relatively rare. In summer all of the precipitation appears to be primarily convective, but at other seasons most of the storms contain both stratiform and convective precipitation simultaneously and in significant amounts.

The occurrence of such extensive convective activity in extratropical cyclones warrants investigation concerning its possible significance to the storm dynamics through release of latent heat and by vertical transport of such quantities as heat, momentum and vorticity. The importance of such effects in tropical storms is recognized, but it has generally been assumed that all of the energy for extratropical cyclones is derived from other sources. An investigation of the role of

SCR-615-B radar 60-mile range
1330 EST $R_e \geq 8$ mm/hr

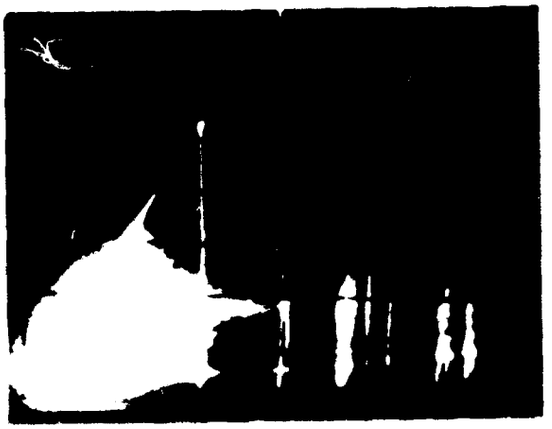

AN/CPS-9 50-mile range
0830 EST Azimuth: 20°

Fig. 40. Radar scope photographs showing areas of intense small showers, 7 November 1963.

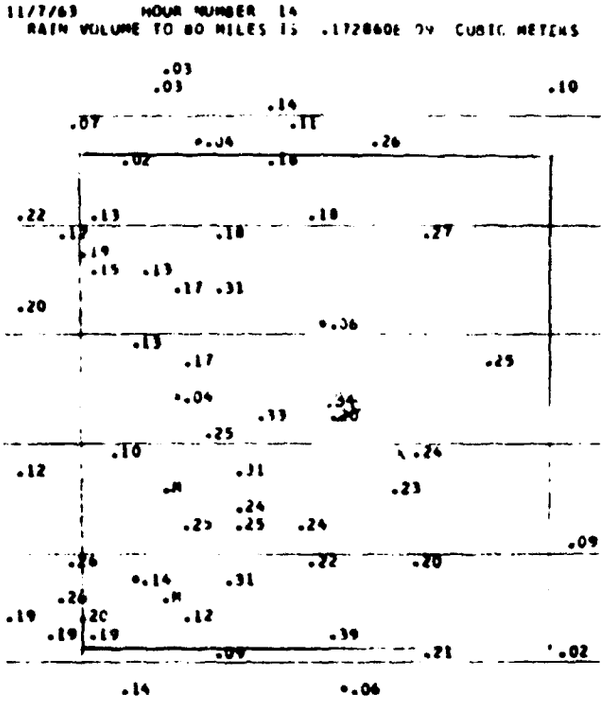

Fig. 41. Computer-plotted hourly rainfall amounts in inches. Added square is 4 x 10^4 km^2. x marks radar site.

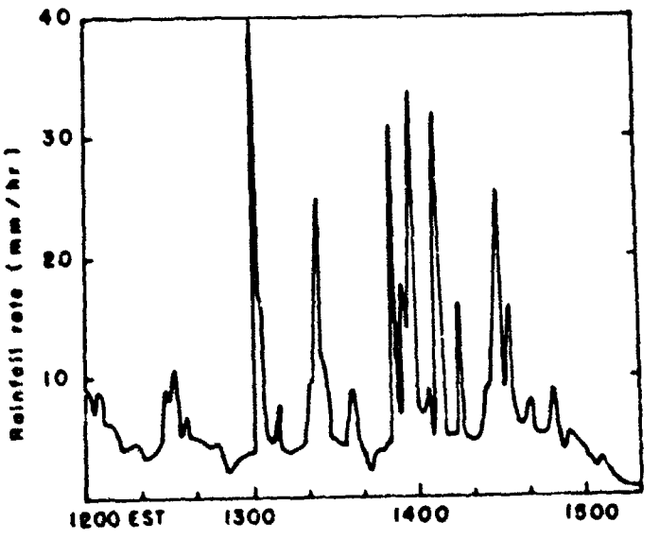

Fig. 42. Detailed rain-gauge record, 7 November 1963.

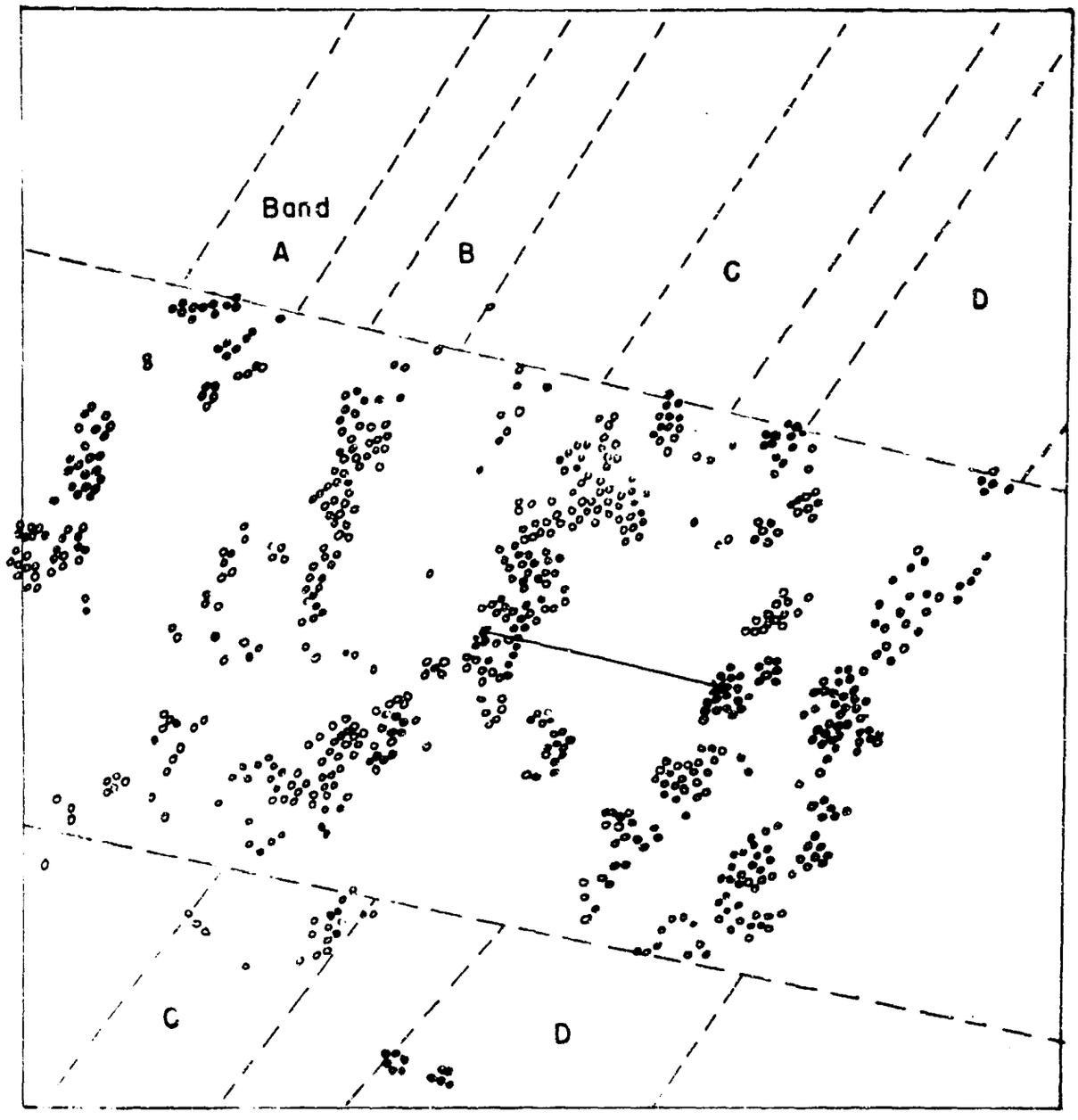

Fig. 43. Detailed precipitation pattern in 200 x 200 km area at 1330 EST, 7 November 1963. Dashed lines show extrapolation of bands beyond range of detection of radar. Steady rain outside of bands is 2.5 mm hr^{-1}, in bands it is 5-6 mm hr^{-1}.

x: radar site
arrow: motion of bands in one-half hour

o: showers at lowest radar intensity level (10-20 mm hr^{-1})
●: showers at second intensity level (40 mm hr^{-1})

small-scale convection in a selected storm is in Section III E of this report.

5. Summary of survey

A survey of all the storms during 1962 and 1963 in the vicinity of Cambridge, Massachusetts, has provided a good deal of information concerning the amount of rain associated with storms of various synoptic types, the seasons when they are likely to occur, and the small-scale characteristics of the precipitation.

One important result is the observation that a fairly large portion of the total precipitation is deposited by relatively few deep extratropical cyclones. In these storms, and also in most of the less intense cyclones, convective activity and mesoscale precipitation areas contribute about as much to the precipitation as does the synoptic-scale circulation itself. Detailed study of individual storms should be helpful in clarifying the physical relationships between the atmospheric circulations on the various scales.

A reasonably objective scheme was presented for describing mesoscale precipitation patterns, and the macroscale storm types in which well-defined precipitation areas ($\sim 10^4$ mi^2 or greater) or bands ($\sim$100 miles in length) are likely to occur were noted. The most significant result concerning the mesoscale patterns was that "small areas" (10^2-10^3 mi^2) are observed in almost all of the storms. Since practically nothing is known concerning the dynamics of these areas, further analysis of their characteristics seemed desirable and has been undertaken. Some of the results are presented in the following section of this report.

The microscale or cellular structure of the storms appears to be more dependent on the season than related to the type of macroscale situation. The infrequency of precipitation which is almost entirely stratiform was noted, and an example was given to illustrate the typically complex combination of general rain and convective cells in cyclonic storms. Relationships between cells and mesoscale precipitation areas are given further consideration in Sections III B and C.

B. Characteristics of Mesoscale Precipitation Areas

1. Selection of storms

Previous analyses have shown that mesoscale precipitation areas appear in almost all New England storms. Further investigation concerning their sizes, shapes, intensities, motions and durations has been undertaken based on radar displays of the averaged range-normalized signal intensity, detailed rain gauge records, and conventional meteorological data. Eight storms were selected for analysis:

Date	Synoptic type
29 August 1962	Coastal low (ex-hurricane)
8 July 1963	Cyclone moving eastward from Great Lakes region
18 May 1963	Overland low plus coastal low
6 December 1962	Cyclone approaching from southwest
17 December 1963	Wave on stationary front
12 January 1963	Wave on stationary front
2 February 1963	Low moving from Great Lakes region
9 June 1965	Air mass (thunderstorm complex)

In no case was there any knowledge of the type of precipitation pattern in a storm before it was chosen. And in no case was a storm rejected because of the precipitation patterns it was found to contain. The storms were selected mostly from those which were primary precipitation producers and to represent as many different synoptic and seasonal situations as possible. Situations which had continuous radar coverage and for which detailed rain gauge traces were available were preferred.

2. Methods of analysis

At the start it was assumed that a precipitation area 10^4 to 10^5 mi^2 in size is on the synoptic scale and that a spot with an area on the order of 1 to 10 mi^2 represents a single convective cell. A mesoscale precipitation area was therefore defined as one larger than 25 mi^2 and smaller than 5000 mi^2, i.e. on the order of 10^2 to 10^3 mi^2. Early in the analysis, however, it became apparent that some of the precipitation patterns contained areas of two distinct sizes both within the mesoscale range where several small mesoscale areas would be located within a larger but less intense one. The definition was therefore amended to distinguish between large mesoscale areas (LMSA's) which contain 500 to 5000 mi^2 and small mesoscale areas (SMSA's) which are 25 to 500 mi^2 in size.

Synoptic-scale precipitation areas were identified from the hourly maps based on records from the rain-gauge network, since the radars do not depict the full extent of these areas. Intensity of the precipitation was estimated from the rain-gauge maps and the detailed rain-gauge records. The sizes, motions and durations of synoptic-scale precipitation areas were not determined because their horizontal dimensions were greater than those of the region of study.

Mesoscale areas and cells were identified from intensity level sequences on the PPI. In Fig. 44, for example, the entire band is a large mesoscale area. Six small mesoscale areas A1 to A6 are indicated in it. Fig. 45 shows two blob-shaped LMSA's. There is some subjectivity in determining what constitutes a separate SMSA, but essentially it appears as a separate area at some intensity level and maintains its identity through a number of PPI sequences. The synoptic-scale area indicated by the rain gauges is shown by the 0 contour. Several cells appear in A4, some not completely resolved, and one in A2.

In each storm representative mesoscale areas were selected for detailed study and their characteristics were tabulated. From the PPI maps, the sizes and shapes were determined. The average size was computed for each mesoscale area from a number of individual observations during its lifetime. The SMSA's and cells located within each LMSA and the cells within each SMSA were counted and the numbers averaged. The average density of SMSA's within each LMSA (number per thousand square miles) was also computed as well as the density of cells within the SMSA's (number per hundred square miles). Motions and durations of the mesoscale areas were determined by tracking them from one PPI sequence to the next.

Precipitation intensity in the mesoscale areas was estimated from the rain gauges over which they passed and from the equivalent rainfall rates indicated by the radars. For a LMSA, the intensity was estimated for the area outside of the SMSA's and cells; for the SMSA's the intensity was estimated for the area outside of the cells.

Cells were identified on the radar maps as precipitation areas less than 25 mi^2 in area. Precise sizes and shapes could not be determined because their dimen-

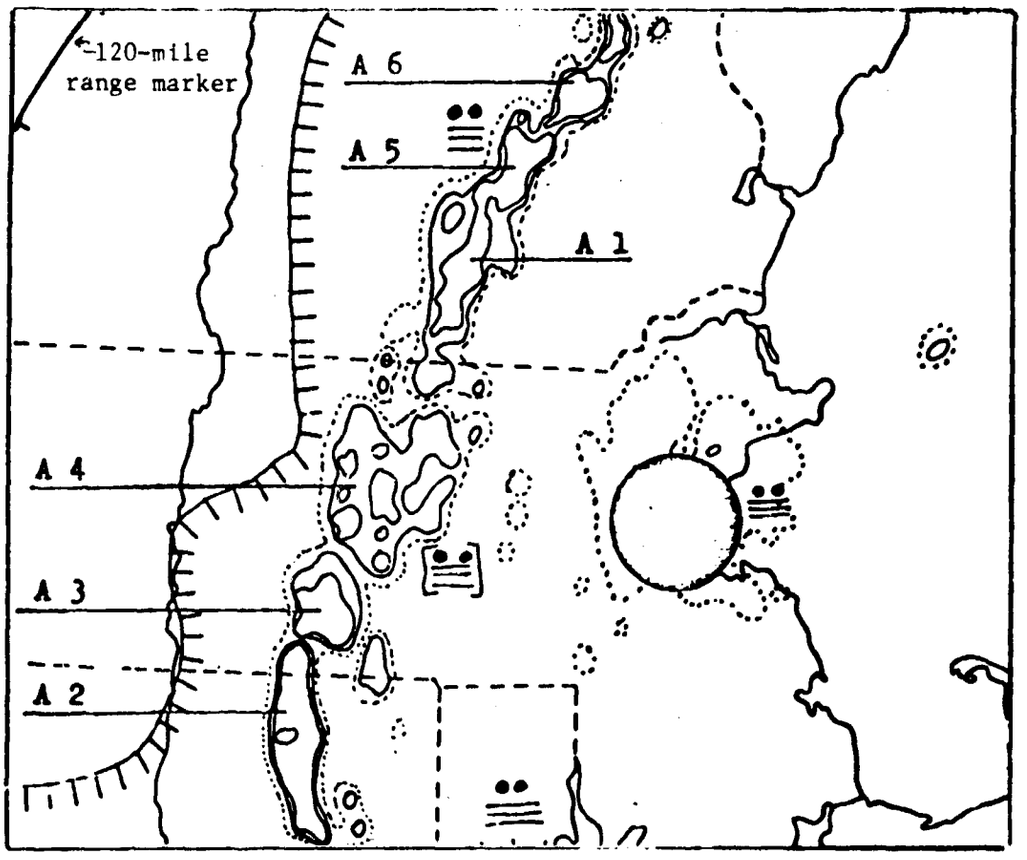

Fig. 44. Precipitation pattern for 0440 EST, 29 August 1962, containing band-shaped large mesoscale area.
Contours: 0(⊥⊥⊥), 2(·····), 6, 12 and 24 mm hr^{-1}.
Circle represents radar site and ground clutter.

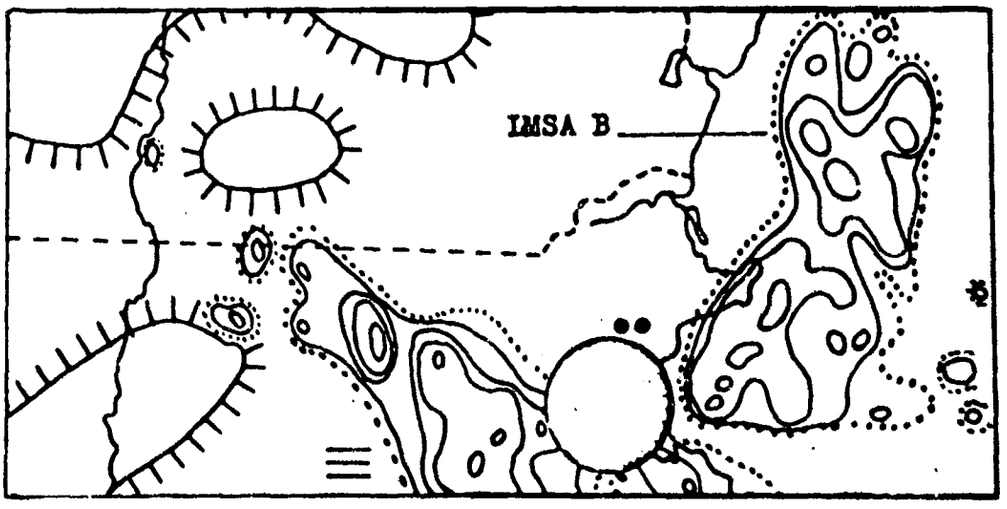

Fig. 45. Precipitation pattern for 0635 EST, 8 July 1963, with blob-shaped large mesoscale area.
Contours: 0(⊥⊥⊥), 1(·····), 2, 4, 8 and 16 mm hr^{-1}.

sions were close to the limit of horizontal resolution of the radars. Most of them appeared to be close to 3 mi^2 in area, and this value was adopted as a representative cell area. Motions, durations and intensities were computed for the cells in the same manner as for the mesoscale areas.

Depth and location of the layer containing the cells was determined from RHI displays and radiosonde data. The tops of the cells were assumed to coincide with the tops of the precipitation columns appearing on the RHI, although lack of detectability may have caused the heights to be slightly underestimated. The bases of cells were more difficult to locate since precipitation falls to the ground and echoes may extend below the level where overturning is occurring. If the precipitation trailed off at an angle from a vertical column, then the level at which it began to trail off was assumed to be the bottom of the cell; also, if the soundings showed a stable layer near the surface, the bottoms of the cells were assumed to be at the top of the stable layer. Depth of the lighter precipitation surrounding the cells was also determined from the RHI displays. This precipitation could be detected only at very close ranges and appeared to remain about the same during any one storm, hence the observed depth was applied to both LMSA's and SMSA's.

The motions of convective elements is generally thought to be governed by the mean wind in the layer which contains them. Therefore, in each storm the wind near the center of the layer containing the cells is referred to as the "steering level wind".

In addition to the quantitative observations (size, motion, duration, etc. of precipitation areas), qualitative observations were made from the radar displays and detailed rain-gauge traces concerning the extent of cellular activity in the various storms. Since there are 5 db between thresholds in the intensity levels, and since the spatial resolution of the radar beams is marginal for arrays of small cells, it is quite possible that a simple count of the small spots at a higher intensity level within any SMSA might seriously underestimate the number of cells which it contains.

3. Results and discussion

The rainstorm of 8 July 1963 occurred preceding and during the passage of an occluded front, and it was noted that the character and behavior of the precipitation patterns in the prefrontal rain differed considerably from those in the rain directly associated with the frontal passage. Therefore, this storm was treated as two, the prefrontal phase (PF) and the frontal phase (F), and the results are presented for a total of nine storms.

In seven of the nine storms, synoptic-scale precipitation areas were observed, although in one case it was weak, that is, all of the gauges did not record precipitation but there were surface reports of drizzle and overcast. Within five of the seven synoptic-scale areas, large mesoscale areas of more intense precipitation were observed, and in the other two they may have been present, but data are inconclusive because the radar was operating on a 60-mile range and a relatively small region was under observation. All of these storms contained small mesoscale areas and cells. In the frontal storm and air mass situation there were no synoptic-scale precipitation areas; the frontal storm contained a large mesoscale area, band shaped, SMSA's and cells. The thunderstorm complex contained only a small mesoscale area and cells.

Altogether 8 large mesoscale areas, 25 small mesoscale areas and 125 cells

were examined. It is recognized that results drawn from such a small sample can not be regarded as statistically verified, but some characteristics were quite consistently observed and are believed to be significant. A summary of the observed quantities is in Tables 11 and 12.

Although by definition LMSA's may be anywhere from 500 to 5000 mi^2 in area, all eight in the sample were in the relatively narrow range between 900 and 1800 mi^2. Similarly the SMSA's were defined as having any area between 25 and 500 mi^2, but as shown in Fig. 46 the distribution peaked very sharply in the vicinity of 100 mi^2.

The average number of SMSA's within each LMSA at any given time varied from 3 to 6 and the density from 2 to 5 SMSA's per 1000 square miles. The number of cells varied from 1 to 7 per SMSA at one time with densities from 1 to 24 cells per 100 square miles. The qualitative observations on cellular structure also suggested wide variability in the density of cells, and indicated that the PPI data do tend to underestimate the number of cells. With the exception of the frontal band on 8 July 1963, the higher cell densities (more than 4 per 100 mi^2) were found in winter storms where the cells were in a relatively shallow layer aloft. Depths of layers containing cells and of the surrounding general precipitation are in Fig. 47.

Durations of both large and small mesoscale areas varied over nearly an order of magnitude. For SMSA's the range is from 0.3 to 3 hours with a median value of one hour; for LMSA's the range is from one to twelve hours with the most probable value appearing to be in the vicinity of four hours. The one with an extremely long duration was the frontal band. Durations of cells were generally only a few minutes; distributions in the various storms are in Fig. 48. There is a roughly linear relation between duration, depth and intensity of cells. When the average values of these quantities for each day are plotted against each other, the lines of best fit indicate that cells last approximately four minutes for every 5000 ft of depth and for every 8 mm hr^{-1} of intensity.

During the lifetime of a LMSA, then, a number of small mesoscale areas build and dissipate within it. Similarly, during the lifetime of each SMSA, cells are building and dissipating within it. The precipitation rate in the mesoscale areas varies considerably from storm to storm, but in general in a LMSA it is about twice as great as that in the synoptic-scale area surrounding it and in a SMSA it is about twice as large as in the LMSA. In the cells the intensity is anywhere from 2 to 10 times as large as in the SMSA's which contain them. The relative amounts of water deposited by precipitation areas of the various sizes are in Table 13; the percentage attributed to cells may be an underestimate, as pointed out earlier. For the three winter storms where the LMSA's could not be adequately defined and for the thunderstorm complex where there was no LMSA, it was found that in the SMSA's about half of the total precipitation (40 to 60 per cent) fell from the cells and the other half from the region surrounding the cells. It may be concluded that although the ratios vary from storm to storm, the amounts of precipitation deposited by precipitation areas of the four scales under consideration are comparable in magnitude.

Concerning the motions, it was found that in all of the storms the average cell motions were in fair agreement (±25 degrees in direction; ±50% in speed) with the steering level flow. Motions of mesoscale areas could be determined only roughly because they are continuously changing shape. The motions of SMSA's were

Table 11. Observed characteristics of large mesoscale areas

Date	LMSA	Shape	Ave. Size (mi^2)	Duration (min)	Intensity ($mm\ hr^{-1}$)	No. of SMSA's	Density of SMSA's (per $10^3\ mi^2$)
29 Aug 1962	A	Band	1500	240	5	5	3
8 July 1963 (PF)	B	Blob	1200	80	2.5	3	2
	C	Blob	1300	>80		4	3
18 May 1963	D	Blob	1200	200	2-3	3	2
	E	Blob	900	240		4	4
17 Sept 1963	H	Blob	1300	>210	0.5-1	5	4
	I	Blob	1800	>210		6	3
8 July 1963 (F)	P	Band	1000	720	0.5-5	5	5

Table 12. Observed characteristics of small mesoscale areas

Date	SMSA	Ave. area (mi^2)	Duration (min)	Intensity ($mm\ hr^{-1}$)	Intensity in cells ($mm\ hr^{-1}$)	Average no. of cells	Density of cells (per 100 mi^2)
29 Aug 1962	A1	300	65	10	15-20	5	2
	A7	75	85			4	5
8 July 1963 (PF)	B1	125	20	5	10-20	5	1
	B2	125	40			4	2
	C1	125	25		10-40	3	?
	C2	200	>30			7	4
18 May 1963	D1	175	20	5	10-15	1	1
	D2	125	>60			1	1
	D3	50	>30			1	2
	E1	275	55			2	1
	E2	75	50			1	1
	E3	50	>35			1	2
6 Dec 1962	F1	50	45	3-6	10-50	2	4
	G1	100	>35			5	5
17 Sept 1963	H1	100	140	2	4-15	2	2
	I1	175	>195			1	1
12 Jan 1963	J1	100	35	1-2	3-4	-	-
	K1	150	65			5	3
	L1	75	35			6	8
	M1	50	>30			4	8
	M2	25	90			6	24
2 Feb 1963	N1	100	>95	2-3	5-10	6	6
	N2	100	>85			2	2
8 July 1963 (F)	P1	50		5-25	20-100	5	10
9 June 1965	Q1	100	150	5-20	45-90	3	3

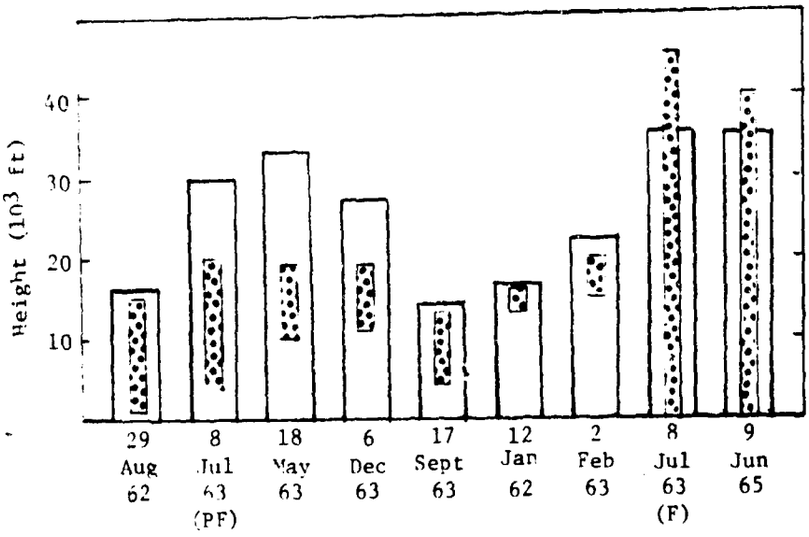

Fig. 47. Diagram showing for each storm the layer containing the cells (shaded) and the layer of lighter precipitation surrounding the cells (unshaded).

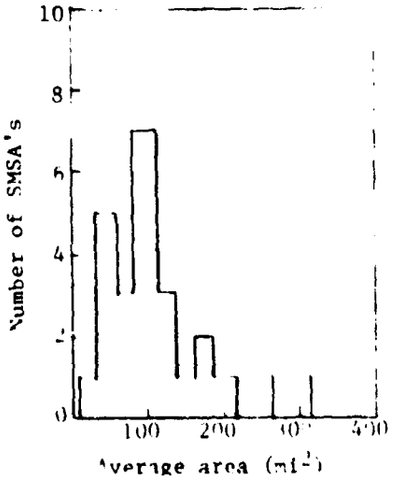

Fig. 46. Size distributions of small mesoscale areas.

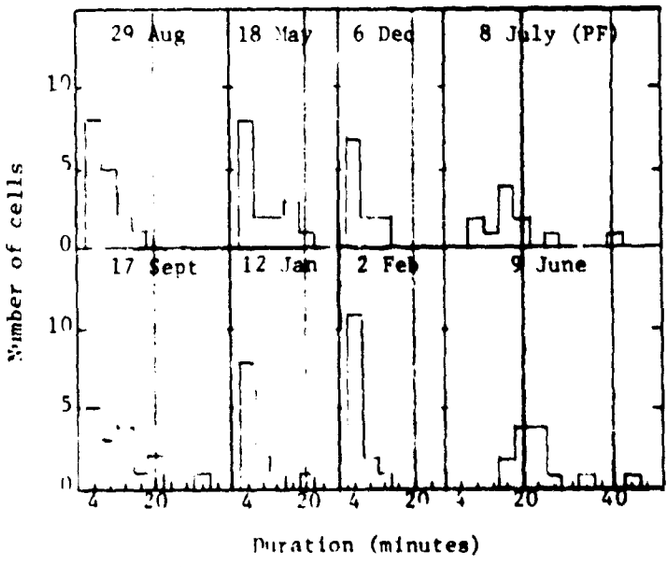

Fig. 48. Duration of cells observed in various storms.

generally the same as those of the cells within them. One exception is noted; the thunderstorm complex of 9 June 1965 moved to the right of the cell velocities. Blob-shaped LMSA's moved approximately in the same manner as the cells and SMSA's which they contained. The frontal band appeared to move in conjunction with the occluded front, while LMSA A was almost stationary.

Table 13. Water deposited by the various parts of the large mesoscale areas.
P_L = average volume of water per unit time from LMSA outside of SMSA's and cells
P_s = average volume of water per unit time from SMSA's outside of cells
P_c = average volume of water falling from cells

Date	LMSA	Total deposit (10^7 m^3 hr^{-1})	P_L %	P_s %	P_c %
29 Aug 1962	A	32.7	22	69	9
8 July 1963 (PF)	B	10.4	51	44	5
	C	15.7	27	48	25
18 May 1963	D	10.4	52	42	6
	E	7.1	33	65	2
17 Sept 1963	H	2.8	37	42	21
	I	3.4	29	55	16
8 July 1963 (F)	P	31.2	11	54	35

4. Resumé of mesoscale precipitation areas

There appear to be two distinct sizes of mesoscale precipitation areas so that altogether we can define four scales: synoptic-scale precipitation areas on the order of 10^4 mi^2 or greater; large mesoscale areas (LMSA's) from 500 to 5000 mi^2 in area; small mesoscale areas (SMSA's) from 25 to 500 mi^2; and cells, which are smaller than 25 mi^2. In cyclonic storms all four scales are usually present, although the synoptic-scale area may be only drizzle or widespread cloudiness. In frontal or air mass storms the synoptic-scale area or even a LMSA may not appear. Within a precipitation area of any given scale, however, all of the smaller scales are usually present. The LMSA's normally contained 3 to 6 SMSA's at any given time, whereas the SMSA's contained anywhere from 1 to 24 cells.

There is a definite size preference within the defined ranges as follows: cells, $\sim$3 mi^2; SMSA's, 100-150 mi^2; and LMSA's, 900-1800 mi^2. Typically, the cells lasted 0.1-0.5 hr, SMSA's 0.5-3 hr, LMSA's 2-5 hr, and synoptic-scale areas longer than 10 hr. Thus, within an area of a given scale the pattern of smaller sized areas was constantly changing.

Estimates of the amount of precipitation deposited by areas of each scale are not very precise, but they appear to be comparable in magnitude although there is considerable variation from storm to storm. No scale of motion is either predominant or negligible with respect to the overall precipitation regime.

The average cell velocities were in approximate agreement with the winds at

their steering levels (mid-cell heights). Thus, advection must have been the dominant process influencing the cell motions. SMSA's moved with approximately the same velocities as the cells they contained.

The physical basis for the occurrence of mesoscale precipitation areas is not known at this time. It is hoped that these descriptions of their characteristics will lead to a better understanding of them, and it is certainly desirable that the observations be extended to a larger sample. A close relationship between cells and small mesoscale areas is suggested by the similarity of their motions and the fact that they are always observed in conjunction.

C. Structure and Behavior of Thunderstorm Complexes

1. General description

Ever since the work on the Thunderstorm Project over twenty years ago (Byers and Braham, 1949) it has been recognized that new cells or updrafts tend to develop very close, a distance of only a few miles, to existing or dissipating ones. On the radar the precipitation associated with these updrafts appears as small spots of relatively high intensity on the PPI or as columns on the RHI. If the radar is sufficiently sensitive these spots or cores are surrounded by lighter echo corresponding to a region about ten to twenty miles in dimension (small mesoscale areas). The term "thunderstorm complex" has been introduced to designate the mesoscale precipitation area and the intense cells or cores associated with it. Thunderstorm complexes often occur in organized squall lines, but sometimes they are scattered about in apparently random locations. In a study of the internal sturcture of nine squall lines in New England, Cochran (1961) showed that the average spacing between intense storms in the lines was 25 to 30 miles, the storms lasted one to two hours, and their motion was consistently slower than and to the right of the 700-mb wind. In about half of the cases observed by Cochran there was a tendency for new storms to develop off the southwest end of the line (squall lines in New England are almost always oriented northeast-southwest), while in the others new storms appeared within the existing line.

After the improvement in sensitivity of the SCR-615-B radar late in 1964, the areas of lighter rain surrounding the cores in thunderstorm complexes could be much more readily observed. Two studies have been made concerning the relative behavior of the intense cores and the lighter echoes, both based on data taken during the summer of 1965.

2. Comparison of complexes in squall line and scattered thunderstorms

In the first study the structure and motions of thunderstorm complexes in a well organized squall line, 19 August 1965, and in an air mass situation, 28 August 1965, were investigated in as much detail as permitted by the resolution o the radar data. The progress and development of the line within radar range is shown in Fig. 49 by composite maps of the range-normalized signal intensity levels. The echoes observed by the radar were actually from the southwesterly end of a squall line which apparently was over 400 miles long. Hourly Precipitation Amounts for New England, indicate that between the hours of 1200 and 1800 EST the line extended in a northeasterly direction all the way across the state of Maine, though how continuous it was cannot be deduced from the rather sparse rain-gauge data.

In the analysis all echoes which reached intensity level 5 (R_e = 35 mm hr^{-1}) or greater were tracked. They are designated as "storms", while the very small

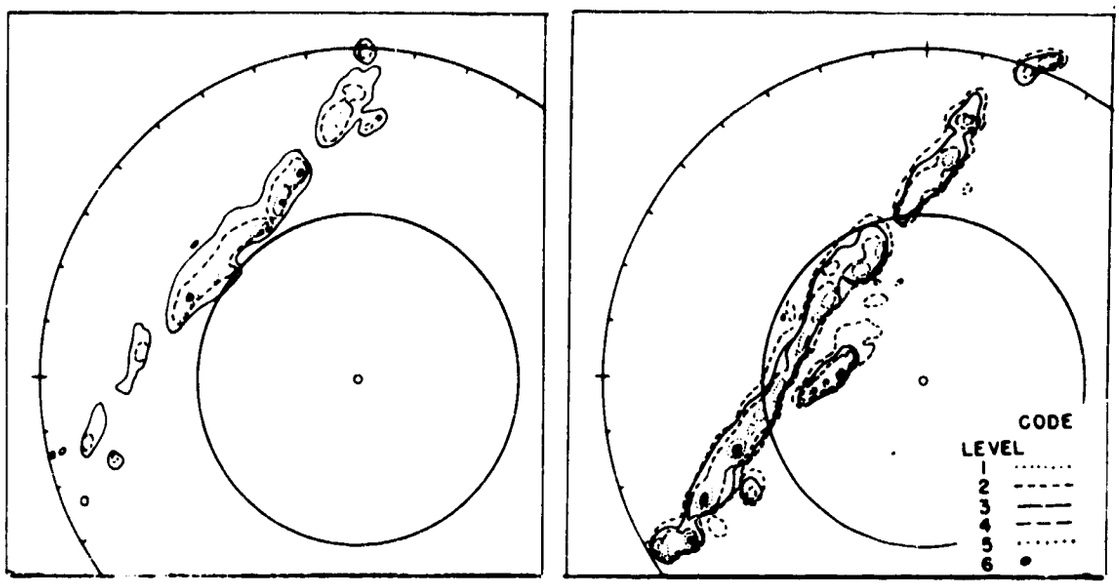

Fig. 49. Maps of range-normalized signal intensity on the SCR-615-B radar showing storm development in the squall line of 19 August 1965.

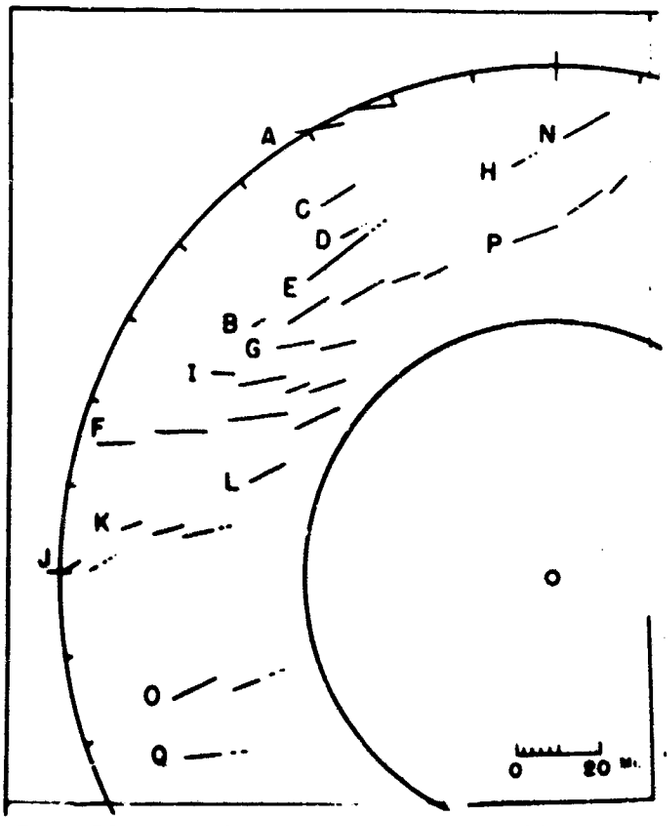

Fig. 50. Tracks of the intense cells within the squall line. Dashed lines indicate when cell motion can no longer be followed.

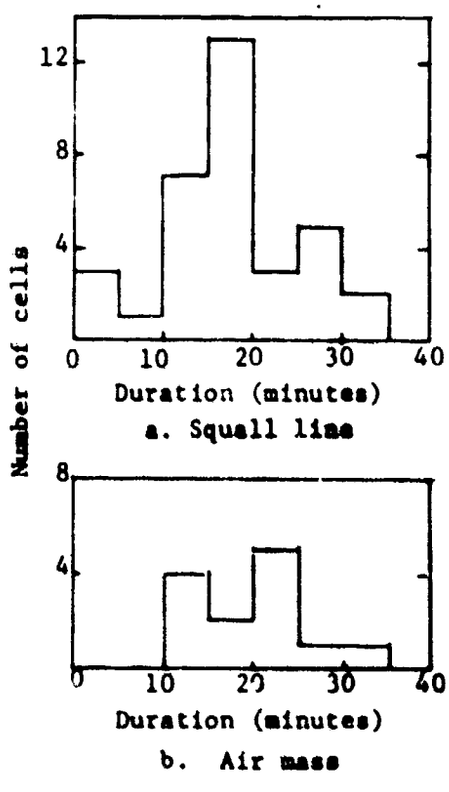

Fig. 51. Thunderstorm cell durations.

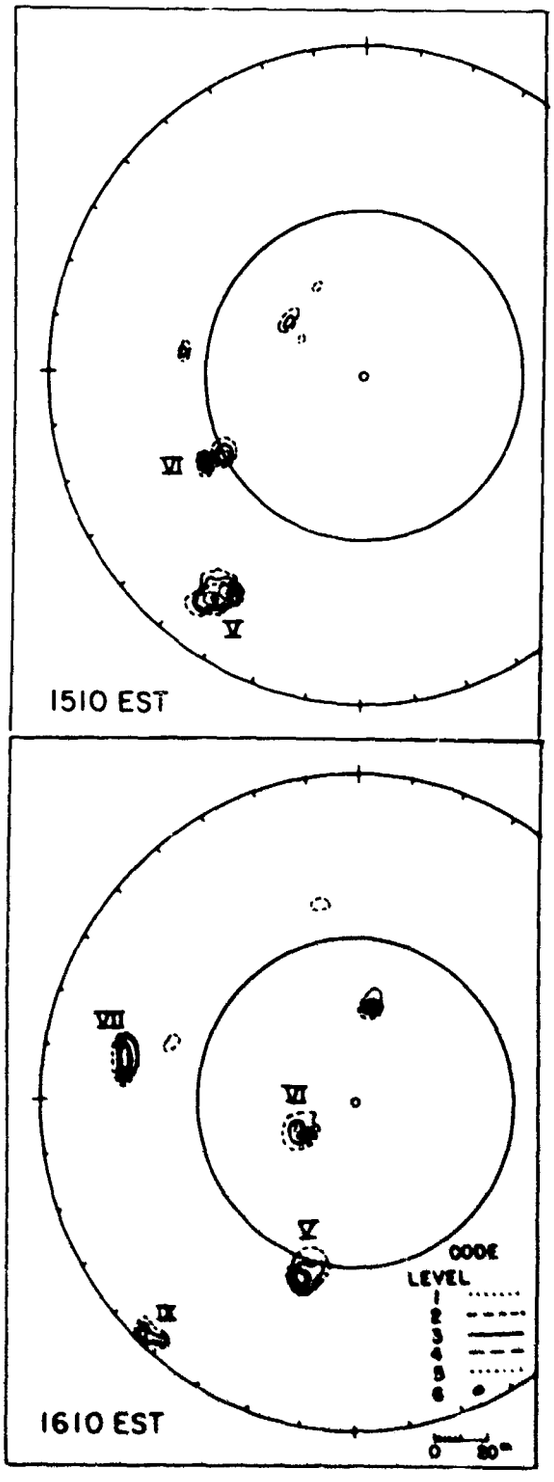

Fig. 52. PPI maps showing some of the air mass storms of August 28, 1965.

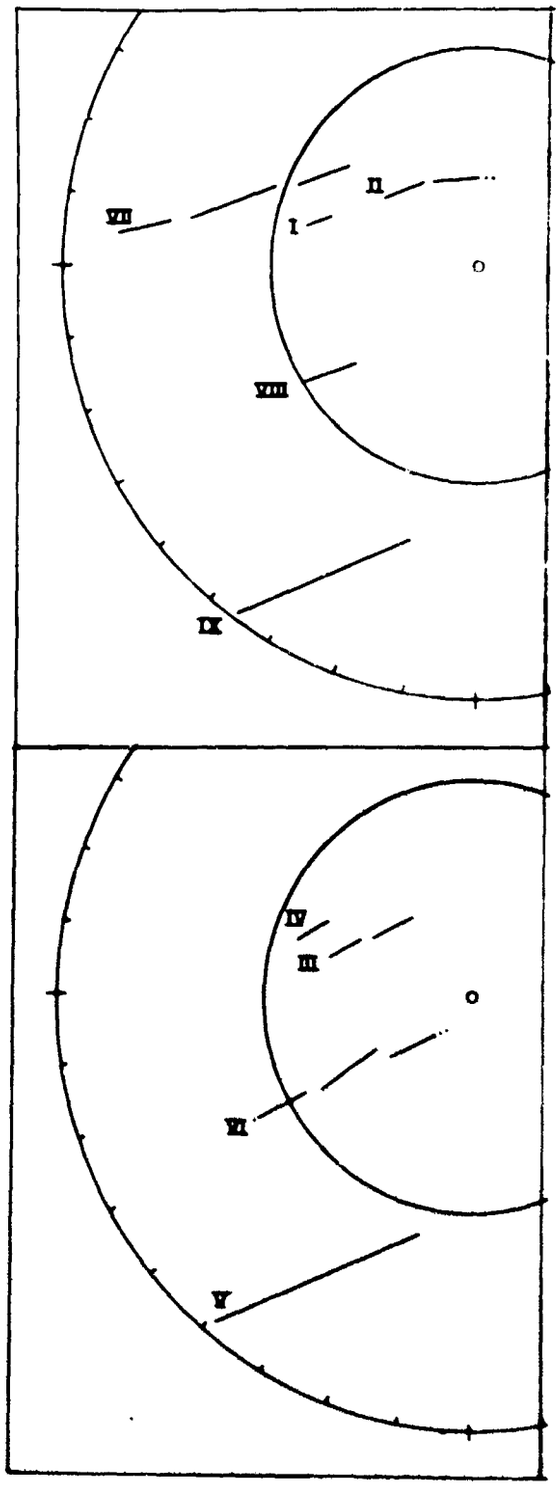

Fig. 53. Tracks of the air mass thunderstorms. Dashed lines indicate when storm motion can no longer be followed.

spots were regarded as "cells". Cells were less than five miles in diameter, usually only one or two, while the "storms" ranged from 5 to 15 miles in dimension. Fifteen storms, as defined, were identified within the squall line between 1250 and 1600 EST, and were labelled by letters of the alphabet the order corresponding to the time of appearance. Each contained from one to five cells; tracks of the cells are in Fig. 50. It can be seen from the figure that new storms did not consistently develop on the southwesterly end of the line, but there was a tendency for them to do so.

Most of the storms contained a succession of cells; in nearly every case the new cell track commenced at the same time or within two minutes of the termination of the old one. A preferred position for the formation was two to four miles to the right (southerly side) of the old one; this was the case for 23 out of 28 cells which were observed to form in the vicinity of old ones. Three cells formed to the north (in storms A and F) and for two the relative positions were not clear. Observed cell motions varied from 235° to 270° in direction and from 20 to 44 mph in speed. The wind in the 700 to 500 mb layer was from 230° increasing from 30 to 50 mph. Clearly advection was an important factor in the motions. Most frequent cell duration was 15 to 20 minutes, Fig. 51; storm lifetimes were from 20 minutes, for single celled ones, to about 1 1/4 hours.

Reflectivity maps and individual cell tracks for the air mass thunderstorms are in Figs. 52 and 53. These thunderstorms also consisted of one or several individual cells in sequence, and as before the new cells generally formed slightly to the right of the old ones. Average motions were in close agreement with ambient winds. Most frequent duration was between 20 and 25 minutes, Fig. 51.

The mesoscale patterns on these two days were quite different. On one a well organized line progressed steadily across the region. On the other there were spots 50 or more miles apart, and there was a tendency for recurrence with more than one storm following roughly the same track at intervals of one to two hours. In Fig. 53 the similarity of position of storm IV with the last cell in VII, VIII with the first cell in VI and of storms V and IX can be noted. The similarity in structure and behavior of the individual thunderstorm complexes on these two days therefore appears significant. In both cases individual cores appeared in sequence, each lasted about 20 minutes, and their motions were roughly in agreement with the ambient winds. The frequently observed motions of complexes to the right of the wind appear to be associated with the tendency of new cells to build to the right of old ones.

3. Relation between intense cores and the surrounding rain

In a thunderstorm complex the mesoscale area of lighter rain appears to be guided by the behavior of the cells within it. This fact suggests that the precipitation within the small mesoscale area may have been formed in convective elements and then been spread by divergence near the top of the layer containing the cells. Each successive cell would add to this general rain area as well as producing a short-lived core of intense rain. This hypothesis appears reasonable in view of the observations of Braham (1952) who analyzed the convergence-divergence pattern in the vicinity of air mass thunderstorms and concluded that the amount of condensate left aloft is twice as great, on the average, as that which is deposited by precipitation. With so much condensate diverged aloft it would not be surprising for a sequence of cells to form a mesoscale area of rain.

The second study concerned with thunderstorm complexes was designed to test

this hypothesis. Several thunderstorm complexes were studied in detail for their entire lifetimes with particular attention being paid to the relation between development of the mesoscale areas and that of the cells during the early stages. Also the total amounts of water deposited by the cells and by the portions of the complexes outside of the cells were computed in order to see whether the entire amount deposited by each complex was of a magnitude which could reasonably have been produced in the observed number of cells. Computed rainfall amounts were based on observed echo areas and computed equivalent rainfall rates. Six thunderstorm complexes were selected which were within range of the radar and were under observation during their entire lifetimes. In addition, a squall line which developed within range of the radar was studied as it formed.

In five of the thunderstorm complexes the first echo was the initial cell. The area of lighter rain formed around this cell and increased in size until the last cell developed. It then diminished in size and disappeared at the termination of the final cell. Examples are in Fig. 54 which shows tracings of the complexes from the PPI at intervals of a few minutes and also the tracks of the cells which each contained. In the sixth case, two separate cells were observed initially and an area of lighter precipitation evolved about each until they combined to form the complex. In the developing squall line on 24 June 1965 the first echoes were also cells. Five of them appeared between 0958 and 1014 EST separated by distances of approximately ten miles, and four others were detected within the following fifteen minutes. Small mesoscale areas formed about each cell; they spread and joined to form a line which was a combination of overlapping complexes containing a number of cells. Thirty cells were observed up to 1100 EST.

RHI data were not taken continuously, hence a detailed history of vertical structure is not available. In the spot observations, often only a single cell surrounded by lighter rain can be seen at a particular azimuth, as in Fig. 55 a. Sometimes both a new cell, the taller nearer one in Fig. 55 b, and a dissipating one can be seen simultaneously. In Fig. 55 c there are two cells and also a broad anvil which has blown out ahead of the complex.

Summaries of the observations and computations are in Table 14-16. Distribution of cell durations is in Fig. 56.

From Table 15 it can be seen that the cell motions were generally in the same range in both direction and speed as the winds in the layer between 700 and 500 mb as reported from the nearest three radiosonde stations. Exceptions are three very slowly moving cells and the cells in complex IV which moved to the right of the wind direction. The motions of the complexes clearly reflect a combination of cell motion and preferred positions for development of new cells. In complexes I, II and VII where most of the new cells formed to the right of the old ones, the complex moved to the right of the average cell motion; the effect is especially pronounced in case II where the cells formed well to the right and the rear. In IV both new cells formed to the left and forward and the complex moved faster and slightly to the left. In several of the complexes the differences in motion are slight.

Computations of the relative amounts of precipitation in Table 16 indicate that the total amount of rainfall outside of the cells is from two to four times as great as that deposited in the intense cores. Since these amounts are of the same order of magnitude and are compatible with the ratios computed by Braham (1952) between deposited precipitation and condensate left aloft, they appear to support

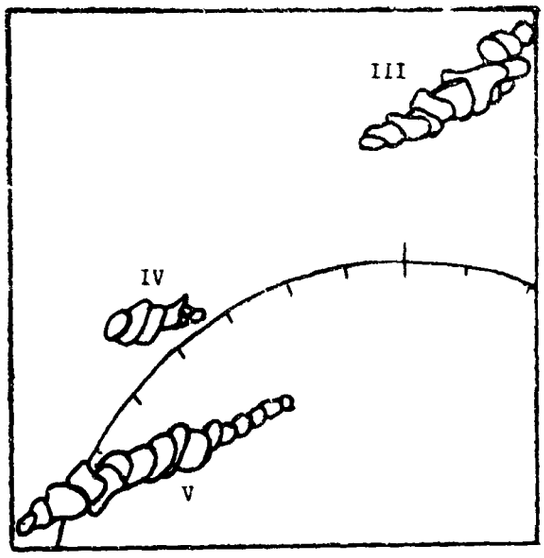

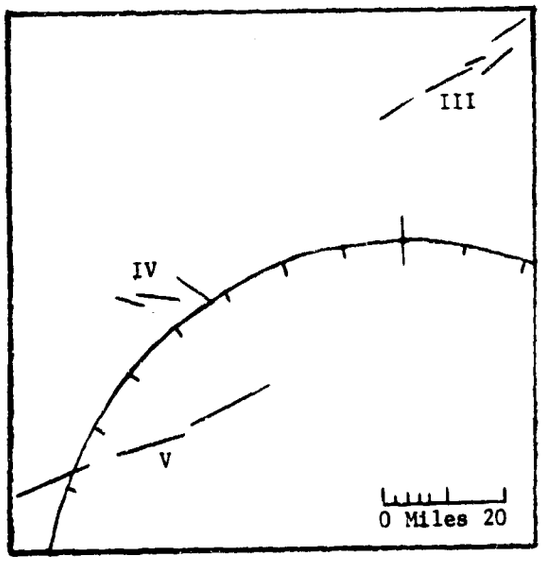

Fig. 54. Motions and development of three thunderstorm complexes on 23 June 1965, and tracks of the individual cells (lower figure).

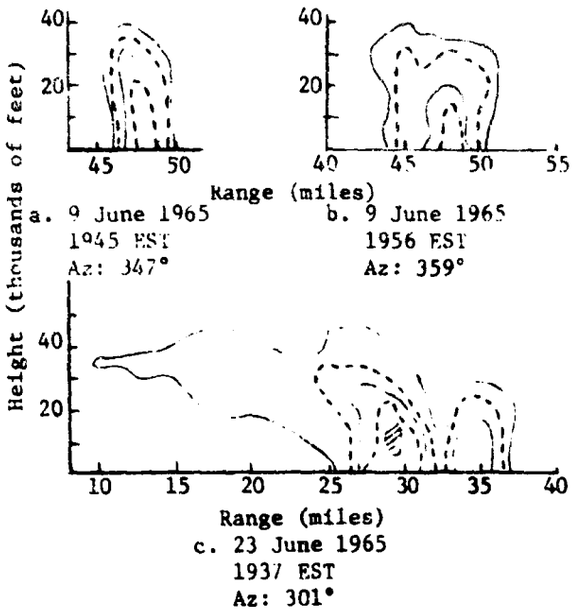

Fig. 55. Examples of vertical structure of thunderstorm complexes. Intensity levels on SCR-615-B radar

Level:	1	3	4	6	8
Key:					
R_e (mm hr^{-1}):	1.5	4	10	45	>100

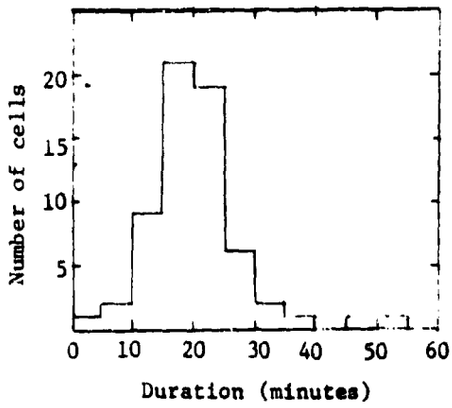

Fig. 56. Distribution of durations of cells in thunderstorm complexes.

the hypothesis. In addition, computations were made of the updraft speeds which would be required to produce the total precipitation in each complex if the cross sections of the assumed updrafts are equal to the average cell area, their depths equal to the depth of the layer containing the cells and their duration the sum of the durations of the cells in the complex. Depending on various assumptions which were made regarding entrainment and amount of condensate evaporated or left aloft as cloud, the computed updraft speeds varied from 4 to 27 meters per second. This range of values is in very good agreement with observed updraft speeds in thunderstorms (Braham, 1952).

Table 14. Durations of complexes and cells and positions of new cell formations.

Case	No. of cells	Duration (min) Complex	Cells (ave.)	Position of new cells relative to prior ones* Initial cell	Right Rear	Right Forward	Left Rear	Left Forward	Center Forward
9 June									
I	3	60	28	1	2				
II	14	150	24	2	12				
23 June									
III	5	65	18	1		2		2	
IV	3	25	15	1				2	
V	3	75	25	1				1	1
24 June									
VI	30		27	9	9	3	3	4	2
28 Aug									
VII	13	120	20	2		5		4	2
Total	71			17	23	10	3	13	5

*Distances between new and old cells are 2-4 km.

4. Requirements for model of thunderstorm complex

The characteristics of all of the thunderstorm complexes which were analyzed for the two studies described here are remarkably similar. We may, therefore, conclude that they provide a reliable and representative description for thunderstorm complexes in general, at least for those which occur in New England. The manner in which they develop and move, the sequence of relatively short-lived intense cores, the order of magnitude of the rainfall rates, and the relative amounts of water deposited by the intense cores and by the small mesoscale precipitation areas around them have been determined. Aspects of the vertical structure have also been observed and described.

The next step will be to develop a model of individual convective elements and mesoscale circulations which would produce precipitation patterns of the type which have been described. The hypothesis has been advanced that all of the precipitation is condensed out in the strong updrafts, which have relatively small dimensions, and then some of the condensate is spread by divergence of the air near the top of the cells and forms the small mesoscale areas of apparently stratiform pre-

Table 15. Comparison of cell motions with wind field and motions of complexes

Case	Wind (700-500 mb)		Cell motions		Complex motion relative to average cell motion	
	Dir* (deg)	Speed (mph)	Dir* (deg)	Speed (mph)		
9 June						
I	250-280	20-40	260-265	18-25	20° right	same speed
II			260-280	7-28	50° right	slower
23 June						
III	235-255	20-40	235-245	16-34	same	
IV			280-300	21-28	10° left	faster
V			240-250	32-45	10° left	same speed
24 June						
VI	240-265	25-55	255-270	20-43	10° right	same speed
28 Aug						
VII	240-260	35-75	230-250	30-49	10° right	same speed

* Direction from which air and cells move.

Table 16. Rainfall rates and amounts in complexes and cells

Case	Rainfall rate ($mm\ hr^{-1}$)		Precipitation Amounts ($10^{11}\ m^3$ of water)		
	in cells (ave)	outside of cells	in cells	outside of cells	Total
9 June					
I	15	1-10	0.5	2.2	2.7
II	70	1-25	31	36	67
23 June					
III	30	1-20	1.8	3.9	5.7
IV	8	1-4	0.2	0.5	0.7
V	20	1-8	0.9	3.3	4.2
24 June					
VI	20	1-15	5	14	19
28 Aug					
VII	60	2-40	13	29	42

cipitation. In this context stratiform is used to mean that the precipitation is fairly uniform in the horizontal over distances which are large compared with its depth. The observations and computations appear to support this hypothesis.

The model, then, should take into account the transient nature of the cores by incorporating some form of the bubble theory of convection. The model developed by the Thunderstorm Project (Byers and Braham, 1949) for the basic circulation appears to be applicable in principle to the thunderstorm complexes in New England. It should be amplified, however, to include a more specific description of the mesoscale convergence-divergence pattern and the entrainment mechanism so that an explanation is provided for the manner in which some of the precipitation particles spread into a mesoscale area while others remain in a well defined core. The role of wind shear should also be included in the model because in real situations there is usually significant shear in the layer containing the cells. Finally, the growth of individual hydrometeors and the manner in which they fall, both relative to the air and relative to the earth, clearly must affect the resulting precipitation patterns which are depicted by the radar, and they must therefore be taken into account.

D. Cell Model for Computing Vertical Transport from Radar and Rain Gauge Data

1. Background considerations

There is no doubt that small-scale convection is an extremely common phenomenon in the atmosphere. In fact, some evidence of convective activity can be seen in almost every cloud formation and precipitation pattern, even those which are generally stratiform in structure. The effects of this convection may well be significant to the dynamics and energetics of the larger-scale circulation through release of latent heat and vertical transport of such quantities as momentum, sensible heat and vorticity. It is generally recognized that in the tropics the latent heat released in convective showers provides energy for the initiation and maintenance of larger-scale air motions. Extensive convective activity and mesoscale phenomena which radar has shown to occur in extratropical cyclones may well have a similar effect. The need for a better understanding of small-scale circulations and their relations to the larger-scale events has become clear, but the problem is a difficult one to attack. Techniques employed to investigate the larger-scale motions (numerical integration of the dynamic equations or statistical analyses similar to those employed by Starr and others, 1966) would require an observational network of such density as to be prohibitive, except for limited studies or particular occurrences. Furthermore, dynamic studies of small-scale phenomena are greatly complicated by the necessity of including in the equations the effects of latent heat release and the forces exerted by falling hydrometeors.

Because of the difficulties encountered in attempting a direct and comprehensive analysis, either descriptive or dynamic, of small-scale convective phenomena in the atmosphere, we have adopted an indirect approach, based on a detailed and quantitative description of the distribution of precipitation. After evaluation of the relative amounts of precipitation produced by stratiform and convective lifting, the small-scale air motions required to produce the observed patterns are deduced. Such an approach is feasible because of the availability of radar and rain-gauge records which permit a description of the precipitation in three dimensions and its variation with time. The approach should also prove fruitful because the occurrence of precipitation, which is the observed quantity, is intimately related both to the release of latent heat and to small-scale convection.

The very steep lapse rates required for significant convection to take place without condensation are infrequent. Therefore an analysis of the precipitation in a particular region over a period of time would include all situations with significant small-scale convective activity, and would provide statistics concerning its characteristics and frequency of occurrence.

It is recognized that motion fields cannot be deduced directly and unequivocably from the precipitation patterns which they produce. However, the resulting precipitation patterns do prescribe limits for the motions which are sufficiently definite to permit meaningful investigation of their role in the vertical transport of various quantities.

2. Cell model relating vertical motion and precipitation

For convective cells the dimensions, durations, precipitation rate, and total water deposited can be deduced directly from the data. In the model, which relates total amount of lifting to total amount of precipitation, certain assumptions are made regarding the vertical velocity profile, the entrainment and divergence at various levels, and the amount of condensate which remains aloft as cloud. After the model is described the magnitude of the uncertainties associated with these assumptions will be considered.

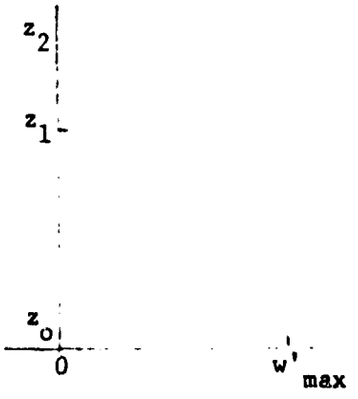

Fig. 57. Linear profile for updraft speed.

It is assumed that the updraft starts from an initial disturbance near the bottom of the unstable layer, z_o in Fig. 57. As the initial parcel of air rises its vertical speed, w', increases linearly until it reaches a maximum at level z_1; it then decreases to zero at z_2. The heights z_o and z_2 are obtained from the data as described in section III, B, 2; z_1 is near the level where buoyant forces are ceasing and further lifting is due to inertia. This level is likely to be considerably nearer to z_2 than z_o; if its location cannot be deduced from the radiosonde data it is reasonable to place it in the upper third of the layer which contains the cells. Primed quantities indicate those inside the updraft and unprimed ones those in the environment. The environmental values of temperature, humidity and horizontal wind are obtained from radiosonde soundings. Inside the updraft the air must be saturated and the temperature is assumed to be equal to that of the environment at the same level. Actually, it must be slightly greater whenever the updraft speed is increasing, but empirical evidence and dynamic considerations indicate that the difference is small (Austin, 1951).

In order to maintain mass continuity, air is entrained from the sides and also enters from the base of the updraft below the initial parcel. The cross section of the updraft is assumed to remain constant and the variation of air density with height is neglected at this stage of the discussion. In applying the model to individual storms where the depth and position of the layer containing the cells are known, the density variation can be taken into consideration. For simplicity in this presentation we assume a density of one kilogram per cubic meter.

Vertical mass transport through any layer and the total amount of condensate are both considered in terms of the mass of air which rises through level z_1. For every cubic meter of air rising through z_1, equal parts have been drawn from all levels below and they are assumed to mix thoroughly in the updraft. Similarly, equal amounts of air are diverged out of the updraft in each layer above z_1 up to z_2. Thus for every parcel of air rising through z_1 the entire layer is involved since a small portion of it started near z_o at some previous time and a small portion of it will eventually come close to z_2. We cannot assume that the updraft speed actually begins and ends at a zero or infinitesimal value because the length of time required for the disturbance to go from the bottom to the top of the layer would then be infinite. In fact, any computed value for the time of rise is more dependent on the selected initial and final values of updraft speed than on the value assigned to w'_{max}. Fortunately, the model does not require specific assumptions about the time scale. These comments point up the fact that in an actual situation the original disturbance must be finite.

We further note that as the initial disturbance rises, the top of the cloud (or cell, if it is already embedded in cloud or precipitation) rises through the layer, the region above it being undisturbed and the region below it forming the updraft. Any parcel of air in the updraft follows the same pattern of entrainment and increasing vertical velocity below z_1 with divergence and slowing above z_1 as outlined for the initial disturbance. It is not necessary, however, for the updraft to reach a stage where it extends all the way from the bottom to the top of the layer as a complete column of rising air. Rising motion may cease in the lower portions before the initial disturbance reaches the top. Moreover the value of w'_{max} does not have to be identical for all parcels; it may build up and decrease during the lifetimes of the updraft or may vary over its horizontal cross section. But the entrainment and divergence pattern and the condensation amounts, as discussed below, are assumed to be the same for each kilogram of air rising through z_1.

Continuity requires that at any level downward mass transport in regions outside of the cells must equal the amount which is transported upward within the updrafts. This transport is assumed to take place as a uniform downward shift over a relatively large area.

We consider now the amount of condensate. For every cubic meter or kilogram of air rising through z_1, the fraction $dz/(z_1 - z_o)$ is drawn from a layer of thickness dz at any level z below z_1. The mixing ratio of this air is q(z). By the time it has been raised to level z_1 it has a mixing ratio of $q'(z_1)$ and the amount of moisture which has been condensed out is:

$$\frac{dz}{z_1 - z_o} [q(z) - q'(z_1)] \qquad (7)$$

In this expression q(z) is the mixing ratio indicated by the radiosonde at level z and q'(z) is the saturation mixing ratio for the temperature observed at z. Above

z_1 moisture is condensed out at the moist adiabatic rate and simultaneously air is lost to the environment through divergence. For every kilogram which goes through z_1 the fraction $dz/(z_2-z_1)$ is diverged into a layer of thickness dz at any level z, and the moisture condensed out of it during its rise from z_1 to z is:

$$\frac{dz}{z_2-z_1}\,[q'(z_1) - q'(z)] \tag{8}$$

The total amount of moisture condensed out for each kilogram of air rising through z_1, during its entire ascent is then:

$$\frac{1}{z_1-z_o}\int_{z_o}^{z_1}[q(z) - q'(z_1)]\,dz + \frac{1}{z_2-z_1}\int_{z_1}^{z_2}[q'(z_1) - q'(z)]\,dz \tag{9}$$

These integrals can be evaluated for a particular occasion by inserting the appropriate values of heights and mixing ratios.

In reality, the moisture condensed in the updraft exceeds the precipitation deposited by the shower because the air which diverges to the environment above z_1, doubtless contains condensate. Braham (1952) estimated that for an average air-mass thunderstorm condensate evaporated from the sides or left as cloud is nearly twice as much as that which is deposited as precipitation. For kinematic models of cells in a saturated atmosphere, Kessler (1967) found the amount left as cloud to be about one-third of that precipitated. If the assumption is made that equal amounts of condensate are precipitated and are left as cloud or evaporated aloft, the error in estimating the total condensate and the corresponding vertical transport of air would be less than a factor of two.

Braham (1952) also estimated a large amount of condensate to be evaporated in the downdraft of a thunderstorm. This effect is not included here because the upward transport of air required to condense out this moisture would be balanced by the downward transport in the downdraft.

If, instead of a linear profile, as in Fig. 57, a constant updraft with no entrainment is assumed, all of the air is transported from z_o to z_2 and the total condensate for each cubic meter rising through z_1 is doubled. If it is assumed that the entrainment and divergence are greater near the base and top of the cell, respectively, than near the center, as for example in a parabolic updraft profile, the vertical mass transport required to produce a given amount of condensate is less than for the linear profile but greater than for the constant updraft.

It appears, then, that there are uncertainties of a factor of 2-3 in computations of the vertical transport of air by small-scale convection based on measured amounts of convective precipitation and observations of the top and bottom of the layer containing the cells. The uncertainties arise primarily from lack of knowledge concerning the details of entrainment and the amounts of condensate lost to the environment through divergence rather than being deposited as precipitation.

3. Vertical transport of other quantities

Once the mass transport of air from one level to another by small-scale convection is determined, the transport of any other quantity which varies with height in the layer can be computed. In the case of horizontal momentum the wind values at any level are assigned from rawinsonde data. The horizontal momentum of the rising air at any level inside the cells is the integrated value over the layers

from which the air was drawn. That of the descending air is the environmental or synoptic-scale value at the given level. If, for example, the wind is westerly and increases linearly with height in the layer between z_0 and z_1, the ascending air at z_1 has a horizontal speed equal to $\frac{U(z_1) + U(z_0)}{2}$ while that of the descending air is $U(z_1)$. Therefore, for each kilogram of air which rises through z_1 in the updraft there is a net downward transport of westerly momentum of $\frac{U(z_1)-U(z_0)}{2}$ kg m sec^{-1}.

Vertical transports of sensible heat and moisture can be computed in a manner similar to that outlined for horizontal momentum. In the case of vorticity, transports can be computed if the environmental values at different levels are known. In addition, however, there may be generation of vorticity through the divergence and vertical motions associated with the cells. This source of vorticity and its effect on the large-scale pattern must be investigated.

It is recognized that none of the quantities, either directly observed or derived through application of the model, are known accurately, that is, within a few percent. Moreover, one cannot make a general estimate of the overall reliability because the accuracy with which the precipitation is depicted by the radar varies considerably from storm to storm. At each step the uncertainties appear to be no worse than a factor of two, so that computations of the vertical transports should certainly give the correct order of magnitude and probably be reliable within a factor of four. This accuracy is sufficient to determine the significance of these effects as compared with the transports accomplished by the larger-scale circulations. There is every reason to believe that as more detailed quantitative radar data become available and are analyzed, the details of cellular convection will be better understood and greater accuracy can be achieved through suitable refinement of the model.

E. The Role of Cellular Convection Within an Extratropical Cyclone

1. Introduction

The National Hurricane Research Project has established the importance of cellular convection to the development and maintenance of tropical cyclones. In the present view, hurricanes are forced circulations driven by the latent heat released in organized convection. Riehl and Malkus (1961) have demonstrated that important dynamic and thermodynamic processes are concentrated into narrow convective zones within the hurricane core region and have shown that a hurricane's intensity is related to the mass of air channeled up through "hot towers" as opposed to that lifted by "mass circulations".

Although radar investigations have demonstrated that cellular convection frequently occurs within extratropical cyclones, it has generally been considered a relatively unimportant dynamic entity to the storm system. Though efforts have been made recently to formulate some of the effects of convection by parameterizing them with respect to the large-scale flow, synoptic-scale motions and processes are still assumed to dominate within intense mid-latitude cyclones.

The purpose of this study is to examine the validity of such an assumption by determining the convective motions within a selected storm and assessing their importance. This is done by ascertaining the extent to which the vertical mass flux and other physical processes are concentrated into convective cells within the storm system rather than being uniformly distributed over synoptic-scale regions.

More specifically, the quantities to be considered are the relative and absolute contributions of the cumulus and synoptic-scale lifting to the total precipitation deposited, latent heat released, and vertical transports of mass, momentum, and heat.

2. Convective precipitation and latent heat release

The major cyclonic development that occurred over the eastern United States, 29-30 November 1963, was chosen for analysis. The storm developed rapidly while moving northeastward from the Gulf of Mexico along the Appalachians into New England (Fig. 58). The circulation both at the surface and aloft dominated the eastern third of North America. Copious rainfall accompanied the storm, and both surface synoptic reports and radar indicated the presence of extensive convective shower activity. Maximum precipitation rates and the bulk of convective activity appeared to be concentrated north of the low and just east of the inverted trough that lay parallel to and ahead of the warm front. Precipitation rates and total amounts for the storm became more uniform the further west one proceeded from the warm front.

The investigation was restricted to an area of around 7.4×10^5 km^2 extending southward from Maine to North Carolina, and westward to eastern Tennessee and Ohio. The track of the low pressure center was such that a relatively symmetric sample of the storm was obtained in both space and time as it passed through the region on into Canada. The region was subdivided into squares 1° latitude by 1° longitude and an average total precipitation amount was determined for each from precipitation totals listed in the U.S. Weather Bureau Climatological Data. The average areal depth for the entire region was 1.4 inches, so that the total volume of water deposited was 2.7×10^{10} m^3, corresponding to a total latent heat release of 6.7×10^{16} kj. Averaged over the thirty hour storm duration the rate of latent heating is 6.2×10^{11} kj sec^{-1}, which corresponds to a value found by Palmen and Halopainen (1962) (8.4×10^{11} kj sec^{-1}) near the central part of an intense extratropical cyclone.

The characteristics and amount of convective activity were determined from detailed analysis of tipping-bucket raingauge records at 28 stations scattered about the region and radar data from M.I.T., Nantucket (ACK), Atlantic City (ACY), Washington (DCA), Buffalo (BUF), and Cincinnati (CVG). Resolution of the gauges was on the order of one minute. This proved to be adequate in depicting the difference between steady stratiform rain and rainfall fluctuating rapidly in space and time as is produced in convective cells (Fig. 59). The first four radars show very similar PPI patterns with both individual cells and groups of cells imbedded within stratiform precipitation. In marked contrast, those at Buffalo and Cincinnati showed only general stratiform precipitation except for an occasional cell or cell group at Buffalo. Individual cells averaged around 1-2 km in diameter while areas containing cell arrays averaged 20 x 30 km in horizontal dimension. Although RHI photographs were available only for the M.I.T. radar, it appeared from the observer's comments on the Weather Bureau radar data sheets that the vertical structure of the cells was similar to those which occurred near M.I.T. Cell heights were generally between four and five kilometers. Raingauges indicated an average precipitation rate beneath the cells of 20 mm hr^{-1} (.8" hr^{-1}), but rates often exceeded 50 mm hr^{-1} (2" hr^{-1}).

The percentage of the total rain that was produced in convective cells at each recording gauge station was estimated as follows: for each hour that precipitation was recorded, the fairly steady rate, or plateau, out of which the shower

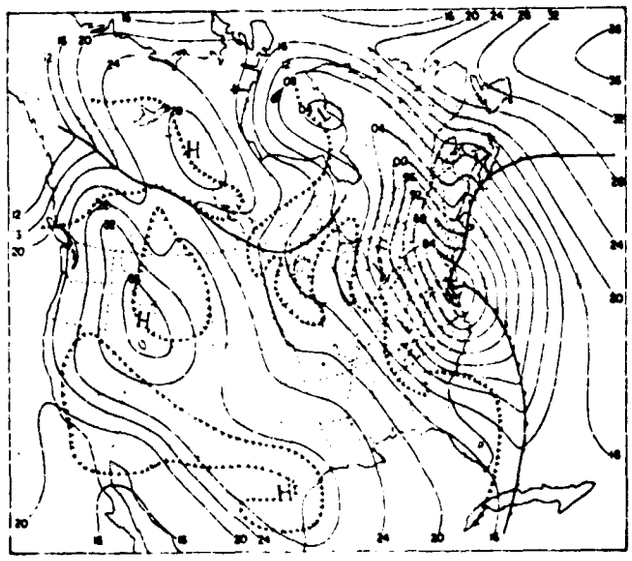

Fig. 58. Surface analysis, 00Z 30 November 1963. (after Danielsen, 1966)

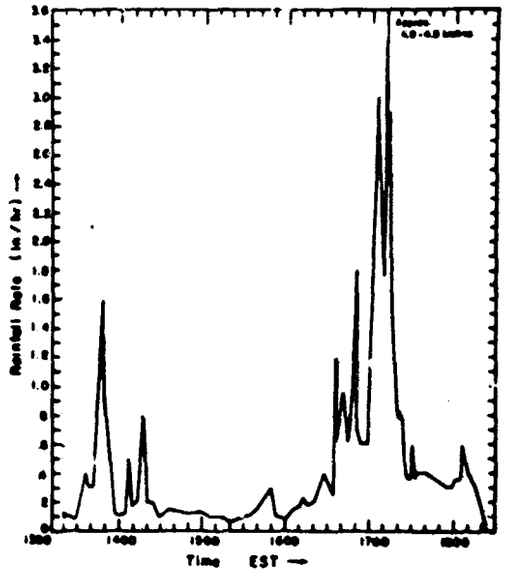

Showery type
(Boston)

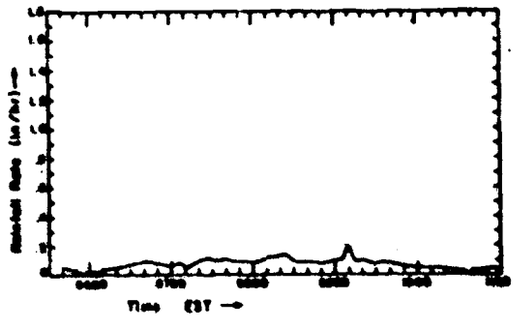

Non-convective
(Parkersburg, W. Va.)

Fig. 59. Examples of rain-gauge records, 30 November 1963.

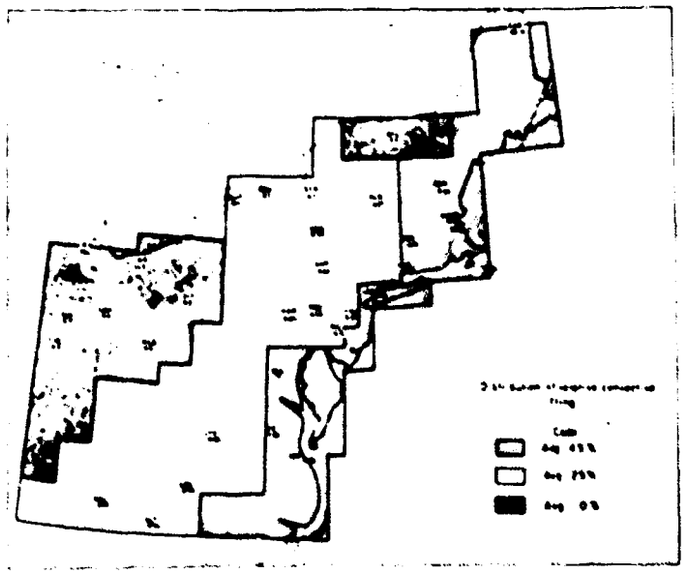

Fig. 60. Distribution of relative contribution of convective lifting to total precipitation in storm of 29-30 November 1963.

peaks rise was determined. The difference between this and the hourly total is ascribed to cellular convection. In this way the precipitation formed within the sharp and transient vertical currents of the cells is separated from that produced by the relatively uniform upglide motion of the synoptic-scale lifting. The ratio between the sum of the hourly convective amounts to the total precipitation at the station was taken to be the percent convective contribution for that station. An important point to be noted is that within a cell group the precipitation rate between the cells is generally somewhat greater than that of the large-scale environment. This seems to indicate that the small areas containing cell arrays are as a whole a region of enhanced upward motion. More specifically, it appears that the cell arrays are within a convergent field one order larger than the convective scale and one order smaller than the synoptic scale; however, because the horizontal extent of such mesoscale areas, as they are termed, is much larger than their vertical dimensions, the enhanced rate between the cells is partitioned to large-scale lifting. Any consideration of the significance of the mesoscale areas in themselves to the precipitation and vertical transports must await a suitable dynamic model to describe their circulations.

The distribution of the relative contribution of the convective-scale motions to the total precipitation is presented in Fig. 60. The breakdown into regions was aided by an apparent relationship between the total rainfall for any given hour and its convective contribution. For example, .1" to .2" in one hour generally had a 20-40% convective contribution. For a few stations in regions where there were no data from tipping-bucket gauges, this relationship was used to estimate the percent contributions of convective precipitation from the reported hourly amounts.

Readily apparent in Fig. 60 are three well-defined bands parallel to the coast and to the mean position of the warm front, with decreasing values as one proceeds inland. The 16% figure recorded by the Trenton, New Jersey (TTN) gauge appears unrepresentative in light of the hourly totals of surrounding stations. In the region as a whole, 30% of the total water produced by the storm can be attributed to the convective cells, the balance being produced by the synoptic-scale rising motion of the cyclonic system. Equal percentages of latent heat are released on each scale.

3. Vertical mass transports

The vertical transport of mass accomplished by the cellular mode of lifting was deduced using a slightly modified version of the model described in the previous section. Instead of assuming a linear vertical velocity profile, the model was modified so that a greater portion of the air is entrained near the cell base, and a correspondingly larger portion is diverged near the top of the cell. For this storm, z_1 was around 700 mb, and the mass flux upwards through this level was evaluated to be 2.6×10^{15} kg.

The mass flux produced by large-scale lifting was also evaluated on the basis of the precipitation deposited by that scale. Radar data and radiosonde soundings indicated that stratiform precipitation was being produced in a saturated environment up to a height of 6.5 km. Assuming moist adiabatic ascent to 6.5 km, a constant updraft speed of 1 cm/sec, and a mean vertical temperature distribution for the region based on the soundings, an average large-scale precipitation rate may be obtained from the diagram of Fulks (1935). At this precipitation rate, the time necessary to produce the observed volume of stratiform precipitation was determined. Multiplied by a mean air density, the area of the region, and the assumed

vertical velocity of 1 cm/sec, this time establishes the mass transport. It should be recognized that the use of an arbitrary value of the vertical velocity prescribes a corresponding arbitrary time interval, but does not affect the computed mass flux required to produce a given amount of precipitation.

On the basis of these considerations, the stratiform mass flux through 700 mb was evaluated to be 1.4×10^{15} kg. Within the limits of accuracy of the calculations, the factor of two difference between this result and that obtained for the convective flux is probably not significant. They are of the same order of magnitude indicating that roughly the same amount of air is funnelled by convective cells upwards through 700 mb as is carried through this level by the cyclonic-scale lifting.

4. Vertical momentum transports

It is possible to calculate the vertical transport of momentum by the cumulus and synoptic-scale motions repectively by assuming that each transports downward through a given level precisely the same amount of mass it has transported upwards. On the large scale, the sinking motion of the storm system follows immediately behind the area of rising motion and precipitation. On the convective scale, the compensating downward currents are presumed to occur as a uniform downward shift of mass between the cells.

A non-zero vertical momentum transport requires a correlation between the wind velocity and the mass flux. For this study, only the momentum associated with the zonal wind component, U, is considered. If the value of U for the air transported upwards through a given level is smaller than that for the air brought down, the correlation is negative. That is, momentum has been transported downwards from higher to lower levels.

The transport through a level may be written as $M_u U'_u + M_d U'_d$ where U'_u and U'_d are the departures of the zonal wind component from some space and time mean, $\bar{U}$, in the rising and sinking region respectively.

The large-scale momentum transport was first evaluated at the 500 mb level, which in this storm lies well above the cells. Vertical velocity computations performed for this storm by Danielsen (1966) were used to pinpoint the regions of ascent and descent on the large scale. By superimposing the vertical velocity field upon the 500-mb NMC maps, it was readily apparent that the descending air had a larger westerly wind component than that which was ascending; hence, a downward momentum transport. A quantitative estimate of the transport was obtained as follows: at each NMC grid point over eastern North America the average of the U value between 12Z Nov 29 and 00Z Nov 30 was obtained. $\bar{U}$ was taken to be the space average of these values, with U'_u and U'_d the average departures therefrom in the rising and sinking region respectively. On the basis of these considerations the momentum transport was determined to be 22×10^{15} kg m sec^{-1}. At 700 mb there was little correlation between U and the mass flux, and the computed large-scale transport was several orders of magnitude smaller.

The cumulus-scale transport through 700 mb was evaluated by assuming that the air entrained into a cell at any level would tend to conserve its horizontal momentum as it rose rapidly in a narrow channel through this level. From the radiosonde data and radar echo velocities, it was apparent that the lower portion of the cells was imbedded in a region of intense vertical shear. Consequently, since $\partial U/\partial z > 0$, the momentum of the air at 700 mb immediately surrounding the cells would be greater

than that of the air within the cells. For computation purposes this difference, U'_u, was taken as one-half of the average of $(U_{950} - U_{700})$ of all radiosonde stations in areas where convective activity was occurring. The numerical value ascertained was around -5 m sec^{-1}. U'_d was assumed zero. The momentum transport, MU'_u, is therefore downwards, having a magnitude of 20 x 10^{15} kg m sec^{-1}. This value is nearly equal in sign and magnitude to that obtained for the large-scale transport of momentum at 500 mb. The obvious conclusion, then, is that the large-scale motions of the storm system are performing the momentum transport at high levels, whereas the bulk of the transport at low levels is accomplished by the cellular mode of motion.

5. Vertical transports of sensible heat

The sensible heat transport may be written as $C_p(M_uT'_u + M_dT'_d)$ where C_p is the specific heat of air at constant pressure. T'_u and T'_d for the large-scale motions were obtained in a manner exactly analagous to that used to ascertain U'_u and U'_d. For the cellular motion, the difference between the temperature of the rising air and the environmental air was taken as 0.2°C.

At 700 mb it was found that the sensible heat transport upwards by the large-scale motions was 9 x 10^{18} cal. Transport by cellular motions was two orders of magnitude smaller.

It is interesting to note that the large-scale heat transport was of the same magnitude as the total release of latent heat.

6. Conclusion

It has been shown that cellular convection imbedded within an intense extra-tropical cyclone accounts for a significant fraction of the total precipitation produced, latent heat energy released, as well as of the vertical transports of mass and momentum. It appears to be of less importance to the vertical transport of sensible heat.

In so far as this storm is representative of other intense mid-latitude cyclones, it appears that certain physical processes usually attributed solely to the cyclone scale are to a significant degree highly concentrated into regions of narrow horizontal extent. The implications of such localization, especially to numerical forecasting, should receive close scrutiny.

IV. CONCLUSION

The question regarding the usefulness of radar as an instrument for measuring precipitation either at the surface or aloft has been a controversial one for the past two decades. It has been recognized that this instrument has unique potential as far as coverage is concerned, but that the accuracy is inherently limited because precipitation rate and radar reflectivity are not directly related. Sufficient research has now been done at various laboratories in the United States and other countries to permit quantitative evaluation of its performance and potential, and to provide a basis for determining the conditions where the value of the information justifies the expense of installation and maintenance. In this report recent contributions of the Weather Radar Research Project at M.I.T. have been summarized and the following conclusions have been drawn.

The uncertainties related to drop-size distributions are approximately a factor of two in measured rainfall rate provided the best empirical Z-R relation is used for a particular geographical location. This factor does not necessarily represent the ultimate limit in accuracy which can be achieved. There is evidence that when the physical processes which determine the drop-size distributions are better understood, it may be possible to make allowance for differences from storm to storm and the results will be better than those obtainable with a single general empirical relation. The procedure will, however, have to be more meaningful than the rather subjective classification into "continuous rain", "showers", and "thunderstorms", which has been tried and does not give significant improvement.

In storms which are primarily convective, the above-mentioned accuracy of a factor of two can be achieved over areas on the order of 10^5 km^2 provided the instrumental errors are kept to a minimum, about ± 2 db. Moreover, this represents a higher degree of accuracy for areal amounts and distributions than can be obtained with a network of rain gauges since they cannot adequately sample convective showers. Presence of hail in intense convective storms sharply increases the reflectivity factor. For each region where observations are made it is necessary to determine the critical value of Z which is indicative of hail and to consider the corresponding equivalent rainfall rate as the maximum which occurs.

In widespread rain, uncertainties which may be quite large, say a factor of three or four, may be introduced by changes in the character or intensity of the precipitation as it falls to the ground from the volume sampled by the radar. The corresponding discrepancies between the precipitation indicated by the radar and that reaching the surface would not be constant but would increase with range. Radar measurements of rainfall in widespread storms should therefore be interpreted with caution and should be correlated closely with rain-gauge observations.

In the case of snowstorms empirical Z-R relations are based on a much smaller sample than for rain and are very uncertain. Also the reflectivity diminishes rapidly with height. Therefore both types of error are large for snowstorms and, at this stage, satisfactory measurements of precipitation rates cannot be made with a radar.

In order to achieve instrumental accuracy of ± 2 db it is necessary to have circuits for averaging the fluctuating signals and techniques for proper calibration, which includes direct measurement of the radar parameters particularly the antenna gain and the power pattern in the beam. Furthermore, it is mandatory that the wave length be long enough so that measurements are not affected by attenuation

in heavy rain or melting snow. Computations and observations have demonstrated that at 10 cm attenuation is negligible and at 3 cm it is prohibitive. Experimental evidence at 5.5 cm is lacking; it appears that this wave length would be satisfactory in many situations but would suffer from attenuation in intense convective storms.

Instrumenting a radar for accurate quantitative measurements is neither easy nor inexpensive. With modern integrated circuits and solid state components, however, and with the prototype devices already constructed and tested, the cost is moderate (perhaps 20 per cent of the cost of the radar itself) while the value of the data is increased by an inestimable amount when it progresses from qualitative to quantitative. In the opinion of this author, one of the major sources of disillusionment in the potential of radar for measuring precipitation lies in the poor results of experiments in which the observers failed to recognize large uncertainties in the data which were present because the radars were not adequately instrumented and calibrated.

Equipment which employs digital techniques for signal averaging, range normalization, and quantization into intensity levels has been designed and constructed at the Weather Radar Laboratory at M.I.T. and is described in this report. Also a special-purpose computer for on-the-spot data processing and digital display is under construction. This device employs a new computational technique which is particularly suited to the handling of weather radar data because of the large storage capacity.

Instrumentation for quantitative measurements has been developed at two or three other research laboratories, but they employ analog methods and hence lack the reliability and stability which the digital instruments have displayed. Use of auxiliary equipment for quantitative measurements has not yet been extended to operational installations. It is recommended that where 10-cm radars with adequate sensitivity and resolution are in operation such instruments be added as soon as possible, because the enhanced value of the data would undoubtedly offset the cost of the equipment. Also it is strongly urged that in the tropics and other regions where convective showers are the predominant form of precipitation, properly instrumented 10-cm radars be set up, since it is doubtful that satisfactory observations of the precipitation can be obtained by any other means.

In addition to providing information on amounts and distribution of precipitation, quantitative radar observations are proving to be exceedingly valuable in basic meteorological research concerned with mesoscale circulations, convective lifting and precipitation processes. The studies summarized in this report provide detailed descriptions of the structure and behavior of mesoscale precipitation areas and convective cells both in extratropical cyclones and in thunderstorm complexes. Such descriptions will serve as a basis for physical and numerical studies of mesoscale phenomena. Also, pilot studies have been performed to demonstrate the feasibility of and to illustrate techniques for using quantitative radar data to explore the dynamic and energetic interdependence of small-scale and synoptic-scale atmospheric circulations. The promising results of these preliminary studies certainly warrant continuation of this type of research.

REFERENCES

Atlas, D., 1964: Advances in radar meteorology. Advances in Geophysics, Vol. 10, Academic Press, N.Y., pp 317-478.

Austin, J.M., 1951: Cumulus convection and entrainment. Compendium of Meteor., Amer. Meteor. Soc., Boston, 694-704.

Austin, P.M., 1952: A study of the amplitude distribution function for radar echoes from precipitation. Tech. Rep. No. 17, Weather Radar Research, Dept. of Met., M.I.T.

Austin, P.M. and S.G. Geotis, 1960: The radar equation parameters. Proc. Eighth Wea. Rad. Conf., Amer. Met. Soc., Boston, pp 15-22.

Austin, P.M. and E.L. Williams, Jr., 1951: Comparison of radar signal intensity and precipitation rate. Tech. Rep. No. 14, Weather Radar Res., Dept. of Met., M.I.T.

Battan, L.J., 1959: Radar Meteorology, Univ. of Chicago Press, Chicago, 161 pp.

Battan, L.J., and B.M. Herman, 1962: The radar cross section of "spongy" ice spheres. J. Geophys. Res. 67, 5139-5145.

Boucher, R.J., 1951: Results of measurement of raindrop size. Proc. Conf. on Water Resources, Ill. State Water Survey Bull. 41, Urbana.

Braham, R.R., Jr. 1952: The water and energy budgets of the thunderstorm and their relation to thunderstorm development. J. Met. 9, 227-242.

Byers, R.H., and R.R. Braham, Jr. 1949: The Thunderstorm, Report of the Thunderstorm Project, Dept. of Commerce, Washington, 287 pp.

Cochran, H.G., 1961: A numerical description of New England squall lines. S.M. Thesis, Dept. of Meteor., M.I.T.

Danielsen, E.F., 1966: Research in four-dimensional diagnosis of cyclonic cloud systems. Scientific Rep. No. 1, Contract No. AF19(628)4777, The Univ. of Cal. at Los Angeles, 33 pp.

Donaldson, R.J., Jr., 1961: Radar reflectivity profiles in thunderstorms. J. Meteor. 18, 292-305.

Douglas, R.H., 1960: Size distributions, ice contents, and radar reflectivities of hail in Alberta. Nubila III, 5-11.

Douglas, R.H., and W. Hitschfeld, 1961: Radar reflectivities of hail samples. Proc. 9th Wea. Radar Conf. Amer. Meteor. Soc., Boston, 147-152.

Dumoulin, G., and A. Cogomblea, 1966: A comparison of radar values of precipitation intensities and rainfall rate from a raingauge. Proc. 12th Conf. on Radar Meteor., Amer. Meteor. Soc., Boston, 190-197.

Fulks, J.R., 1935: Rate of precipitation from adiabatically ascending air. Mon.

Wea. Rev., 63, 291-294.

Geotis, S.G., 1963: Some radar measurements of hailstorms, J. Appl. Meteor., 2, 270-275.

Geotis, S.G., 1968: Drop-size distributions in eastern Massachusetts. Proc. 13th Radar Meteor. Conf., Amer. Meteor. Soc., Boston, 154-157.

Gill, A., 1962: Introduction to the theory of finite-state machines. McGraw Hill Book Co., New York.

Gunn, K.L.S., and T.W.R. East, 1954: The microwave properties of precipitation particles. Quart. J. Roy. Meteor. Soc., 80, 522-545.

Gunn, K.L.S. and J.S. Marshall, 1958: The distribution with size of aggregate snowflakes. J. Meteor., 15, 452-466.

Herman, B.M., and L.J. Battan, 1961a: Calculation of Mie back scattering of microwaves from ice spheres. Quart. J. Roy. Meteor. Soc., 87, 223-230.

Herman, B.M., and L.J. Battan, 1961b: Calculation of Mie back scattering from melting ice spheres. J. Meteor., 18, 468-478.

Hoegl, D.U., 1965: An F-M sweep integrator for quantitative radar displays. Res. Rep. No. 37, Weather Radar Research, Dept. of Meteor., M.I.T.

Imai, I., M. Fujiwara, I. Ichimura, and Y. Toyama, 1955: Radar reflectivity of falling snow. Papers in Meteor. Geophys. 6, Tokyo, 130-139.

Joss, J. and A. Waldvogel, 1967: Ein spektrograph fur niederschlagstropfen mit automatischer auswertung. Pure and Appl. Geophys. Vol. 68, 240-246.

Kessler, E. 1967: On the continuity of water substance. Tech. Memo IERTM-NSSL 33, U.S. Dept. of Commerce, ESSA, 125 pp.

Kodaira, N., 1959: Quantitative mapping of radar weather echoes. Res. Rep. No. 30, Weather Radar Res., Dept. of Meteor., M.I.T.

Marshall, J.S., and W. Hitschfeld, 1953: The interpretation of the fluctuating echo for randomly distributed scatterers. Part I. Can. J. Phys., 31, 962-994.

Marshall, J.S. and W.M.K. Palmer, 1948: The distribution of raindrops with size. J. Meteor., 5, 165-166.

McCallister, J., J.L. Teague and C.E. Vicroy, 1966: Operational radar rainfall measurements. Proc. 12th Conf. on Radar Meteor., Amer. Meteor. Soc., Boston, 208-215.

Mie, G., 1908: Beitrage zur optik truber medien, speziell kolloidaler metallosungen. Ann. Phys. XXV, 377.

Mueller, E.A., 1966: Radar cross sections from drop spectra. Appendix to Tech. Report ECOM-00032-F, Ill. State Water Survey, Univ. of Illinois, Urbana.

Mueller, E.A., and A.L. Sims, 1966: The influence of sampling volume on raindrop size spectra. Proc. 12th Conf. on Radar Meteor., Amer. Meteor. Soc., Boston, 135-141.

Palmen, E., and E.O. Halopainen, 1962: Divergence, vertical velocity, and conversion between potential and kinetic energy in an extratropical disturbance. Geophysics, 8, 87-113.

Riehl, H. and J.R. Malkus, 1961: Some aspects of Hurricane Daisy, 1958: Rep. No. 35, National Hurricane Research Project, 63 pp.

Schaffner, M.R., 1963: A processor for weather radar data. Proc. 10th Weather Radar Conf., Amer. Meteor. Soc., Boston, 384-388.

Schaffner, M.R., 1966: The circulating page loose system, a new solution for data processing. Res. Rep. No. 15, Radio Meteor. Project, Smithsonian Astrophysical Observatory and Harvard College Observatory, Cambridge, Mass.

Starr, V.P., et al., 1960: Observational studies of the atmospheric general circulation. Scientific Rep. No. 2, Planetary Circulation Project, Dept. of Meteorology, M.I.T.

Stout, G.E., and E.A. Mueller, 1968: Survey of relationships between rainfall rate and radar reflectivity in the measurement of precipitation. J. Appl. Meteor., 7, 465-474.

Tokunagu, K., and T. Tanaka, 1964: Experimental results of microwave attenuation due to rain along a path. J. Inst. Elec. Com. Egrs., 47, Japan, 204-290.

Wexler, R., and P.M. Austin, 1954: Radar signal intensity from different levels in steady snow. Res. Rep. No. 23, Weather Radar Res., Dept. of Meteor, M.I.T.

Widrow, B., 1956: A study of rough amplitude quantization by means of Nyquist sampling theory. Trans. IRE/PGCT.

Williams, E.L., Jr., 1949: The Pulse Integrator, Part A: Description of the instrument and its circuitry. Tech. Rep. No. 8, Weather Radar Res., Dept. of Meteor., M.I.T.

Security Classification

DOCUMENT CONTROL DATA - R & D

(Security classification of title, body of abstract and indexing annotation must be entered when the overall report is classified)

1. ORIGINATING ACTIVITY (Corporate author) Massachusetts Institute of Technology Department of Meteorology Cambridge, Massachusetts 02319	2a. REPORT SECURITY CLASSIFICATION Unclassified 2b. GROUP N/A

3. REPORT TITLE
Application of Radar to Measurement of Surface Precipitation

4. DESCRIPTIVE NOTES (Type of report and inclusive dates)
Final Report

5. AUTHOR(S) (First name, middle initial, last name)
Pauline M. Austin

6. REPORT DATE March 1969	7a. TOTAL NO. OF PAGES 93	7b. NO. OF REFS 45
8a. CONTRACT OR GRANT NO. DAAB07-67-C0319 b. PROJECT NO. IT061102B53A-19 c. d.	9a. ORIGINATOR'S REPORT NUMBER(S) 9b. OTHER REPORT NO(S) (Any other numbers that may be assigned this report) ECOM 0319-F	

10. DISTRIBUTION STATEMENT
This document is subject to special export controls and each transmittal to foreign governments or foreign nationals may be made only with prior approval of CG, US Army Electronics Command, Fort Monmouth, N.J. ATTN: AMSEL-BL-AP

11. SUPPLEMENTARY NOTES None	12. SPONSORING MILITARY ACTIVITY US Army Electronics Command AMSEL-BL-AP Fort Monmouth, New Jersey 07703

13. ABSTRACT

This report contains two major sections. In the first, consideration is given to the accuracy and practicality of measuring surface precipitation by radar. The second summarizes studies which have been made regarding mesoscale precipitation patterns and their relation to larger-scale circulations.

It is concluded that for convective storms a properly instrumented 10-cm radar can provide more accurate measurements of rainfall over an area than can a network of gauges. A wave length as short as 3 cm is shown to be unsatisfactory for measuring precipitation because of attenuation.

In widespread storms appreciable errors, occasionally a factor of two or three, may result from differences between the precipitation in the volume sampled by the radar and that reaching the surface. Observations of such effects are presented and discussed.

Advantages and liabilities both of the radar and of a network of gauges for measuring precipitation over an area are illustrated by experiments in which simultaneous measurements by the two methods are compared.

The second section of this report presents detailed descriptions of the structure and behavior of mesoscale precipitation areas and convective cells both in extratropical cyclones and in thunderstorm complexes. These descriptions will serve as a basis for physical and numerical studies of mesoscale phenomena.

DD FORM 1473 REPLACES DD FORM 1473, 1 JAN 68, WHICH IS OBSOLETE FOR ARMY USE. (7)

Security Classification

Security Classification

14. KEY WORDS	LINK A		LINK B		LINK C	
	ROLE	WT	ROLE	WT	ROLE	WT
Meteorology Weather Radar Precipitation						

ESC-FM 2189 - 69

(6)

Security Classification